

This work addresses the numerical determination of effective properties of a cellular media and its topology optimization. Two optimization approaches are addressed: the maximization of a linear combination of the components of the homogenized tensor of elastic properties and the mechanical tailoring of the effective properties of a cellular material.

Advisor: Eduardo Lenz Cardoso

Joinville, 2016

YEAR
2016



SANTA CATARINA STATE UNIVERSITY - UDESC
COLLEGE OF TECHNOLOGICAL SCIENCES - CCT
MASTER IN MECHANICAL ENGINEERING - PPGEM

BRUNO GUILHERME CHRISTOFF | ANALYSIS AND OPTIMIZATION OF THREE DIMENSIONAL MICROSTRUCTURES

MASTER THESIS
**ANALYSIS AND OPTIMIZATION
OF THREE DIMENSIONAL
MICROSTRUCTURES**

BRUNO GUILHERME CHRISTOFF

JOINVILLE, 2016

BRUNO GUILHERME CHRISTOFF

**ANALYSIS AND OPTIMIZATION OF THREE
DIMENSIONAL MICROSTRUCTURES**

Master thesis presented to the Mechanical Engineering Department at the College of Technological Sciences of the Santa Catarina State University, in fulfilment of the partial requirement for the degree of Master in Mechanical Engineering.

Advisor: Eduardo Lenz Cardoso

**JOINVILLE, SC
2016**

C556a

Christoff , Bruno Guilherme

Analysis and optimization of three dimensional microstructures / Bruno Guilherme Christoff . -
2016.

204 p. : il. ; 21 cm

Orientador: Eduardo Lenz Cardoso

Bibliografia: p. 165-174.

Master dissertation – Santa Catarina State University, College of Technological Sciences, Post
Graduation Program in Mechanical Engineering, Joinville, 2016.

1. Porous materials. 2. Cellular materials. 3. Homogenization. 4. Topology optimization.
5. Three dimensional microstructures. I. Cardoso, Eduardo Lenz. II. Santa Catarina State
University, College of Technological Sciences, Post Graduation Program in Mechanical
Engineering. Title.

CDD 620.1 – 23.ed.

BRUNO GUILHERME CHRISTOFF

ANALYSIS AND OPTIMIZATION OF THREE DIMENSIONAL

MICRO STRUCTURES

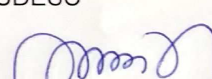
Dissertação apresentada ao Curso de Mestrado Acadêmico em Engenharia Mecânica como requisito parcial para obtenção do título de Mestre em Engenharia Mecânica na área de concentração “Modelagem e Simulação Numérica”.

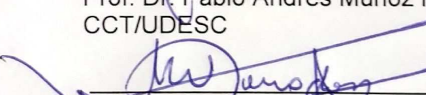
Banca Examinadora

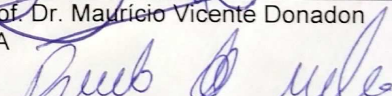
Orientador:

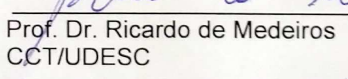

Prof. Dr. Eduardo Lenz Cardoso
CCT/UDESC

Membros


Prof. Dr. Pablo Andrés Muñoz Rojas
CCT/UDESC


Prof. Dr. Mauricio Vicente Donadon
ITA


Prof. Dr. Ricardo de Medeiros
CCT/UDESC


(vídeo-conferência)
Prof. Dr. Markus Merkel
HOCHSCHULE AALEN - Alemanha

Joinville, SC, 06 de junho de 2016.

ACKNOWLEDGEMENTS

I would like to express my deepest gratitude to the following persons, who directly or indirectly helped me in some stage of the development of this thesis.

To my advisor Eduardo Lenz Cardoso for the enormous support in every aspect of this work, for the patience, for being a great professional, besides being a good friend inside and outside the university and for all the coffees and beers.

To professor Pablo Andrés Muñoz Rojas for all the bibliography provided, for all the discussions concerning several aspects of this work and also for the possibility of letting me visit an university abroad.

To professor Markus Merkel for kindly receiving me at Hochshule Aalen.

To the Mechanical Engineering Department of the Santa Catarina State University for the opportunity to carry on this master.

To CAPES for the concession of the master's scholarship.

To my parents Lenir and Carlos, and to my brother Luis for the endless support and for being part of my life in every step I take.

To all my friends of LAMEC for relieving the burden in the stages of development of this work.

To the undergraduate Thiago Ponciano da Silva for the help with the 3D printer.

To Rafa, Klein, Xanxa and Elvis for the Rock and Roll.

*"Take the risk of thinking for yourself,
much more happiness, truth, beauty,
and wisdom will come to you that
way."*

Christopher Hitchens

ABSTRACT

CHRISTOFF, Bruno Guilherme. **Analysis and Optimization of Three Dimensional Microstructures.** 204 pages. Master Thesis (Post Graduation Program in Mechanical Engineering) - Santa Catarina State University, Joinville, 2016.

Cellular materials are a wide spread class of material found in nature. As example one can list wood, cork and tubercular bone. As this kind of structure provides excellent properties to the material and as presently the rapid prototyping process allow a high resolution artificial material manufacturing, several researches are conducted in the artificial materials area. Thus, this work develops a computational code for the determination of the effective properties of a three dimensional media formed by the periodic repetition of a base cell and for the optimization of such cell. Three well established tools into the computational mechanics field are used. The first one is the Homogenization by Asymptotic Expansion, used to evaluate the effective properties of the three dimensional media. The second one is the Topology Optimization and the third one is the Finite Element Method, used to solve the equilibrium problems. The homogenization algorithm is used to evaluate the variation of the effective mechanical and conductivity thermal properties of a hollow sphere structure with regard to the geometrical parameters of its base cell. The optimization algorithm is used in order to obtain a base cell which maximizes a linear combination of the components of the homogenized elasticity tensor of the media and to obtain the geometry of a base cell which better approximates the mechanical properties of a human bone, using as base material, the properties of a biocompatible titanium alloy.

Key-words: Porous Materials. Cellular Materials. Homogenization. Topology Optimization. Three Dimensional Microstructures

RESUMO

CHRISTOFF, Bruno Guilherme. **Análise e Otimização de Microestruturas Tri-Dimensionais.** 204 páginas .Dissertação (Programa de Pós Graduação em Engenharia Mecânica) - Universidade do Estado de Santa Catarina, Joinville, 2016.

Materiais celulares são um classe especializada de material muito encontrada na natureza. Como exemplos destes materiais pode-se citar a madeira, a cortiça e o osso tubercular. Como este tipo de estrutura proporciona ao material excelentes propriedades com um volume relativo baixo e como atualmente os processos de prototipagem rápida permitem a fabricação de materiais contendo microestruturas em escala bastante reduzida e com alta precisão, diversas pesquisas são conduzidas relacionadas à materiais celulares artificiais. Assim, este trabalho consiste no desenvolvimento de um código computacional para obtenção das properiedades efetivas de um meio tri dimensional formado pela repetição de uma célula base e para o projeto otimizado de tal célula base. Três ferramentas bastante difundidas na literatura são utilizadas. A primeira é a Homogeneização por Expansão Assintótica, utilizada para a determinação das propriedades efetivas do meio. A segunda é a otimização topológica e a terceira o método dos elementos finitos, utilizado para a solução dos problemas de equilíbrio. O algoritmo de homogeneização é utilizado para a obtenção das propriedades mecânicas e de condutividade térmica efetivas num meio formado por esferas ocas. O algoritmo de otimização é utilizado para a obtenção de geometrias que maximizam uma combinação linear qualquer das componentes do tensor elástico efetivo do meio e para a obtenção da geometria da célula base que aproxime as propriedades mecânicas de um osso humano, utilizando como material base as propriedades mecânicas de uma liga de titânio bio compatível.

Palavras-chave: Materiais Porosos. Materiais Celulares. Homogeneização. Otimização Topológica. Microestruturas Tri-Dimensionais.

LIST OF FIGURES

Figure 1 – Design domain, periodic material and base cell	38
Figure 2 – Base cell and corresponding periodic material	39
Figure 3 – Microstructure of the Base Cell	40
Figure 4 – Base cell and corresponding periodic material	40
Figure 5 – Base cell and corresponding periodic material	41
Figure 6 – A quarter of base cell and corresponding periodic material	41
Figure 7 – Base cell and corresponding periodic material	42
Figure 8 – Periodic expansion of a base cell. x are the macroscopic coordinates and y are the microscopic coordinates	47
Figure 9 – Micro and macroscopic behaviour of the function	48
Figure 10 – Adopted topology	59
Figure 11 – Load case 1	59
Figure 12 – Load case 2	60
Figure 13 – Load case 3	61
Figure 14 – Load case 4	62
Figure 15 – Load case 5	62
Figure 16 – Load case 6	63
Figure 17 – Periodicity consideration	67
Figure 18 – Example for periodicity consideration	68
Figure 19 – Reference for the mesh generation	71
Figure 20 – Solution of the linear systems	76
Figure 21 – Mechanical homogenized coefficients	77
Figure 22 – Thermal homogenized coefficients	78
Figure 23 – Algorithm of the analysis program	79
Figure 24 – Parametric optimization	89
Figure 25 – Shape optimization	89
Figure 26 – Topology optimization	90
Figure 27 – SIMP	94
Figure 28 – The checkerboard problem in a compliance minimization problem for several finite element mesh sizes. Mesh with a) 300 ; b) 1200 ; c) 4800; and d) 19200 finite elements	96
Figure 29 – The mesh-dependency problem in a compliance minimization problem for several finite element mesh sizes. Mesh with a) 300 ; b) 1200 ; c) 4800; and d) 19200 finite elements	97
Figure 30 – Algorithm of the optimization program	113
Figure 31 – Algorithm of the optimization procedure	114

Figure 32 – Hollow sphere - model 1	114
Figure 33 – Hollow sphere - model 2	115
Figure 34 – Hollow sphere structure - Case 1	117
Figure 35 – Hollow sphere structure - case 2	118
Figure 36 – C_{1111}^H values obtained for the first model	119
Figure 37 – C_{1122}^H values obtained for the first model	120
Figure 38 – C_{1212}^H values obtained for the first model	120
Figure 39 – Kt_{11}^H values obtained for the first model	121
Figure 40 – Surface and simulated points for the C_{1111}^H component, reinforcement of $R_R = 0.2$	122
Figure 41 – Surface and simulated points for the C_{1111}^H component, reinforcement of $R_R = 0.3$	122
Figure 42 – Surface and simulated points for the C_{1111}^H component, reinforcement of $R_R = 0.4$	122
Figure 43 – Surface and simulated points for the C_{1111}^H component, reinforcement of $R_R = 0.5$	123
Figure 44 – Surface and simulated points for the C_{1122}^H component, reinforcement of $R_R = 0.2$	123
Figure 45 – Surface and simulated points for the C_{1122}^H component, reinforcement of $R_R = 0.3$	124
Figure 46 – Surface and simulated points for the C_{1122}^H component, reinforcement of $R_R = 0.4$	124
Figure 47 – Surface and simulated points for the C_{1122}^H component, reinforcement of $R_R = 0.5$	124
Figure 48 – Surface and simulated points for the C_{1212}^H component, reinforcement of $R_R = 0.2$	125
Figure 49 – Surface and simulated points for the C_{1212}^H component, reinforcement of $R_R = 0.3$	125
Figure 50 – Surface and simulated points for the C_{1212}^H component, reinforcement of $R_R = 0.4$	125
Figure 51 – Surface and simulated points for the C_{1212}^H component, reinforcement of $R_R = 0.5$	126
Figure 52 – Surface and simulated points for the Kt_{11}^H component, reinforcement of $R_R = 0.2$	126
Figure 53 – Surface and simulated points for the Kt_{11}^H component, reinforcement of $R_R = 0.3$	127
Figure 54 – Surface and simulated points for the Kt_{11}^H component, reinforcement of $R_R = 0.4$	127
Figure 55 – Surface and simulated points for the Kt_{11}^H component, reinforcement of $R_R = 0.5$	127

Figure 56 – C_{1111}^H values obtained for the second model	129
Figure 57 – C_{1212}^H values obtained for the second model	130
Figure 58 – C_{1122}^H values obtained for the second model	130
Figure 59 – Kt_{11}^H values obtained for the second model	131
Figure 60 – Surface and simulated points for C_{1111}^H	131
Figure 61 – Surface and simulated points for C_{1212}^H	132
Figure 62 – Surface and simulated points for C_{1122}^H	132
Figure 63 – Surface and simulated points for Kt_{11}^H	132
Figure 64 – Mesh detail	135
Figure 65 – Maximization of $C_{1111}^H + C_{2323}^H$, topology obtained for the first initial material distribution	138
Figure 66 – Maximization of $C_{1111}^H + C_{2323}^H$, topology obtained for the second initial material distribution	138
Figure 67 – Maximization of $C_{1111}^H + C_{2323}^H$, topology obtained for the third initial material distribution	139
Figure 68 – Maximization of the components 1111 e 2323	140
Figure 69 – Maximization of $C_{1212}^H + C_{2323}^H + C_{1313}^H$, $V_f = 0.1$	141
Figure 70 – Maximization of $C_{1212}^H + C_{2323}^H + C_{1313}^H$, $V_f = 0.2$	141
Figure 71 – Maximization of $C_{1212}^H + C_{2323}^H + C_{1313}^H$, $V_f = 0.3$	142
Figure 72 – Maximization of $C_{1212}^H + C_{2323}^H + C_{1313}^H$, $V_f = 0.4$	142
Figure 73 – Maximization of $C_{1212}^H + C_{2323}^H + C_{1313}^H$, media with $V_f = 0.1$.	143
Figure 74 – Maximization of $C_{1212}^H + C_{2323}^H + C_{1313}^H$, media with $V_f = 0.2$.	143
Figure 75 – Maximization of $C_{1111}^H + C_{2222}^H + C_{3333}^H$, mesh of $30 \times 30 \times 30$ elements	144
Figure 76 – Maximization of $C_{1111}^H + C_{2222}^H + C_{3333}^H$, mesh of $40 \times 40 \times 40$ elements	145
Figure 77 – Initial material distribution - Case 1	148
Figure 78 – Final material distribution - Case 1	148
Figure 79 – Initial material distribution - Case 2	149
Figure 80 – Final material distribution - Case 2	150
Figure 81 – Initial material distribution - Case 3	150
Figure 82 – Final material distribution - Case 3	151
Figure 83 – Initial material distribution - Case 4	152
Figure 84 – Final material distribution - Case 4	152
Figure 85 – Initial material distribution - Case 5	153
Figure 86 – Final material distribution - Case 5	154
Figure 87 – Media for the mechanical tailoring - case 1	156
Figure 88 – Media for the mechanical tailoring - case 2	157
Figure 89 – Media for the mechanical tailoring - case 3	157
Figure 90 – Media for the mechanical tailoring - case 4	158
Figure 91 – Media for the mechanical tailoring - case 5	158

Figure 92 – Final results	159
Figure 93 – Unidimensional media	175
Figure 94 – Pure bending in a finite element	181
Figure 95 – Low order approximation and exact solution for a bending case	181
Figure 96 – Nodes and coordinates system for the eight node element .	183
Figure 97 – Reinforcement in the planes xy , yz and xz , respectively . .	187
Figure 98 – Young and shear modulus versus volumetric fraction. In the full lines the mixture rule solution. In the discrete points the homogenization solution	189
Figure 99 – Square reinforcement	190
Figure 100 – Circular reinforcement	191
Figure 101 – Young's modulus versus volumetric fraction, square rein- forcement in y direction	192
Figure 102 – Young's modulus versus volumetric fraction, circular rein- forcement in x direction	192
Figure 103 – Hollow sphere model	193
Figure 104 – Young's modulus	194
Figure 105 – Shear modulus	195
Figure 106 – Bulk modulus	195
Figure 107 – Poisson's coefficient	196
Figure 108 – Glass fibre with volumetric fraction of 0.51 in an epoxy matrix	197
Figure 109 – Glass spheres volumetric fraction of 0.54 in an epoxy matrix	197
Figure 110 – Properties of the epoxy matrix reinforced by glass fibres . .	198
Figure 111 – Properties of the epoxy matrix reinforced by glass spheres - Young's modulus	199
Figure 112 – Properties of the epoxy matrix reinforced by glass spheres - Shear modulus	200
Figure 113 – Effective thermal conductivity versus volumetric fraction. In the full line is the mixture rule solution. In the discrete points is the homogenization solution	201
Figure 114 – Open cell hollow sphere structure	202
Figure 115 – Thermal properties validation	202

LIST OF TABLES

Table 1 – Simulation data	118
Table 2 – Maximum error - Case 1	135
Table 3 – Maximum error - Case 2	135
Table 4 – Computational effort	136
Table 5 – Simulation data	137
Table 6 – Components 1111 and 2323 of the homogenized tensor	139
Table 7 – Shear components of the homogenized tensor	142
Table 8 – Normal components of the homogenized tensor	145
Table 9 – Simulations properties	147
Table 10 – Objective function value	155
Table 11 – Relative error	155
Table 12 – Data for the plane reinforcement cases	187
Table 13 – Data for uniaxial reinforcement cases	191
Table 14 – Simulation data	193
Table 15 – Simulation data	197
Table 16 – Data for the plane reinforcement cases	201
Table 17 – Data for the plane reinforcement cases	202
Table 18 – Validation of the analytical derivatives through the central finite difference method	204
Table 19 – Validation of the analytical derivatives through the central finite difference method	204
Table 20 – Validation of the analytical derivatives through the central finite difference method	204

LIST OF ABBREVIATIONS AND ACRONYMS

DLP	Digital Light Processing
FDM	Fused Deposition Modelling
FEM	Finite Element Method
HSS	Hollow Sphere Structures
KKT	Karush-Kuhn-Tucker (Optimality Conditions)
MMA	Method of the Moving Asymptotes
OC	Optimality Criteria
RVE	Representative Volume Element
SIMP	Solid Isotropic Material with Penalization
SLM	Selective Laser Melting
SLP	Sequential Linear Programming
SLS	Selective Laser Sintering

LIST OF SYMBOLS

A	Coefficient matrix
a	Vector
b	Average body force vector
B	Strain-displacement Matrix
b	Known vector
C	Fourth order elasticity tensor
C^*	Target tensor
c_e	centroid of the element e
c_i	centroid of a neighbour element i
c_{kl}	Column kl of the constive fourth order elasticity tensor
C^H	Fourth order homogenized elasticity tensor
Ct	Global conductivity matrix
Ct^e	Local conductivity matrix
\widetilde{Ct}	Reduced global thermal conductivity matrix
d	Search direction
D	Diagonal Matrix (diagonal scaling)
D_{ie}	Euclidian distance between the filtered element and its neighbour
E	Young's Modulus
f	body force vector
f	Objective function
f^{ϵ^0}	Initial strain force vector
f_{kl}	Load vector
f_{kl}^e	Local load vector

$\tilde{\mathbf{f}}$	Reduced force vector
\hat{g}_j	Scalar associated to the j -th constraint
g_j	j -th inequality constraint
\mathbf{H}	Hessian matrix
h_k	j -th equality constraint
\mathbf{K}	Global stiffness matrix
\mathbf{k}^e	Local stiffness matrix
$\widetilde{\mathbf{K}}$	Reduced global stiffness matrix
\mathbf{Kt}	Thermal conductivity tensor
Kt	Thermal conductivity coefficient
\mathbf{L}	Differential linear operator
\mathbf{L}	Lagrangian function
\mathbf{L}_i	Moving asymptote
\mathbf{N}	Diagonal Matrix
N	Total number of nodes in the discrete domain
n	Number of elements on the mesh
n_d	Number of design variables
ng	Number of Gauss points
\mathbf{N}_e	Neighbourhood of an element e
n_g	Number of inequality constraints
n_h	Number of equality constraint
n_1, n_2, n_3	Arbitrary integer numbers
N_i^g	Global shape function associated with the node i and the element type
P	Penalization factor
p_{ji}	Parameter of the MMA

p_{oi}	Parameter of the MMA
\mathbf{p}	vector of tractions inside the holes
\mathbf{Q}_j	Flux vector
\mathbf{Q}_j^e	Local flux vector
$\tilde{\mathbf{Q}}$	Reduced flux vector
q_{ji}	Parameter of the MMA
q_{oi}	Parameter of the MMA
\mathbf{r}	Residue vector
R	Filtering radius
\mathbf{R}^j	Characteristic temperature field relative to the flux case j
$\tilde{\mathbf{R}}$	Reduced characteristic temperature field
R_R	Diameter of the reinforcement of a hollow sphere
r_j	Parameter of the MMA
r_o	Parameter of the MMA
S	Boundary of the cell
\mathbf{s}	Slack variable vector
\mathbf{t}	vector of tractions on the boundaries
\mathbf{T}	Transformation matrix
T_0	Macroscopic scale contribution for the temperature field
T_1	Microscopic scale contribution for the temperature field
\mathbf{T}^ϵ	Total temperature field of the porous media
\mathbf{T}_m	Mechanical transformation matrix
\mathbf{T}_t	Thermal transformation matrix
\mathbf{u}^0	Macroscopic scale contribution for the displacement field

u^1	Microscopic scale contribution for the displacement field
u^2	Eventual smaller scale contribution for the displacement field
u^ϵ	Total displacement field of the porous media
U_i	Moving asymptote
v	virtual displacement vector
V	Volume
\hat{v}	Virtual node displacement vector
V_e	Volume of an element
V_f	Admissible volume for the structure
V^ϵ	set of kinematically admissible displacements
w_e	Weight function associated to the element e
x	Macroscopic coordinates
y	Microscopic coordinates
Y	Size of the base cell
y_1^0	Length of the base cell
y_2^0	Height of the base cell
y_3^0	Depth of the base cell
α_i^k	Parameter of the MMA
α_i	Scalar associated to the i -th component of the homogenized constitutive tensor
β_e	Update parameter
β_i^k	Parameter of the MMA
β^s	Scalar
χ	Characteristic displacement field
$\hat{\chi}$	Nodal displacement relative to the load case kl

χ^{kl}	Characteristic displacement field relative to the load case kl
$\tilde{\chi}$	Reduced characteristic displacement field
ϵ	Small parameter
Γ_t	Boundary
κ	Discrete function
λ	Lagrange Multiplier vector
Λ	Large number
λ_1	Initial parameter of bisection
λ_2	Initial parameter of bisection
μ	Kuhn-Tucker multiplier vector
ν	Poisson's coefficient
Ω	Domain
Ω_f	Feasible region
Ω^{mat}	Region with material
Ω / Ω^{mat}	region without material
$\partial\chi^{kl}$	Strain field of the unit cell in regard to the load case kl
Φ	Error function
Φ	Function
Φ^0	macroscopic value of the field variable
Φ^1	perturbation on the field variable
Φ^2	perturbation on the field variable
Φ^e	Exact value of the field variable
Ψ	Characteristic displacement field
Ψ^s	Step

Ψ^0	Optimization problem
Ψ^k	Optimization sub problem
ρ	Pseudo density vector, design variable vector
ρ^*	Regular point
$\underline{\rho}_i$	Inferior bound for the i -th design variable
$\bar{\rho}_i$	Superior bound for the i -th design variable
ρ_{min}	Minimum admissible pseudo density
ρ_i	Inner diameter of a hollow sphere
ρ_o	Outer diameter of a hollow sphere
ρ_{opt}	Optimum pseudo density vector
ρ_v	Pseudo density of an element
σ	Second order stress tensor
τ	Residual stress tensor
\mathcal{F}	Function
\mathcal{P}	Property
\mathcal{P}^0	Property of the base material
tol	tolerance
\mathbb{Y}	Solid portion of the base cell
E_v^0	Voids Young's Modulus
K_{est}^e	Condensed stiffness matrix
E^0	Base material's Young's Modulus
G^H	Homogenized Shear Modulus
u^h	Displacement approximation
N_a	Shape function of node a
G_v^0	Voids Shear Modulus

E^H	Homogenized Young's Modulus
G^0	Base material's Shear Modulus
E_m	Matrix Young's Modulus
E_f	Fibre Young's Modulus
η	Natural coordinate
γ	Specific weight
ν_f	Fibre Poisson coefficient
ν_m	Matrix Poisson coefficient
ξ	Natural coordinate
ζ	Natural coordinate

CONTENTS

1	INTRODUCTION	33
1.1	CELLULAR MATERIALS	33
1.1.1	Natural Cellular Materials and Engineering Applications	33
1.1.2	Manufacturing	35
1.1.3	Properties Determination	35
1.2	HOMOGENIZATION BY ASYMPTOTIC EXPANSION	36
1.3	OPTIMIZATION OF CELLULAR STRUCTURES	38
1.4	CONTEXTUALIZATION WITHIN THE UNIVERSITY RESEARCH GROUP	39
1.5	OBJECTIVES	42
1.6	OUTLINE OF THIS THESIS	43
2	HOMOGENIZATION	45
2.1	ASYMPTOTIC EXPANSION AND PERIODICITY	47
2.2	ELASTICITY PROBLEM	49
2.2.1	General Elasticity Problem	51
2.2.2	Numerical Solution	54
2.2.3	Physical Interpretation of the Load Cases	58
2.3	THERMAL PROBLEM	63
2.3.1	General Thermal Conductivity Problem	64
2.3.2	Numerical Solution	65
2.4	PERIODIC BOUNDARY CONDITIONS	66
2.5	DESCRIPTION OF THE ALGORITHM	70
2.5.1	Data Input and Initial Calculations	70
2.5.1.1	Mesh Generation	71
2.5.1.2	Compatibility Matrix	71
2.5.2	Base Material	72
2.5.3	Solution of the Linear System	73
2.5.3.1	Conjugate Gradient Method	73
2.5.3.2	Diagonal Scaling	75
2.5.3.3	Parallel Code	75
2.5.4	Mechanical Homogenized Coefficients	76
2.5.5	Thermal Homogenized Coefficients	77
2.5.6	Analysis Problem	78
3	OPTIMIZATION	81
3.1	HISTORICAL CONTEXT	81
3.2	BASIC CONCEPTS	82

3.2.1	Local and Global Minima	83
3.2.2	Necessary and Sufficient Conditions	84
3.2.3	Regular Point	84
3.2.4	Lagrange Multipliers	85
3.2.5	KKT Conditions	86
3.3	STRUCTURAL OPTIMIZATION	88
4	TOPOLOGY OPTIMIZATION	91
4.1	HISTORICAL REVIEW	91
4.2	MATERIAL PARAMETERIZATION	93
4.3	PROBLEMS RELATED TO TOPOLOGY OPTIMIZATION	95
4.3.1	Checkerboard	95
4.3.2	Mesh dependency	96
4.3.3	Restriction Methods	97
4.3.3.1	Filtering Methods	98
4.4	SOLUTION OF THE TOPOLOGY OPTIMIZATION PROBLEM	99
4.4.1	Optimality Criteria	99
4.4.2	Sequential Linear Programming	101
4.4.3	Method of Moving Asymptotes	103
5	FORMULATION	105
5.1	OPTIMIZATION PROBLEMS	106
5.1.1	Linear Combination of the Components of the Homogenized Constitutive Tensor	106
5.1.2	Target Tensor	107
5.2	SENSITIVITY ANALYSIS	107
5.3	ALGORITHM DESCRIPTION	112
5.3.1	Data	112
5.3.2	Optimization Problem	112
5.4	ANALYSIS PROBLEM	114
5.4.1	Least Square Method	115
6	RESULTS	117
6.1	EFFECTIVE PROPERTIES OF HOLLOW SPHERE STRUCTURES (HSS)	117
6.1.1	Numerical Results	118
6.1.1.1	First Hollow Sphere Model	119
6.1.1.2	Second Hollow Sphere Model	129
6.1.2	Summary	134

6.2	MAXIMIZATION OF THE COMPONENTS OF THE HOMOGENIZED TENSOR	136
6.2.1	Maximization of the Linear Combination of the Components 1111 and 2323 of the Homogenized Tensor	137
6.2.2	Maximization of the Linear Combination of the Components 1212, 2323 and 1313 of the Homogenized Tensor	140
6.2.3	Maximization of the Linear Combination of the Components 1111, 2222 and 3333 of the Homogenized Tensor	144
6.2.4	Summary	145
6.3	TAILORING OF MECHANICAL PROPERTIES	146
6.3.1	Topologies	147
6.3.2	Summary	154
7	CONCLUSION	161
7.1	SUGGESTIONS FOR FURTHER WORKS	162
CONCLUSION		162
	BIBLIOGRAPHY	165
	APPENDIX A – UNIDIMENSIONAL HOMOGENIZATION	175
	APPENDIX B – TRILINEAR ISOPARAMETRIC HEXAHEDRAL ELEMENT WITH INCOMPATIBLE MODES	181
	APPENDIX C – VALIDATION OF THE HOMOGENIZATION	187
	APPENDIX D – SENSITIVITY VALIDATION	203

1 INTRODUCTION

The introduction of rapid prototyping processes allows the high resolution manufacturing of cellular materials with a predetermined microstructure, thus increasing the applications of this kind of material in several areas of technology.

The correct prediction of properties in a composite and a cellular, or porous media, plays an important role in engineering applications, due to the fact that a proper material specification can provide lower cost, lower weight and higher strength. Also, abreast the correct prediction of properties, the optimization of these kind of microstructures allows tailoring the effective mechanical properties in order to suit in a given application.

1.1 CELLULAR MATERIALS

Cellular, or porous material, can be understood as a material containing a small structure that can be identified in the material. The most important feature of a cellular material is its relative density, that is, the density of the cellular material, divided by the density of the solid of which the cellular material is made (GIBSON; ASHBY, 1997). Some materials can be made with a relative density as low as 0.001. Also, cellular materials can roughly be divided into two distinct groups, open and closed cell materials (GRENESTEDT, 1999). The open cell materials consists of a interconnected network of rods or beams, whereas the closed cell materials consists in a network of interconnected shells or plates. Also, the material can be partly open and partly closed.

Another way of defining a cellular material is through the concept of composite. According to Mendonça (2005), a composite is a set of two or more different materials, combined into a macroscopic scale in order to work as a single material, aiming the acquisition of properties that none of the base materials present individually. A cellular material can be seen as a particularity of a composite, in which one of the constituent materials is solid and another one is void.

1.1.1 Natural Cellular Materials and Engineering Applications

Cellular materials are widely spread in nature and in engineering applications. This kind of structure provides excellent material properties

like high energy absorption, good formability and excellent insulation. Also, the possibility of tailoring their mechanical, thermal, electrical and other properties makes this an unique class of material. In nature one can find cellular materials in plant bodies and skeletons, applications in which certain mechanical properties with a small amount of material, or a small weight, are required. This natural cellular materials have an adapted microstructure in order to prevail some service conditions, rendering them very mechanically efficient (LUXNER, 2006).

Many natural structural materials are cellular solids, including wood, cancellous bone and cork. Wood is still the world's most widely used material. It has orthotropic behavior and its stiffness is greater in the axial direction, due to the cellular arrangement, showing a natural adaptation of the necessity of a plant. Most bones are an elaborate construction with an outer shell of compact bone and a core of porous cellular cancellous bone within. This arrangement reduces the weight of the bone while still provides a large bearing area, feature that reduces stresses at joints. Also, this configuration forms a low weight sandwich shell, providing a lightweight structure without compromising its primary mechanical function (GIBSON; ASHBY, 1997).

The main area of application of cellular materials is the thermal insulation. The low conductivity of certain foams makes it very useful in applications such as the insulation of booster rockets, refrigerated transport system, among others.

The use of cellular solids is also widespread into the packaging area. This kind of material becomes useful in this kind of application due to two major reasons. The first one is an effective energy absorption in case of impacts, that must be effective to protect the material being transported and the second one is the light weight.

Nowadays, sandwich panels in modern aircraft are made of carbon or glass fibres, separated by honeycomb, or other lightweight material, providing an enormous bending stiffness to the structure. The understanding of the mechanics of the cancellous bone, allows to replace damaged bone to man-made cellular materials with properties approximately equal to the bones.

Cellular materials have been used also in marine buoyancy. Cork has been used for fishing float for millennia. Nowadays, plastic foams are widely used as supports for floating structures. This kind of material is more resistant to damage than other solutions as flotation bags or chambers. Also, they do not rust or corrode and can retain their buoyancy even when

hardly damaged, due to the cellular composition.

1.1.2 Manufacturing

Cellular structures have complex geometries and cannot be manufactured with standard manufacturing processes, such as machining or casting. So, a great challenge faced by the research on cellular materials lies on a viable way of manufacturing this kind of structure. The work of Banhart (2000) shows several techniques of manufacturing cellular materials and metallic foams. Recently, these techniques improved significantly enabling the manufacturing of cellular materials with complex geometries.

One could mention as the main cellular materials manufacturing processes the Selective Laser Melting, SLM, the Selective Laser Sintering, SLS, the Fused Deposition Modelling, FDM and the Digital Light Processing, DLP, which allow the manufacturing of materials with a high complexity in a microscopic scale in regard to the manufactured piece. The above mentioned methods are called Rapid Prototyping processes and allow a controlled and localized melting of a powder metal. The works of Smith, Guan and Cantwell (2013) and Wang (2005) show how the techniques of manufacturing are used in a combined way. These techniques can be used to manufacture either polymeric or metallic media. Still, the use of rapid prototyping combined with biodegradable polymers has become increasingly important in the medical area (LUXNER, 2006).

1.1.3 Properties Determination

The effective properties of a cellular material are dependent on the properties of the base material, the relative fraction and the spatial distribution of material on the domain.

Several analytical models are presented by Gibson and Ashby (1997) to predict the effective mechanical properties of honeycombs, foams and sandwich panels with foam cores. It is also discussed the mechanical behaviour of natural cellular materials as wood, cancellous bone and cork. The work of Grenestedt (1999) uses analytical and numerical techniques in order to predict the effective elastic behaviour of low density regular cellular materials, considering that there are no imperfections in the material. Still, the work of Christensen (2000) investigates the mechanical behaviour for both two and three dimensional low density regular cellular solids. Zhu, Hobdell and Windle (2000) investigates how cell irregularities affects the

elastic properties of open-cell foams using a finite element analysis approach. Sanders and Gibson (2003) analyse the elastic moduli and initial yield strength of body-centred and face-centered cubic packings of hollow sphere foams with finite element models. In the work of Luxner, Stampf and Pettermann (2005), several finite element modelling concepts and linear analyses are used in order to study generic three dimensional structures with the employment of both continuum element and beam element based models.

As mentioned before, a cellular material can be seen as a particularity of a composite, thus, it is worth mentioning some works concerning the properties determination of composites. The effective properties of a composite material are dependent of the properties of each constituent, their relative volume fractions, the arrangement of the inclusions and the quality of the adhesion among each phase. If the material is assumed as periodic or quasi-periodic, one can, under the assumption of linearity, use the well-established concept of representative volume element (RVE) analysis. In the RVE analysis, representative sections of the material distribution are analysed under assumed boundary conditions to obtain the average or effective properties of that mixture (HOLLISTER; KIKUCHI, 1994).

Among the several methods available to obtain the effective properties of a composite, the standard rule of mixtures is the simplest, Jones (1999), although it can only be used with simple mixtures. Other well-established methods found in the literature, like Paul (1960), Hashin (1962), Hashin (1963), Hill (1965), Whitney (1967), Halpin and Tsai (1969), Muskhelishvili (2010), must be used within some specific hypothesis concerning the material distribution, the material properties of the constituents and their relative volume fraction.

One of the RVE methods that can be used in order to account for more general problems, like the mixture of anisotropic materials with complex geometries and cellular materials, is the homogenization by asymptotic expansion (KELLER, 1977) (SANCHEZ-PALENCIA, 1980), (SANCHEZ-HUBERT; SANCHEZ-PALENCIA, 1992). The basic idea of this method, used in this work, is to obtain the macroscopic behaviour of a media formed by a periodic microstructure, as a function of the microscale.

1.2 HOMOGENIZATION BY ASYMPTOTIC EXPANSION

In the context of linear elasticity, the effective properties of a material with a periodic microstructure can be determined by the homog-

enization by asymptotic expansion method. This method is based on the assumption that there is a base cell (or RVE), that is to say, a small part of the domain which repeats itself with a periodicity in the whole domain, that is considerably smaller than the design domain (NEVES; RODRIGUES; GUEDES, 2000).

The development of the method follows three basic considerations (HOLLISTER; KIKUCHI, 1994). The first demands that the property being evaluated can be written as an asymptotic expansion. The second consideration is that the problem can be divided into two scales, one at the macro scale, or design domain, and other in the micro scale. This two scales must be related by an small scalar, ϵ , that should tend to zero, indicating that the macro scale is far bigger than the micro scale. The last consideration is that the boundaries of the RVE are periodic. That means that kinematic constraints are imposed to the RVE, enforcing that the displacement field (for the determination of the elastic properties) and the temperature field (for the determination of the thermal conductivity properties) must have the same values on opposite faces of the RVE.

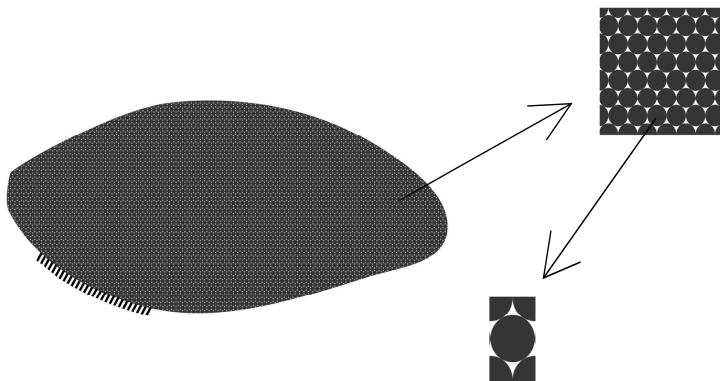
This method allows to obtain the macroscopic behaviour, with the consideration that the required properties can be written as a function of the microscopic behaviour, at the base cell level, in the form of an asymptotic expansion in two or more scales. Thereby, the main objective of the method is to describe the macroscopic behaviour of the cellular material using only the informations of the base cell, avoiding a complicated problem and reducing drastically the computational effort on a finite element problem, due to the fact that, using the homogenization method, only one cell must be discretized and not the whole domain.

The evaluation procedure of effective properties of a media, from a given base cell geometry, can be understood as a direct analysis of the problem. Figure 1 illustrates the basic idea of the method, in which a domain, formed by a repetition of several base cell is shown.

Like the elastic properties, the thermal conductivity properties of a media formed by the repetition of several base cell can be obtained by the homogenization by asymptotic expansion method, using the same consideration as for the mechanical case.

The equilibrium equations needed to obtain the effective properties of a porous, or composite, media can be solved through several numerical methods. At this work, the finite element method is adopted.

Figure 1 – Design domain, periodic material and base cell



Source: Author's production, 2016, based on (NEVES; RODRIGUES; GUEDES, 2000)

1.3 OPTIMIZATION OF CELLULAR STRUCTURES

A quite frequent approach of a homogenization problem, is the so called inverse analysis, that is used combined with the topology optimization method. This approach consists in, given the macroscopic requirements of the porous media, to find the geometry of the base cell who better fits these requirements.

The use of the topology optimization method in the context of a continuum media is well established by Bendsøe and Kikuchi (1988), who define an optimum distribution of material in order to satisfy a function associated to the effective properties of the media, and the homogenization method is used as a tool to evaluate such properties.

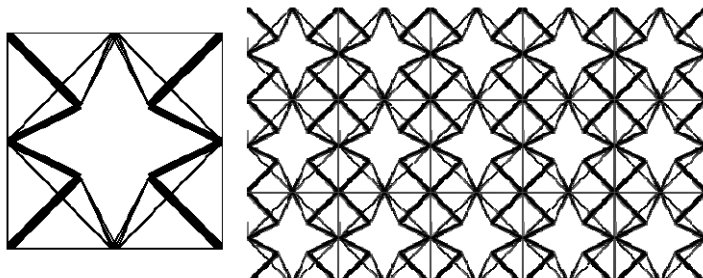
Still in this context, it is worth mentioning the work of Weihong et al. (2007), which uses the methods of homogenization and topology optimization to find the geometry of the base cell that provides the maximization of a linear combination of the components of the homogenized constitutive tensor, and also the work of Lin, Kikuchi and Hollister (2004), which uses both tools to find a bone support with a structure in which the material has elastic properties close to the human bone.

1.4 CONTEXTUALIZATION WITHIN THE UNIVERSITY RESEARCH GROUP

In this section, some works developed in the Mechanical Computational Laboratory (*Laboratório de Mecânica Computacional-LAMEC*) of the Santa Catarina State University (*Universidade do Estado de Santa Catarina - UDESC*), or with a partnership with some member of the research group, are shown.

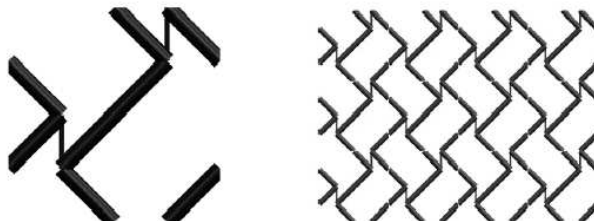
The works of Muñoz-Rojas, Carniel and Öchsner (2011) and Carniel (2009) use sequential linear programming to optimize thermomechanical properties, like the maximization of the shear modulus and the thermal conductivity and a given direction. Bi and three dimensional results are presented, although, the use of small moving limits requires a high number of iterations to the convergence. To solve this issue, the authors propose the use of an alternative algorithm of mathematical programming. To improve the previous work, Muñoz-Rojas et al. (2011) suggest an hybrid approach composed by an optimization without derivatives, the Globalized Bounded Nelder-Mead Method - GBNM, followed by an optimization with derivatives, the Sequential Linear Programming - SLP. With this approach it is possible to achieve new topologies with improved results, when compared with the previous work. Figures 2 and 3 show the micro structures obtained by maximizing the ratio between the shear component of the elasticity homogenized tensor and the thermal conductivity component of the thermal homogenized tensor for both works.

Figure 2 – Base cell and corresponding periodic material



Source: (CARNIEL, 2009)

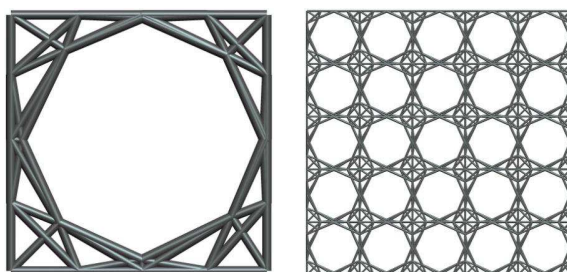
Figure 3 – Microstructure of the Base Cell



Source: (MUÑOZ-ROJAS et al., 2011)

The work of Guth (2012) couples the homogenization method with an optimization algorithm in order to obtain the optimum configuration of materials composed by lattice cells, aiming the improvement of the response of mechanical and thermal solicitations, including for some cases, symmetry restrictions. Figure 4 shows an optimized base cell for the maximization of thermal conductivity with thermal isotropy symmetry and its correspondent periodic material.

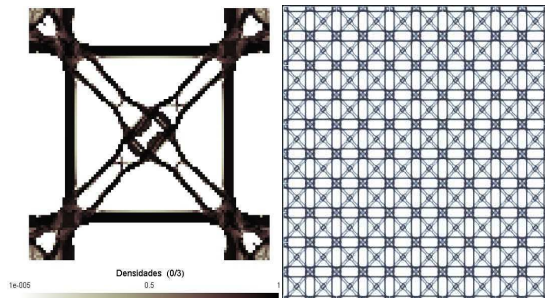
Figure 4 – Base cell and corresponding periodic material



Source: (GUTH, 2012)

Franco (2014) studies an optimized design of titanium micro structures, in order to minimize the difference between the elasticity tensor of the human bone and the material properties of a prosthesis, using the topology optimization method and the plane stress consideration. Several topologies achieve a satisfactory result and one of them is shown in figure 5, together with the correspondent periodic material.

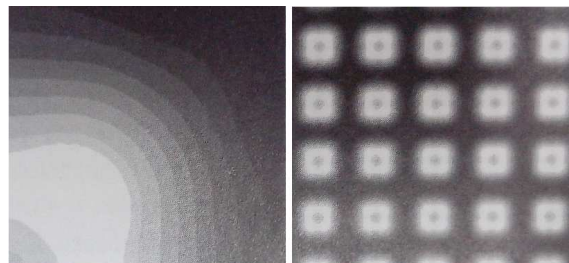
Figure 5 – Base cell and corresponding periodic material



Source: (FRANCO, 2014)

It is worth mentioning the work of Muñoz-Rojas et al. (2008), that uses shape and topology optimization to achieve a maximization on the thermal conduction properties on cellular materials. Figure 6 shows an unitary cell obtained for the maximization of the sum of the thermal properties in both principal directions and the correspondent periodic material.

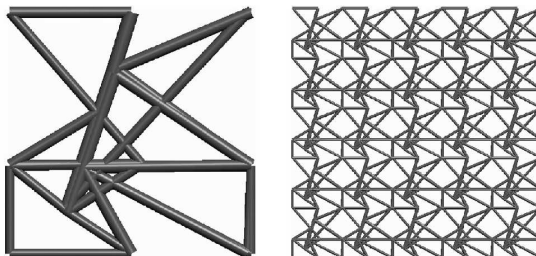
Figure 6 – A quarter of base cell and corresponding periodic material



Source: (MUÑOZ-ROJAS et al., 2008)

To conclude, the work of Guth, Luersen and Muñoz-Rojas (2012) shows the lattice periodic material optimization, with symmetry restrictions into the homogenized elastic constitutive tensor. Figure 7 shows the base cell obtained for the minimization of the Poisson's coefficient, with isotropy restriction on the elasticity tensor and its correspondent periodic material.

Figure 7 – Base cell and corresponding periodic material



Source: (GUTH; LUERSEN; MUÑOZ-ROJAS, 2012)

1.5 OBJECTIVES

The present work has two main objectives. The first one consists in, given a three dimensional base cell who represents the smallest repetitive part of a porous media, to find the effective mechanical and thermal properties of this media, the so called direct analysis. The second one consists in, given an elastic constitutive parameters of the porous media, to find the geometry of the base cell who better satisfies these requirements, the so called inverse analysis.

It is developed a computational code using the Julia Language (BEZANSON et al., 2012), using the finite element method (FEM) as a tool combined with the homogenization by asymptotic expansion theory for the direct analysis. In addition, a computational code for topology optimization is also developed. All stages of development of the algorithms and the computational code are made by the author and the visualization of the topologies is made by using the Gmsh software (GEUZAIN; REMACLE, 2009)

Furthermore, as specific objectives, one can highlight:

- Review, understand and register the finite element method, the homogenization and the topology optimization theories;
- Implementation of a three dimensional finite element software for the determination of the displacement, strain and stress fields in a given domain, including the mesh generation;
- Implementation of a homogenization software for the determination of the mechanical and thermal tensors of a porous media formed by

the repetition of a base cell, bearing in mind that all calculation are made at the base cell level;

- Implementation of a topology optimization software to be used combined with the homogenization software, in order to determinate the geometry of a base cell that satisfies some requirements of the porous media formed by the repetition of these cells;
- Direct Analysis: To study the mechanical and thermal behaviour of a porous media throughout the geometry of the base cell;
- Inverse Analysis to mechanical applications: To find the optimum geometry of the base cell to maximize the linear combination of the components of the homogenized tensor and to find the geometry of the base cell whose homogenized tensor approximates a given elasticity tensor.

1.6 OUTLINE OF THIS THESIS

The work is structured following the sequence:

- Chapter 2 presents the main concepts associated to the determination of the properties of a porous media through the homogenization method. The concept of asymptotic expansion and the expressions for the determination of the mechanical and thermal effective tensors are obtained. Finally, the developed algorithm for the determination of the equivalent properties of a porous media is explained;
- Chapter 3 presents the basic concepts of optimization in a general approach. A historical review, the basic concepts to understand an optimization problem, and the classification of the structural optimization approaches are shown;
- Chapter 4 presents the the topology optimization method. The concept of material parameterization is explained. Problems associated to the method, and some of the approaches to avoid them are shown. Last of all, the methods used in this work to solve a topology optimization problem are presented;
- Chapter 5 presents the formulation of the problems addressed in this work. Initially, the proposed optimization problems are shown. The first one consists in to find the geometry of the base cell of a porous

media whose linear combination of any components of its mechanical tensor is maximized. The second one is the elastic tailoring of the properties of a human bone. The formulation of the optimization problems are presented, as well as the sensibility analysis. Finally, the proposed solution algorithm is presented. Besides the optimization problems, an analysis problem is proposed. It consists in, given the topology of two distinct hollow spheres models, to find the effective mechanical and thermal properties of the media with regard to their base cell's geometrical parameters. The models proposed and the least square method, used to approximate an equation relating the effective properties of the media and the geometrical parameters, are presented;

- Chapter 6 shows the results of the developed work. Initially the results for the hollow sphere structures analysis are shown. Then, the results involving the optimization problems, the maximization of a linear combination of the components of the constitutive mechanical tensor and the obtainment of a target tensor are shown;
- Chapter 7 shows the conclusions of the work and the suggestions for future works.

2 HOMOGENIZATION

The effective properties of a heterogeneous material, with a regular or nearly regular micro structure, can be determined through the homogenization by asymptotic expansion method.

The urge of the use of a particular method to obtain the effective properties of this kind of media becomes clear when two approaches to determine the behaviour of the material are considered. The first one is the numerical approach. If a method such as the FEM is used to predict the behaviour of the media, it would be necessary an extremely refined mesh in order to represent the heterogeneities, rendering the problem very difficult or even impracticable due to the computational effort needed. The second one is to find the effective properties of the media through experimental tests. It is clear that this approach may become impractical due to the high number of experiments needed to be performed and the cost associated. The homogenization method is a way to overcome these issues and consists, basically, in replacing the heterogeneous material to an equivalent material model.

In a mathematical way, one can see the homogenization as a limit theory used to substitute differential equations with rapidly oscillating coefficients under the assumption of periodicity and using an asymptotic expansion, by differential equations with constant, or quasi constant coefficients.

The earliest studies on the homogenization field can be attributed to Sanchez-Palencia (1974), Larsen (1975) and Keller (1977). Studies regarding mathematical aspects and engineering applications were developed in parallel in the late seventies by several authors, as Benssousan, Lions and Papanicolau (1978), Ciaranescu and Paulin (1979), Sanchez-Palencia (1980). From then on, several authors refined the method, and contributions that are worth mentioning are the works of Léné and Leguillon (1982) and Guedes and Kikuchi (1990), that use the finite element method in order to solve the homogenization equations.

The effective properties of a porous material are dependent on the properties of the base material, the relative volume of material in regard to the whole domain, and the spatial distribution of material. In a composite, both base material properties and their adhesion also influence the effective properties. If the material is assumed as periodic or quasi-periodic, one can, under the assumption of linearity, use the well-established concept of representative volume element (RVE) analysis. In the RVE analysis, repre-

sentative sections of the material distribution are analysed under assumed boundary conditions to obtain the average or effective properties of the media (HOLLISTER; KIKUCHI, 1994). One of the RVE methods that can be used in order to account for more general problems, like the determination of properties of a mixture of anisotropic materials with complex geometries or porous materials, is the homogenization by asymptotic expansion.

The basic idea of the homogenization by asymptotic expansion, used in this work, is to obtain the macroscopic behaviour of a media formed by a periodic micro structure as a function of the micro scale, in other words, to predict the effective behaviour by an analysis only on the RVE of the material. It consists, basically, in solving an equilibrium problem to obtain the displacement, or temperature, field on the microscopic level, with which is possible to determine the effective homogenized elasticity tensor of the media. In the work of Hollister and Kikuchi (1992) it is shown that the effective properties of composites with a periodic structure, such as stiffness and local strain, are better approximated using the homogenization theory instead of the before mentioned approaches.

The development of the method follows three basic considerations (HOLLISTER; KIKUCHI, 1994). The first demands that the displacement field of the media can be written in an asymptotic expansion as

$$u^\epsilon(x, y) = u^0(x, y) + \epsilon u^1(x, y) + \epsilon^2 u^2(x, y) + \dots, \quad (2.1)$$

where x and y are the coordinates in the macroscopic and in the microscopic levels, respectively, u^ϵ is the total displacement field and u^0 , u^1 and u^2 are the contributions for the displacement of the macroscopic scale, microscopic scale, and eventual smaller scales, respectively. The second consideration is that the coordinates at each level are related by a small parameter, ϵ , in the form

$$y = \frac{x}{\epsilon}. \quad (2.2)$$

As the coordinates in the microscopic scale are smaller than their macroscopic relatives, the parameter ϵ should tend to zero. The last main consideration is that the displacements on the boundaries of the RVE are periodic, in other words, the value of the displacement are the same in opposite sides of the representative volume.

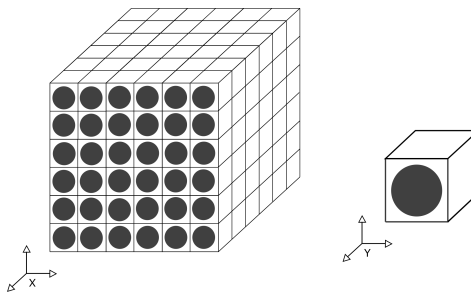
This chapter presents the basic definitions and the mathematical formulation concerning the homogenization method. At first the concepts of periodicity and asymptotic expansion are presented. Hereupon, the method is used in the context of linear elasticity, in order to obtain the

effective fourth order mechanical tensor of a periodic media. Like for the mechanical case, the method is also used to predict the effective thermal conductivity tensor of the material. Both analytical and numerical developments are shown. Finally, the algorithm, used to evaluate the mechanical and thermal effective properties of a porous media, developed in this work is explained.

2.1 ASYMPTOTIC EXPANSION AND PERIODICITY

Among all classes of materials, one can emphasize one which has a regular periodicity. This kind of material contains a regular and periodic structure, and it is represented by a base cell, or a representative volume element (RVE), the smallest structure on the domain in which one can find a pattern of repetition. Figure 8 shows an example of a periodic material in three dimensions where the microstructure is made of fibres embedded in a matrix.

Figure 8 – Periodic expansion of a base cell. x are the macroscopic coordinates and y are the microscopic coordinates



Source: Author's production, 2016, based on (SIGMUND, 1994)

Materials containing this kind of structure obey the relation

$$\mathcal{F}(x + NY) = \mathcal{F}(x), \quad (2.3)$$

where \mathcal{F} is a scalar, vectorial or even tensorial function, x contains the spacial coordinates in the macroscopic scale, N is a diagonal matrix, given by

$$N = \begin{bmatrix} n_1 & 0 & 0 \\ 0 & n_2 & 0 \\ 0 & 0 & n_3 \end{bmatrix}, \quad (2.4)$$

where n_1 , n_2 and n_3 are arbitrary integer numbers, which are responsible for the translation of the function analysed in the principal directions, and vector \mathbf{Y} represents the period of the base cell, that is to say, the size of the base cell. In \mathbb{R}^3 , \mathbf{Y} is a rectangular base cell, defined as

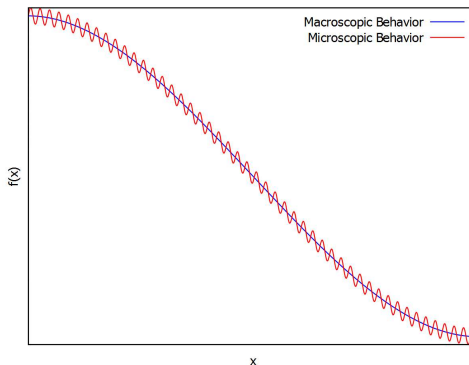
$$\mathbf{Y} = [0, y_1^0] \times [0, y_2^0] \times [0, y_3^0], \quad (2.5)$$

where y_1^0 , y_2^0 and y_3^0 are, respectively, the horizontal length, vertical length and depth of the RVE.

The period of repetition of the base cell, \mathbf{Y} , when compared with the dimension of the whole domain, is assumed to be very small. This consideration leads to the fact that, for these heterogeneous media, a characteristic function will rapidly vary in a small neighbourhood of a point of the domain. Therefore, it is defined an auxiliary position vector, on the microscopic scale, given by $\mathbf{y} = (y_1, y_2, y_3)$, which is responsible for the description of the rapid oscillations of the function. Conversely, the vector \mathbf{x} is responsible for the description of a slow variation, or the effective macroscopic behaviour of the function (HASSANI; HINTON, 1998a). The relation between the length of the vectors in the macroscopic and in the microscopic scales are given by equation 2.2.

Figure 9 shows the behaviour of a function which obeys the relation of the equation 2.3. The highly oscillating function represents the microscopic behaviour of the function, as the result of the variations on the micro structure, on the other hand, the non oscillating function represents the global, or macroscopic behaviour of the function.

Figure 9 – Micro and macroscopic behaviour of the function



Source: Author's production, 2016

The two scale asymptotic expansion method is classical in the field of mechanic vibrations, when a small perturbation modify a motion which should be otherwise periodic in time (SANCHEZ-PALENCIA, 1986). This approach can be used in regard to the homogenization method, in order to predict the effective properties of a media with a highly heterogeneous micro structure.

Let $\Phi^\epsilon(x)$ be a general function describing the behaviour of the problem being analysed. The relevant field variables can be approximated by an asymptotic expansion in two (or more) scales as

$$\Phi^\epsilon(x, y) = \Phi^0(x, y) + \epsilon\Phi^1(x, y) + \epsilon^2\Phi^2(x, y) + \dots, \quad (2.6)$$

where Φ^ϵ is the exact value of the field variable, Φ^0 is the macroscopic or average value of the field variable, Φ^1 and Φ^2 are the perturbations on the field variable due to the micro structure, x and y are the vectors of the coordinates into the macroscopic and microscopic scales, respectively and ϵ is the scalar who relates both scales. The functions Φ^1, Φ^2, \dots are periodic with regard to y and the period is Y . If a function Φ is periodic, its derivatives are also periodic with the same period and its integral, over the period, equals zero. Also, if the function Φ depends both on x and implicitly in y and y depends on x its derivatives can be written as

$$\frac{d\Phi}{dx_i} = \frac{\partial\Phi}{\partial x_i} + \frac{\partial\Phi}{\partial y_i} \frac{dy_i}{dx_i}, \quad (2.7)$$

and, as the both scales are related by the scalar ϵ , equation 2.7 becomes

$$\frac{d\Phi}{dx_i} = \frac{\partial\Phi}{\partial x_i} + \frac{1}{\epsilon} \frac{\partial\Phi}{\partial y_i}. \quad (2.8)$$

2.2 ELASTICITY PROBLEM

The characteristics of each type of materials relating the kinematics and the equilibrium considerations are called constitutive equations. For the elasticity problem, these laws relate one stress to one strain measure. The simplest case, used in this work, is the linear elastic behaviour.

The Hooke's generalized law is used to describe such behaviour. This law is the simplest model and establishes a relation between the strain and stress states. For a three dimensional case this relation is written as

$$\sigma_{ij} = C_{ijkl}\epsilon_{kl}, \quad (2.9)$$

where σ is the second order stress tensor, ε is the second order strain tensor and C is the fourth order elasticity tensor containing the elasticity constants of the material. The indexes i , j , k and l can assume values between 1 and 3. This model is able to describe isotropic, orthotropic and anisotropic materials within the elastic linear consideration.

Now, considering the symmetries

$$C_{ijkl} = C_{jikl} = C_{ijlk} = C_{jilk} \quad (2.10)$$

and

$$C_{ijkl} = C_{klji}, \quad (2.11)$$

the number of components needed to determine the constitutive law is 21. Consequently, the constitutive tensor can be written in the matrix form as

$$C = \begin{bmatrix} C_{1111} & C_{1122} & C_{1133} & C_{1112} & C_{1123} & C_{1113} \\ & C_{2222} & C_{2233} & C_{2212} & C_{2223} & C_{2213} \\ & & C_{3333} & C_{3312} & C_{3323} & C_{3313} \\ & & & C_{1212} & C_{1223} & C_{1213} \\ & & & & C_{2323} & C_{2313} \\ & & & & & C_{1313} \end{bmatrix}. \quad (2.12)$$

For an unidimensional case, the Hooke's law becomes

$$\sigma = E\varepsilon, \quad (2.13)$$

where E is the Young's modulus of the material.

The Hooke's Law is valid in each point of the domain and for homogeneous materials, the fourth order elasticity tensor is constant in the domain. For the case of non homogeneous materials with a micro structure, its properties vary rapidly in the micro scale. In this case, the homogenization method can be used in order to determine equivalent properties, valid in the whole macroscopic domain, whose tensor can be used for an analysis into the macro scale. This tensor is called Homogenized tensor and is designated by C^H . This tensor represents an equivalent homogeneous tensor, used to approximate the heterogeneous behaviour of the media.

As a way of enlightenment, appendix A shows the evaluation of the effective mechanical properties using the homogenization by asymptotic expansion method for an unidimensional case.

2.2.1 General Elasticity Problem

This section aims to show a summary of the homogenization method applied to the determination of the mechanical properties of a three dimensional media.

The method is based on a two-scale asymptotic expansion of the properties of a highly heterogeneous media with a periodic, or quasi-periodic microstructure. For a highly heterogeneous media, its properties may vary within a small neighbourhood of a given point, hence, two scales, one in the macroscopic level and another in the microscopic level, are considered for this development. Also, it is used the concept of RVE, with the consideration that the dimension of the unit cell tends to zero and that there is a small parameter, ϵ , relating both macroscopic and microscopic scales.

The displacement field \mathbf{u} , function of both macroscopic and microscopic scales, is written as

$$\mathbf{u}^\epsilon(\mathbf{x}) = \mathbf{u}(\mathbf{x}, \mathbf{y}), \quad (2.14)$$

where the index ϵ refers to the dependency of the displacement field in the micro scale, and it can be written using an asymptotic expansion. In this case, it is used an expansion in two scales,

$$\mathbf{u}^\epsilon(\mathbf{x}, \mathbf{y}) = \mathbf{u}^0(\mathbf{x}) + \epsilon \mathbf{u}^1(\mathbf{x}, \mathbf{y}) + \epsilon^2 \mathbf{u}^2(\mathbf{x}, \mathbf{y}) + \mathcal{O}(n), \quad (2.15)$$

where the indexes 0 and 1 refer, respectively, to the contributions of the macro scale and of the micro scale and $\mathcal{O}(n)$ refers to higher order terms. The linear stress-strain and the infinitesimal strain-displacement relations are given, respectively, by

$$\sigma_{ij}^\epsilon = C_{ijkl}^\epsilon \epsilon_{kl}^\epsilon \quad (2.16)$$

and

$$\epsilon_{kl}^\epsilon = \frac{1}{2} \left(\frac{\partial u_k^\epsilon}{\partial x_l} + \frac{\partial u_l^\epsilon}{\partial x_k} \right), \quad (2.17)$$

where σ_{ij}^ϵ , ϵ_{kl}^ϵ and C_{ijkl}^ϵ are, respectively, the stress, strain and elasticity tensor within the solid domain, Ω_ϵ .

Applying the principle of virtual displacements for linear elasticity, one gets

$$\begin{aligned} \int_{\Omega^\epsilon} C_{ijkl} \frac{\partial u_k^\epsilon}{\partial x_l} \frac{\partial v_i}{\partial x_j} d\Omega &= \int_{\Omega^\epsilon} f_i^\epsilon v_i d\Omega + \int_{\Gamma_t} t_i v_i d\Gamma \\ &+ \int_{S^\epsilon} p_i^\epsilon v_i dS, \\ \forall \mathbf{v} \in \mathbf{V}^\epsilon, \end{aligned} \quad (2.18)$$

where C_{ijkl} is the fourth order elasticity tensor, \mathbf{f} is the body force vector, \mathbf{t} is the vector of tractions on the boundaries Γ_t , \mathbf{p} is the vector of tractions inside the holes, \mathbf{v} is the virtual displacement vector, Ω is the domain, S is the boundary of the cell and \mathbf{V}^ϵ is the set of kinematically admissible displacements. The dependency of the quantities on the inhomogeneity is indicated by the index ϵ .

Using the two scale expansion, equation 2.15, and the derivatives for a function dependent on both scales, equation 2.8, one can expand the principle of virtual displacements, equation 2.18, in terms of the small parameter ϵ .

As the virtual displacement is an arbitrary function, one can choose it only as a function of the microscopic scale,

$$\mathbf{v} = \mathbf{v}(\mathbf{y}). \quad (2.19)$$

By doing so it can be shown that

$$\mathbf{u}^0 = \mathbf{x}^0(\mathbf{x}), \quad (2.20)$$

that is, the first term of the asymptotic expansion depends only on the macroscopic scale \mathbf{x} (HASSANI; HINTON, 1998a).

Alternatively, if the virtual displacement is arbitrarily chosen as a function only of the macroscale,

$$\mathbf{v} = \mathbf{v}(\mathbf{x}) \quad (2.21)$$

and considering only the first order terms, in which \mathbf{u}^0 and \mathbf{u}^1 represents, respectively, the macroscopic and the microscopic behaviour, it is possible to find the homogenized elasticity tensor such that the virtual displacement equation can be constructed into the macroscopic system of reference, without explicitly using the parameter ϵ (HASSANI; HINTON, 1998a).

The development of the method is well established in the literature, and as found in Sanchez-Palencia (1986), Hassani and Hinton

(1998a), Guedes and Kikuchi (1990) and Muñoz-Rojas, Carniel and Öchsner (2011), the general elasticity problem can be summarized as:

1. Find χ and Ψ , which represent the displacement field at the microscopic level, using the equations

$$\int_{\mathbb{Y}} C_{ijpq} \frac{\partial \chi_p^{kl}}{\partial y_q} \frac{\partial v_i}{\partial y_j} dY = \int_Y C_{ijkl} \frac{\partial v_i}{\partial y_j} dY \quad (2.22)$$

and

$$\int_{\mathbb{Y}} C_{ijpq} \frac{\partial \Psi_k}{\partial y_q} \frac{\partial v_i}{\partial y_j} dY = \int_S p_i v_i dY, \quad (2.23)$$

where \mathbb{Y} represents the solid portion of the base cell, C is the fourth order elasticity tensor of the base material, Y is the vector with the dimensions of the base, y is the position vector on the micro scale, p is the traction vector on the boundary, v is a virtual displacement field and S is the boundary of the cell.

2. Find C_{ijkl}^H , τ_{ij} and b_i by using

$$C_{ijkl}^H(x) = \frac{1}{|Y|} \int_{\mathbb{Y}} \left(C_{ijkl} - C_{ijpq} \frac{\partial \chi_p^{kl}}{\partial y_q} \right) dY, \quad (2.24)$$

$$\tau_{ij}(x) = \frac{1}{|Y|} \int_{\mathbb{Y}} C_{ijkl} \frac{\partial \Psi_k}{\partial y_l} dY \quad (2.25)$$

and

$$b_i(x) = \frac{1}{|Y|} \int_{\mathbb{Y}} f_i dY, \quad (2.26)$$

where C^H is the homogenized fourth order elasticity tensor, x is the position vector in the macroscopic scale, b is the average body force vector and τ is the residual stress tensor.

With the homogenized tensor it is possible to solve the macroscopic equilibrium problem, set as

$$\begin{aligned} \int_{\Omega} C_{ijkl}^H \frac{\partial u_k^0(x)}{\partial x_l} \frac{\partial v_i(x)}{\partial x_j} d\Omega &= \int_{\Omega} \tau_{ij}(x) \frac{\partial v_i(x)}{\partial x_j} d\Omega + \int_{\Omega} b_i(x) v_i(x) d\Omega \\ &+ \int_{\Gamma_t} t_i v_i(x) d\Gamma, \end{aligned} \quad (2.27)$$

where Ω is the global domain, \mathbf{u}^0 is the displacement field in the macro scale, \mathbf{t} are the tractions on the boundaries and Γ is the boundary. It is interesting to notice that the macroscopic and microscopic problems are not coupled, so, the global equilibrium is not a function of the micro scale.

The displacement field, χ^{kl} , is the periodic solution of the equation 2.22 and it is used in the equation 2.24 to find the elastic constants of the effective tensor, 21 for the general three-dimensional case. For this case, the indexes i, j, p, q, k and l can assume values between 1 and 3 and, in order to obtain all the elastic constants, the so called "load cases" $kl = 11, kl = 22, kl = 33, kl = 12, kl = 23$ and $kl = 13$ must be solved. There are several ways to solve the integral equations of the homogenization method. In this work, the base cell is discretized using the finite element method.

2.2.2 Numerical Solution

In a general way, the determination of the homogenized coefficients can be achieved in the sequence shown in the previous section. If the body forces are not considered, the elastic constants can be obtained by solving the equilibrium problem into the microscopic scale, equation 2.22, and then solving the equation 2.24 in order to evaluate all the elastic constants of the media. In this work, the finite element method based on Fang, Sun and Tzeng (2004) and Hassani and Hinton (1998b), is used to evaluate these equations.

For sake of simplicity, it is adopted that

$$\mathbf{C} = [c_{11} \quad c_{22} \quad c_{33} \quad c_{12} \quad c_{23} \quad c_{13}], \quad (2.28)$$

where c_{kl} are the columns of the constitutive fourth order tensor of the base material,

$$\frac{\partial \chi_p^{kl}}{\partial y_q} = \boldsymbol{\epsilon}(\chi^{kl}) \quad (2.29)$$

and

$$\frac{\partial \nu_i(y)}{\partial y_j} = \boldsymbol{\epsilon}(\nu). \quad (2.30)$$

Overall, the equation 2.22 can be written as

$$\int_Y \boldsymbol{\epsilon}^T(\nu) C_{ijkl} \boldsymbol{\epsilon}(\chi^{kl}) dY = \int_Y \boldsymbol{\epsilon}^T(\nu) c_{kl} dY. \quad (2.31)$$

If the domain is divided into a finite number of elements, in order to use a finite element formulation, the virtual displacements, \boldsymbol{v} , and the characteristic displacements of the unitary cell, χ^{kl} , can be written using the concept of shape functions as

$$\boldsymbol{v} = \sum_{i=1}^N N_i^g \hat{\boldsymbol{v}}_i = \mathbf{N}^g \hat{\boldsymbol{v}} \quad (2.32)$$

and

$$\chi^{kl} = \sum_{i=1}^N N_i^g \hat{\chi}_i^{kl} = \mathbf{N}^g \hat{\chi}^{kl} \quad (2.33)$$

where $\hat{\boldsymbol{v}}$ is the nodal virtual displacement vector, with

$$\hat{\boldsymbol{v}} = \{\hat{v}_1 \quad \dots \quad \hat{v}_i\}^T, \quad i = 1, \dots, N, \quad (2.34)$$

$\hat{\chi}_i^{kl}$ is the nodal displacement relative to the load case kl , with

$$\hat{\chi}^{kl} = \{\hat{\chi}_1^{kl} \quad \dots \quad \hat{\chi}_i^{kl}\}^T, \quad i = 1, \dots, N, \quad (2.35)$$

and

$$N_i^g = \begin{bmatrix} 1 & 0 & 0 \\ 0 & 1 & 0 \\ 0 & 0 & 1 \end{bmatrix} N_i^g, \quad (2.36)$$

where N_i^g is the global shape function associated with the node i and the element type and N is the total number of nodes in the discrete domain. For the general three dimensional case,

$$\boldsymbol{\chi} = \begin{Bmatrix} \chi_1 \\ \chi_2 \\ \chi_3 \end{Bmatrix} \quad (2.37)$$

represents the displacements of a point within an element and

$$\hat{\boldsymbol{\chi}}_i = \begin{Bmatrix} \hat{\chi}_{i1} \\ \hat{\chi}_{i2} \\ \hat{\chi}_{i3} \end{Bmatrix} \quad (2.38)$$

represents the displacement of a node i .

Taking the differential linear operator, defined by,

$$\mathbf{L} = \begin{bmatrix} \frac{\partial}{\partial y_1} & 0 & 0 \\ 0 & \frac{\partial}{\partial y_2} & 0 \\ 0 & 0 & \frac{\partial}{\partial y_3} \\ \frac{\partial}{\partial y_2} & \frac{\partial}{\partial y_1} & 0 \\ 0 & \frac{\partial}{\partial y_3} & \frac{\partial}{\partial y_2} \\ \frac{\partial}{\partial y_3} & 0 & \frac{\partial}{\partial y_1} \end{bmatrix}, \quad (2.39)$$

one can obtain the associated global strain matrix, given by

$$\mathbf{B} = \mathbf{L}\mathbf{N}^g, \quad (2.40)$$

and one can write

$$\boldsymbol{\epsilon}(v) = \mathbf{L}\mathbf{v} = \mathbf{L}\mathbf{N}^g\hat{\mathbf{v}} = \mathbf{B}\hat{\mathbf{v}} \quad (2.41)$$

and

$$\boldsymbol{\epsilon}(\chi^{kl}) = \mathbf{L}\chi^{kl} = \mathbf{L}\mathbf{N}^g\hat{\chi}^{kl} = \mathbf{B}\hat{\chi}^{kl}. \quad (2.42)$$

Using equations 2.42 and 2.41, the equation 2.31 can be written as

$$\hat{\mathbf{v}}^T \int_Y \mathbf{B}^T \mathbf{C} \mathbf{B} dY \hat{\chi}^{kl} = \hat{\mathbf{v}}^T \int_Y \mathbf{B}^T \mathbf{c}_{kl} dY. \quad (2.43)$$

As $\hat{\mathbf{v}}$ represents a nodal virtual displacement, it can be eliminated from both sides of the above equation, yielding

$$\int_Y \mathbf{B}^T \mathbf{C} \mathbf{B} dY \hat{\chi}^{kl} = \int_Y \mathbf{B}^T \mathbf{c}_{kl} dY. \quad (2.44)$$

Equation 2.44 is very similar to a standard finite element stiffness equation, and can be written as

$$\mathbf{K} \hat{\chi}^{kl} = \mathbf{f}_{kl}, \quad (2.45)$$

where \mathbf{K} is the global stiffness matrix, $\hat{\chi}^{kl}$ is the characteristic displacement field of the base cell and \mathbf{f}_{kl} represents a load vector, which induces an unitary strain in the kl case analysed. Thus, in order to obtain all elastic constants, equation 2.45 must be solved for the six distinct "load cases".

For a single element, the local stiffness matrix is given by

$$\mathbf{K}^e = \int_Y \mathbf{B}^{eT} \mathbf{C} \mathbf{B}^e dY, \quad (2.46)$$

where \mathbf{B} is the strain-displacement matrix, \mathbf{C} is the constitutive elasticity matrix of the element, and the load vector is given by

$$\mathbf{f}_{kl}^e = \int_Y \mathbf{B}^{eT} \mathbf{c}_{kl} dY, \quad (2.47)$$

where \mathbf{c}_{kl} is the column of the constitutive matrix relative to the load case kl analysed. For one element, e , and for a single node, i , the strain-displacement matrix is given by

$$\mathbf{B}_i^e = \begin{bmatrix} \frac{\partial N_i^e}{\partial y_1} & 0 & 0 \\ 0 & \frac{\partial N_i^e}{\partial y_2} & 0 \\ 0 & 0 & \frac{\partial N_i^e}{\partial y_3} \\ \frac{\partial N_i^e}{\partial y_2} & \frac{\partial N_i^e}{\partial y_1} & 0 \\ 0 & \frac{\partial N_i^e}{\partial y_3} & \frac{\partial N_i^e}{\partial y_2} \\ \frac{\partial N_i^e}{\partial y_3} & 0 & \frac{\partial N_i^e}{\partial y_1} \end{bmatrix}, \quad (2.48)$$

where N_i^e is the shape function of the i -th node of the e -th element. For the whole element, one can write

$$\mathbf{B} = [\mathbf{B}_1^e \quad \mathbf{B}_2^e \quad \dots \quad \mathbf{B}_n^e], \quad (2.49)$$

where n is the total number of nodes of the element. The assembly of the global stiffness matrix and the global load vector is usual and is given, respectively by

$$\mathbf{K} = \bigcup_{e=1}^m \mathbf{K}^e \quad (2.50)$$

and

$$\mathbf{f}_{kl} = \bigcup_{e=1}^m \mathbf{f}_{kl}^e, \quad (2.51)$$

where m is the total number of elements of the mesh and \bigcup is the assembly operator (BATHÉ, 2009). With all the definitions above it is possible to obtain the characteristic displacement field of the base cell, χ , using the equation 2.45.

With an analogous procedure, equation 2.24 can be written as

$$C_{ijkl}^H = \frac{1}{|Y|} \int_Y (C_{ijkl} - C_{ij}^T \epsilon(\chi^{kl})) dY, \quad (2.52)$$

and using the operator of equation 2.42, it becomes

$$C_{ijkl}^H = \frac{1}{|Y|} \int_Y \left(C_{ijkl} - c_{ij}^T B \hat{\chi}^{kl} \right) dY. \quad (2.53)$$

The equilibrium problem of the equation 2.45 must be solved for six load cases. Then, the characteristic displacement fields are used in equation 2.53 in order to obtain the 21 components of the homogenized elasticity tensor.

2.2.3 Physical Interpretation of the Load Cases

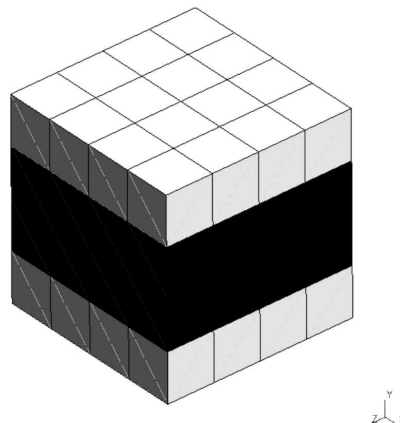
It is interesting to notice that the body force vector used for the determination of the homogenized coefficients has a physical interpretation, which is an initial prescribed strain load case. For the demonstration, it is used the nodal force vector of the element e induced by an initial strain, given by

$$(f^{\varepsilon^0})^e = \int_{Y^e} B^{eT} C \varepsilon^0 dY, \quad (2.54)$$

where ε^0 is the initial strain tensor (ZIENKIEWICZ; TAYLOR, 2000).

A simple base cell is used in order to make the visualization of the force vector induced by the load case kl easier. An unitary domain, discretized by $4 \times 4 \times 4$ elements is used, and a reinforcement in the x and z directions, as shown in figure 10, is used to evaluate these force vectors.

Figure 10 – Adopted topology



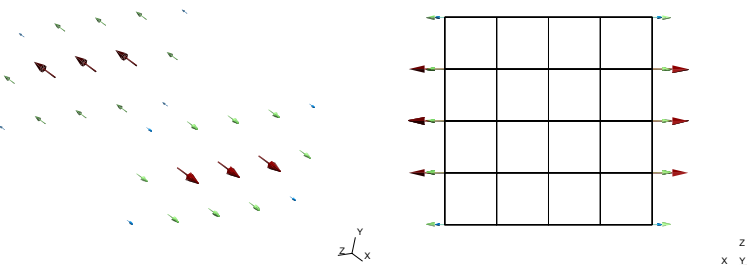
Source: Author's production, 2016.

For the load case 1, in which the indexes assume the values $k = 1$ and $l = 1$, the force vector obtained through the homogenization method is given by

$$\mathbf{f}_{11}^e = \int_{Y^e} \mathbf{B}^{eT} \mathbf{c}_{11} dY, \quad (2.55)$$

and the distribution of forces in the base cell is shown in figure 11.

Figure 11 – Load case 1



Source: Author's production, 2016.

Comparing equations 2.54 and 2.55, it is possible to verify that

$$C\boldsymbol{\varepsilon}^0 = \mathbf{c}_1, \quad (2.56)$$

or

$$\begin{bmatrix} C_{1111} & C_{1122} & C_{1133} & 0 & 0 & 0 \\ C_{1122} & C_{2222} & C_{2233} & 0 & 0 & 0 \\ C_{1133} & C_{2233} & C_{3333} & 0 & 0 & 0 \\ 0 & 0 & 0 & C_{1212} & 0 & 0 \\ 0 & 0 & 0 & 0 & C_{2323} & 0 \\ 0 & 0 & 0 & 0 & 0 & C_{3131} \end{bmatrix} \begin{Bmatrix} \epsilon_{11}^0 \\ \epsilon_{22}^0 \\ \epsilon_{33}^0 \\ 2\epsilon_{12}^0 \\ 2\epsilon_{23}^0 \\ 2\epsilon_{13}^0 \end{Bmatrix} = \begin{Bmatrix} C_{1111} \\ C_{1122} \\ C_{1133} \\ 0 \\ 0 \\ 0 \end{Bmatrix},$$

which implies in

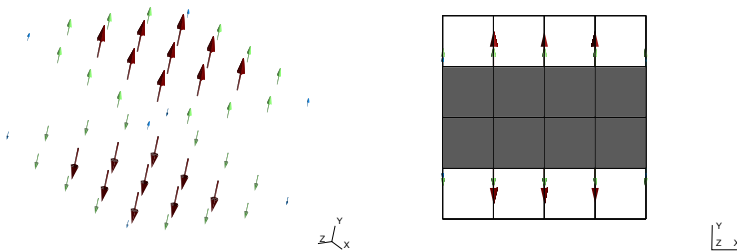
$$\begin{aligned} \epsilon_{11}^0 &= 1 & \epsilon_{22}^0 &= 0 & \epsilon_{33}^0 &= 0 \\ \epsilon_{12}^0 &= 0 & \epsilon_{23}^0 &= 0 & \epsilon_{13}^0 &= 0 \end{aligned}$$

For the load case 2 the indexes assume the values $k = 2$ and $l = 2$ and the homogenized force vector is

$$\mathbf{f}_{22}^e = \int_{Y^e} \mathbf{B}^{eT} \mathbf{c}_{22} dY, \quad (2.57)$$

generating a force distribution in the base cell shown in figure 12.

Figure 12 – Load case 2



Source: Author's production, 2016.

Comparing equations 2.54 and 2.57, the strain induced in each element of the base cell is given by

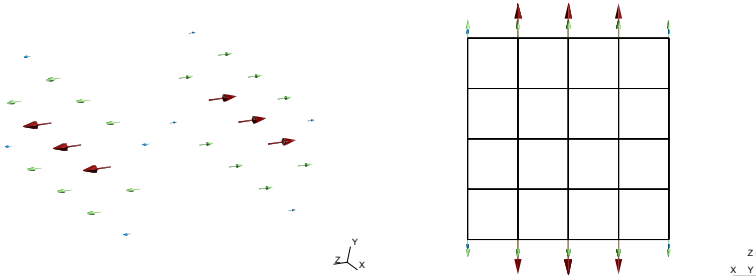
$$\begin{aligned} \epsilon_{11}^0 &= 0 & \epsilon_{22}^0 &= 1 & \epsilon_{33}^0 &= 0 \\ \epsilon_{12}^0 &= 0 & \epsilon_{23}^0 &= 0 & \epsilon_{13}^0 &= 0 \end{aligned}$$

For the third load case the indexes assume the values $k = 3$ and $l = 3$, and the homogenization force vector is given by

$$\mathbf{f}_{33}^e = \int_{Y^e} \mathbf{B}^{eT} \mathbf{c}_{33} dY \quad (2.58)$$

and it is shown in figure 13.

Figure 13 – Load case 3



Source: Author's production, 2016.

Again, with the comparison of equations 2.54 and 2.58 one can obtain the strain induced in each element of the mesh, given by

$$\begin{aligned} \varepsilon_{11}^0 &= 0 & \varepsilon_{22}^0 &= 0 & \varepsilon_{33}^0 &= 1 \\ \varepsilon_{12}^0 &= 0 & \varepsilon_{23}^0 &= 0 & \varepsilon_{13}^0 &= 0 \end{aligned}$$

The same procedure is adopted for the fourth, fifth and sixth load cases, in which the indexes assume, respectively, $k = 1$ and $l = 2$, $k = 2$ and $l = 3$ and $k = 1$ and $l = 3$. The homogenized force vectors are given, respectively, by

$$\mathbf{f}_{12}^e = \int_{Y^e} \mathbf{B}^{eT} \mathbf{c}_{12} dY, \quad (2.59)$$

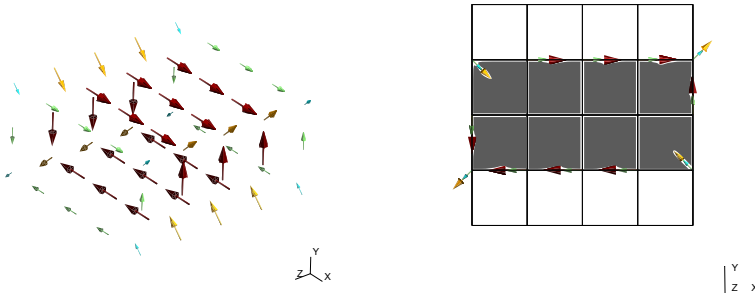
$$\mathbf{f}_{23}^e = \int_{Y^e} \mathbf{B}^{eT} \mathbf{c}_{23} dY \quad (2.60)$$

and

$$f_{13}^e = \int_{Y^e} \mathbf{B}^{eT} c_{13} dY, \quad (2.61)$$

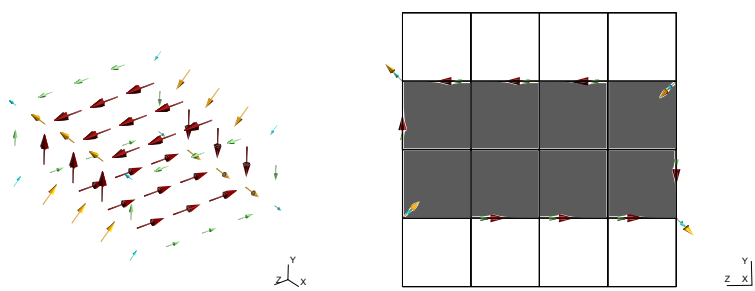
inducing the distribution of forces shown in figures 14, 15 and 16, respectively.

Figure 14 – Load case 4



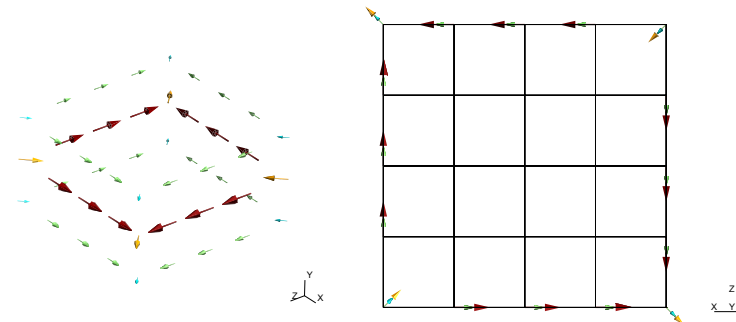
Source: Author's production, 2016.

Figure 15 – Load case 5



Source: Author's production, 2016.

Figure 16 – Load case 6



Source: Author's production, 2016.

Comparing the force vector induced by an initial strain, equation 2.54, and the equations 2.59, 2.60 and 2.61, obtained with the homogenization procedure, one obtains the strain induced in each element of the base cell for the three cases mentioned, respectively given by

$$\begin{aligned}\epsilon_{11}^0 &= 0 & \epsilon_{22}^0 &= 0 & \epsilon_{33}^0 &= 0 \\ 2\epsilon_{12}^0 &= 1 & \epsilon_{23}^0 &= 0 & \epsilon_{13}^0 &= 0'\end{aligned}$$

$$\begin{aligned}\epsilon_{11}^0 &= 0 & \epsilon_{22}^0 &= 0 & \epsilon_{33}^0 &= 0 \\ \epsilon_{12}^0 &= 0 & 2\epsilon_{23}^0 &= 1 & \epsilon_{13}^0 &= 0\end{aligned}$$

and

$$\begin{aligned}\epsilon_{11}^0 &= 0 & \epsilon_{22}^0 &= 0 & \epsilon_{33}^0 &= 0 \\ \epsilon_{12}^0 &= 0 & \epsilon_{23}^0 &= 0 & 2\epsilon_{13}^0 &= 1.\end{aligned}$$

With the development shown above, it can be seen that each load case $k l$ induces an unitary strain in the direction related to these indexes.

2.3 THERMAL PROBLEM

The thermal conductivity in a material can be find through the Fourier Law, given by

$$q = -Kt \nabla T, \quad (2.62)$$

where \mathbf{q} is the heat flux, \mathbf{Kt} is the material's thermal conductivity tensor and ∇T is the temperature gradient. In a matrix form, the Fourier law can be written as

$$\begin{Bmatrix} q_{X_1} \\ q_{X_2} \\ q_{X_3} \end{Bmatrix} = - \begin{bmatrix} Kt_{11} & Kt_{12} & Kt_{13} \\ Kt_{12} & Kt_{22} & Kt_{23} \\ Kt_{13} & Kt_{23} & Kt_{33} \end{bmatrix} \begin{Bmatrix} \frac{dT}{dX_1} \\ \frac{dT}{dX_2} \\ \frac{dT}{dX_3} \end{Bmatrix}. \quad (2.63)$$

As for the elasticity problem, the above equations are valid point to point in the domain. For linear homogeneous materials the conductivity tensor is constant in all the domain. For non homogeneous materials, this tensor vary in the microstructure, and the homogenization method can be used in order to obtain an equivalent homogenized conductivity tensor, designated by \mathbf{Kt}^H that can be used to an analysis in the macro scale.

2.3.1 General Thermal Conductivity Problem

In parallel to the previous section, this one aims to show the basic equations of the homogenization method, when applied to the thermal properties of a three dimensional media. It is assumed that the thermal conductivity tensor, \mathbf{Kt} is an \mathbf{Y} -periodic function, so

$$\mathbf{Kt}(\mathbf{x}) = \mathbf{Kt}(\mathbf{x}, \mathbf{y}) = \mathbf{Kt}(\mathbf{x}, \mathbf{y} + \mathbf{Y}) \quad (2.64)$$

with

$$\mathbf{y} = \frac{\mathbf{x}}{\epsilon}, \quad \epsilon > 0, \quad (2.65)$$

where \mathbf{x} and \mathbf{y} are, respectively, the position vector at the macroscopic and microscopic coordinates and ϵ is a small scalar. The temperature field inside of each unit cell, T , is expanded asymptotically, which yields

$$T^\epsilon = T(\mathbf{x}, \mathbf{y}) = T_0(\mathbf{x}) + \epsilon T_1(\mathbf{x}, \mathbf{y}), \quad (2.66)$$

in which only the first order terms are considered and where, such as for the elasticity problem, the index ϵ refers to the dependency of the variable with the micro structure of the media, and the indexes 0 and 1 refers to the contributions of macro and micro scales, respectively. Also, it is considered that T_1 is periodic, with period \mathbf{Y} , in the micro scale. Having in mind that T depends both on macro and micro scales and that they are related by the scalar ϵ , using the expression for the derivatives, equation 2.7, one can write the temperature gradient as

$$\nabla_x T = \nabla_x T_0(\mathbf{x}) + \epsilon \nabla_x T_1(\mathbf{x}, \mathbf{y}) + \nabla_y T_1(\mathbf{x}, \mathbf{y}). \quad (2.67)$$

In a detailed analysis, Muñoz-Rojas, Carniel and Öchsner (2011) and Muñoz-Rojas et al. (2008) show that the effective properties of the media can be obtained by finding an admissible temperature field at the microscopic level, \mathbf{R} , which satisfies

$$\frac{1}{|Y|} \int_Y [\mathbf{I} - \nabla_y \mathbf{R}(x, y)]^T \mathbf{Kt}(x, y) [\nabla_y \delta T_1(x, y)] dY = 0, \quad (2.68)$$

leading to the homogenized conductivity thermal tensor, given by

$$\mathbf{Kt}^H = \frac{1}{|Y|} \int_Y \mathbf{Kt}(x, y) [\mathbf{I} - \nabla_y \mathbf{R}(x, y)] dY, \quad (2.69)$$

or, in the index form,

$$Kt_{ij}^H = \frac{1}{|Y|} \int_Y \left(Kt_{ij} - Kt_{ip} \frac{\partial R^j}{\partial y_p} \right) dY. \quad (2.70)$$

The temperature field, \mathbf{R}^j is the periodic solution of equation 2.68 and it is used in equation 2.70 in order to obtain all the thermal conductivity constants for the effective tensor. For this case, the indexes i , j and p assume values between 1 and 3. To obtain all the constants, it is sufficient to solve the equations for three "flux cases", represented by the index j . So, the flux cases $j = 1$, $j = 2$ and $j = 3$ must be solved. As for the mechanical case, this flux cases have a physical meaning, a induced unitary temperature gradient in j direction.

2.3.2 Numerical Solution

The procedure of determination of the homogenized coefficients is similar to the procedure presented for the mechanical coefficients. The equation 2.68 can be written as

$$Ct \mathbf{R}^j = \mathbf{Q}_j, \quad (2.71)$$

where Ct is the global conductivity matrix, \mathbf{R}^j is the characteristic temperature field of the unitary cell referent to the flux vector \mathbf{Q}_j , which induces an unitary thermal gradient in j direction.

All coefficients can be obtained by solving the system of equation 2.71 for three distinct "flux cases", $j = 1$, $j = 2$, $j = 3$, inducing an unitary thermal gradient in each principal direction. For a single element, the conductivity matrix can be written as

$$Ct^e = \int_Y \mathbf{B}^{eT} \mathbf{Kt} \mathbf{B}^e dY, \quad (2.72)$$

where \mathbf{B} is the matrix containing the derivatives of the shape functions of the element, \mathbf{Y} is the domain, \mathbf{Kt} is the thermal conductivity matrix of the element. Similarly, the flux vector can be written as

$$\mathbf{Q}_j^e = \int_Y \mathbf{B}^{eT} \mathbf{Kt}^j d\mathbf{Y}, \quad (2.73)$$

where \mathbf{Kt}^j is the column of the conductivity matrix related to the "flux case" j . For one element, e , and for a single node, i , the matrix \mathbf{B} is given by

$$\mathbf{B}_i^e = \begin{bmatrix} \frac{\partial N_i^e}{\partial y_1} \\ \frac{\partial N_i^e}{\partial y_2} \\ \frac{\partial N_i^e}{\partial y_3} \end{bmatrix}, \quad (2.74)$$

where N_i^e is the shape function of the i -th node of the e -th element. For the whole element, one can write

$$\mathbf{B}^e = [\mathbf{B}_1^e \quad \mathbf{B}_2^e \quad \dots \quad \mathbf{B}_n^e], \quad (2.75)$$

where n is the total number of nodes of the element. As for the elastic case, the global thermal conductivity matrix and the global flux vector can be obtained in the usual way, and are given, respectively, by

$$\mathbf{Ct} = \biguplus_{e=1}^m \mathbf{Ct}^e \quad (2.76)$$

and

$$\mathbf{Q} = \biguplus_{e=1}^m \mathbf{Q}^e, \quad (2.77)$$

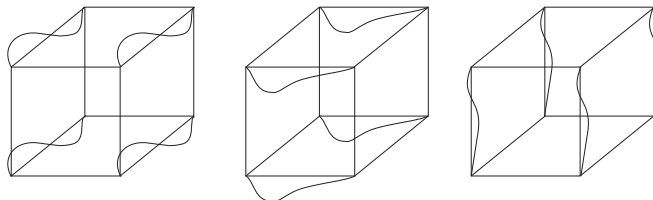
where m is the total number of elements of the mesh. With the procedure above is possible to obtain the characteristic temperature field given in equation 2.71 and all homogenized components of the thermal tensor can be obtained by equation 2.70 if the linear system are solved for three "flux cases".

2.4 PERIODIC BOUNDARY CONDITIONS

As shown in previous sections, it is possible to evaluate all the elastic constants of the media by solving the equilibrium problem of equation 2.45 and all conductivity thermal properties through the equilibrium

problem of equation 2.71. These linear systems are boundary value problems and must be solved, after an appropriate discretization, on the RVE domain. This kind of problem needs essential boundary conditions in order to be solved, and on a homogenization procedure the problems must respect the periodicity considerations, which introduces a kinematic constraint on the RVE. This imposed periodicity constraint enforces that the displacement field, for the mechanical case, and the temperature field, for the thermal conductivity case, have the same values on opposite faces of the RVE. Figure 17 shows a representation of the periodic considerations, in which the opposite borders have same shapes. Also, this consideration reflects the consideration of repeatability of the RVE through the entire macroscopic domain.

Figure 17 – Periodicity consideration



Source: Author's production, 2016

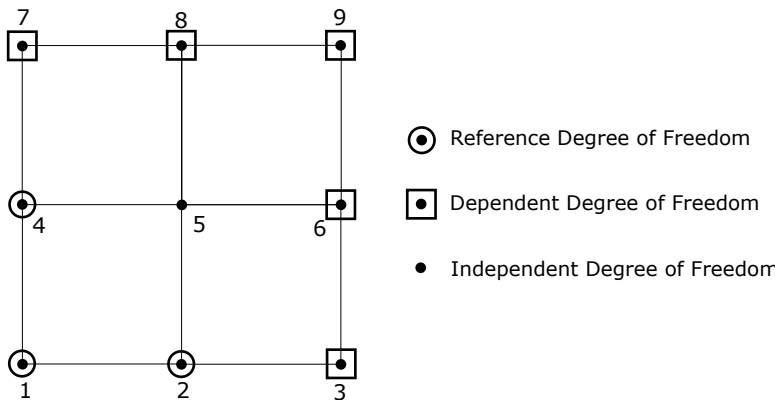
There are several methods that can be used to ensure the periodicity constraints. In this work, the condensation method, presented by Yang and Becker (2004), is used. At first, it is considered that at least one of the vertices of the domain is constrained. The periodicity constraints are obtained by the use of a transformation matrix, T , that relates all the degrees of freedom of the system to the constrained degrees of freedom. For instance, in three dimensional RVE, identical displacements or temperatures must be specified for corresponding nodes on opposite faces. That is, the RVE has the same deformed shapes on opposite faces and the same is valid for the temperature field.

The transformation matrix T has in its rows all the degrees of freedom of the system and in its columns all the reference degrees of freedom, in other words, the degrees of freedom that has a compatibility with another degree of freedom are not included in the columns of the transformation matrix. The matrix is composed only by zeros and ones. If the element on position ij of the transformation matrix is zero, it means that the degree of freedom i have no compatibility with the degree of

freedom j . On the other hand, if this position is an one, both degrees of freedom have a compatibility, that is, these degrees of freedom are in opposite faces of the RVE and must have the same displacement, or temperature.

As a way of enlightenment, the bi dimensional case of figure 18 is considered. For this example, each node of the mesh has a scalar property associated. The degrees of freedom 1, 2 and 4 are the references. The degree of freedom 5 is independent, that is, it has no compatibility nodes. The degrees of freedom 3, 6, 7, 8 and 9 are dependent on the reference degrees of freedom. Yet, the periodicity consideration requires that the nodes 3, 7 and 9 have the same property of the node 1. Also, the node 6 has the same property of the node 4 and the node 8 has the same property of the node 2.

Figure 18 – Example for periodicity consideration



Source: Author's production, 2016

For this simple case, the transformation from the original system to the reduced one can be written as

$$[1 \ 2 \ 3 \ 4 \ 5 \ 6 \ 7 \ 8 \ 9]^T = T \begin{Bmatrix} 1 \\ 2 \\ 4 \\ 5 \end{Bmatrix}, \quad (2.78)$$

and the transformation matrix can be written as

$$\mathbf{T} = \begin{bmatrix} 1 & 0 & 0 & 0 \\ 0 & 1 & 0 & 0 \\ 1 & 0 & 0 & 0 \\ 0 & 0 & 1 & 0 \\ 0 & 0 & 0 & 1 \\ 0 & 0 & 1 & 0 \\ 1 & 0 & 0 & 0 \\ 0 & 1 & 0 & 0 \\ 1 & 0 & 0 & 0 \end{bmatrix}. \quad (2.79)$$

This transformation ensures the periodicity consideration in the opposite faces of the RVE. Now, if a vectorial property is considered, then the degrees of freedom in the same directions on compatible nodes are periodic.

Let $\tilde{\chi}$ be the reduced characteristic displacement field of the RVE. The original displacement field, χ is related to $\tilde{\chi}$ by

$$\chi = \mathbf{T}_m \tilde{\chi} \quad (2.80)$$

where \mathbf{T}_m is the transformation matrix for the mechanical case. Therefore, the global system of equation 2.45 becomes

$$\tilde{\mathbf{K}} \tilde{\chi} = \tilde{\mathbf{f}}, \quad (2.81)$$

in which $\tilde{\mathbf{K}}$ is the reduced global stiffness matrix, that can be written in terms of the transformation matrix as

$$\tilde{\mathbf{K}} = \mathbf{T}_m^T \mathbf{K} \mathbf{T}_m \quad (2.82)$$

and $\tilde{\mathbf{f}}$ is the reduced force vector, that can also be written in terms of the transformation matrix as

$$\tilde{\mathbf{f}} = \mathbf{T}_m^T \mathbf{f}. \quad (2.83)$$

Equation 2.81 is the reduced system of the problem, and must be solved for $\tilde{\chi}$. The recover of the displacement field χ is made through equation 2.80.

A similar procedure is adopted to the thermal equilibrium problem, in which $\tilde{\mathbf{R}}$ is the reduced characteristic temperature field of the RVE, which are related to \mathbf{R} by

$$\mathbf{R} = \mathbf{T}_t \tilde{\mathbf{R}}, \quad (2.84)$$

where \mathbf{T}_t is the transformation matrix for the thermal case. The global reduced equilibrium problem, for this case, is given by

$$\widetilde{\mathbf{C}}\mathbf{t}\widetilde{\mathbf{R}} = \widetilde{\mathbf{Q}}, \quad (2.85)$$

where $\widetilde{\mathbf{C}}\mathbf{t}$ is the reduced global thermal conductivity matrix, given by

$$\widetilde{\mathbf{C}}\mathbf{t} = \mathbf{T}_t^T \mathbf{C}\mathbf{t} \mathbf{T}_t \quad (2.86)$$

and $\widetilde{\mathbf{Q}}$ is the reduced flux vector, written in terms of the transformation matrix as

$$\widetilde{\mathbf{Q}} = \mathbf{T}_t^T \mathbf{Q}. \quad (2.87)$$

Equation 2.87 is the reduced system of the thermal conductivity problem, and must be solved for $\widetilde{\mathbf{R}}$. The recover of the temperature field, with the periodicity constraints, is obtained by equation 2.84.

These transformations ensure the periodicity considerations on the RVE.

2.5 DESCRIPTION OF THE ALGORITHM

This section describes the basic procedure used in order to evaluate the effective properties of a porous media. All computational codes were developed by the authors and written in the free software Julia, and the visualization of the topologies is made with the aid of the free Software Gmsh.

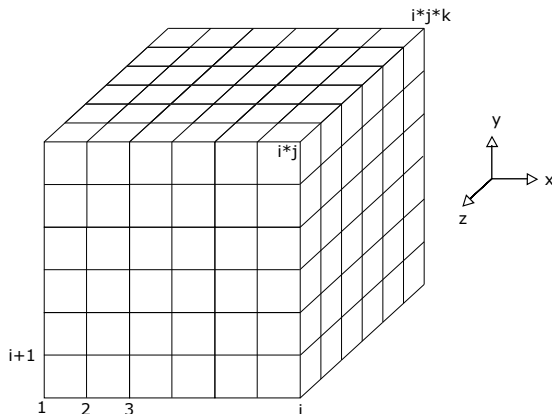
2.5.1 Data Input and Initial Calculations

The information needed to find the equivalent properties of a porous media can be divided into mesh information and material information. As mesh information, it must be informed the dimensions of the domain (length, width and height of the RVE) and the number of finite elements in each direction. As material information, it must be informed the properties of the base material (Young's Modulus, Poisson's Coefficient and the thermal Conductivity coefficient) and the minimum density adopted, in order to model the voids of the domain by using an interpolation scheme. Still, it must be informed which is the material distribution of the domain.

2.5.1.1 Mesh Generation

The mesh generation follows the node numeration and reference system showed in figure 19. In this figure, i , j and k represents the number of nodes in the x , y and z directions, respectively. The code was written in a general way, such that the dimensions of the base cell and the number of elements in each direction must be informed by the user. In this work, for all cases, a structured mesh is employed.

Figure 19 – Reference for the mesh generation



Source: Author's production, 2016

The algorithm is used in order to determine the coordinate matrix of the base cell, containing the spatial coordinates of each node of the mesh and the connectivity matrix, relating each element of the mesh to its nodes.

Also, a vector of the size of the total number of elements of the finite element mesh is used to store the pseudo density of each element. For the analysis case, a position containing an one refers to an element that contains material, and a position containing the minimum density refers to a void element. Several material distribution codes were written in order to analyse different kinds of structures.

2.5.1.2 Compatibility Matrix

The compatibility matrix for the mechanical and for the thermal problems are distinct. The compatibility matrix of the mechanical case

associates three degrees of freedom in opposite nodes, that is, the degree of freedom in x direction has to be associated with the degree of freedom in the x direction of the opposite node and so on. In the thermal problem, a scalar is associated to each node of the mesh. So, only one degree of freedom is associated to each node. The codes were written separately.

2.5.2 Base Material

For all cases studied, the base material is considered isotropic, and its mechanical constitutive tensor is given by

$$\mathbf{C} = \frac{E}{(1+v)(1-2v)} \begin{bmatrix} 1-v & v & v & 0 & 0 & 0 \\ v & 1-v & v & 0 & 0 & 0 \\ v & v & 1-v & 0 & 0 & 0 \\ 0 & 0 & 0 & \frac{1}{2}(1-2v) & 0 & 0 \\ 0 & 0 & 0 & 0 & \frac{1}{2}(1-2v) & 0 \\ 0 & 0 & 0 & 0 & 0 & \frac{1}{2}(1-2v) \end{bmatrix}, \quad (2.88)$$

where E is the Young's Modulus and v is the Poisson's Coefficient, and its thermal conductivity tensor is given by

$$\mathbf{Kt} = \begin{bmatrix} kt & 0 & 0 \\ 0 & kt & 0 \\ 0 & 0 & kt \end{bmatrix}, \quad (2.89)$$

where kt is the thermal conductivity coefficient.

For the analysis case, a scheme of material interpolation is used to determine the properties of all elements of the mesh, post as

$$\mathcal{P} = \rho_v \mathcal{P}^0, \quad (2.90)$$

where \mathcal{P} represents the effective property of the element, \mathcal{P}^0 the property of the base material and ρ_v is the pseudo-density of the element. For a void element, the pseudo-density, ρ_v , is assumed to be very small, so, the influence of the void elements is negligible on the assembly of the global matrices. For a element with material, the pseudo-density, ρ_v , assumes the value one, so, the property of this element is the property of the base material. This approach is used in order to allow the coupling of this code with the topology optimization method.

This interpolation scheme renders the problem simpler, due to the fact that the void elements do not need to be removed from the finite element mesh, thus, the connectivities of the elements do not need to be changed when the material distribution changes. Conversely, this approach is computational inefficient, since the void elements contribute in the assembly of the global matrices.

2.5.3 Solution of the Linear System

The Finite Element Method (FEM), (BATHE, 2009), (HUGHES, 2000), (ZIENKIEWICZ; TAYLOR, 2000), is used to solve the equilibrium problems. The dimensions of a three dimensional finite element equilibrium problem increases in the third power with the number of elements in the mesh. This leads to an expensive computational effort and makes the solution of these problems the most computational demanding part of the algorithm.

If a linear interpolation is used to discrete the domain, poor results may be achieved, and the number of elements needed to achieve a satisfactory result may be large, increasing the computational effort. If a quadratic element is employed, a smaller number of elements may be used, however, this element render the linear system bigger, increasing the computational effort as well. Thus, there is a compromise between the number of elements and the quality of the results to achieve a better result without increasing the computational effort.

For the mechanical case, the element chosen for the discretization is the Trilinear Isoparametric Hexahedral Element with incompatible modes. This element increases the accuracy obtained for the displacement and stress fields and does not affect the computational efficiency of global matrix assembly, when compared to the usual Hexahedral trilinear element. This element was implemented as an expansion of the concepts presented by Hughes (2000) and Cook (1995) for the Four Node Bilinear Isoparametric Element. Appendix B shows the determination of the stiffness matrix and the stress field for this element.

For the thermal case, the usual Trilinear Isoparametric Hexahedral Element is used.

Also, in order to improve the efficiency of this particular part of the algorithm, it was used the conjugate gradient method, together with a diagonal scaling procedure and with a parallel code.

2.5.3.1 Conjugate Gradient Method

The equilibrium problem in a finite element analysis is a system of linear equations of the form

$$\mathbf{A}\mathbf{x} = \mathbf{b}, \quad (2.91)$$

where \boldsymbol{x} is an unknown vector, \boldsymbol{b} is a known vector and \boldsymbol{A} is a known, square, symmetric and positive-definite matrix.

Classic methods, such as the LU decomposition and Cholesky Decomposition, Capra and Canale (2008), can be used to solve the problems. These methods factor matrix \boldsymbol{A} and solve the equations by backsubstitution. If the linear system is very large, factoring the matrix may be impractical due to the memory limitation.

The conjugate gradient method can be used to avoid this issue. This is a memory-efficient iterative method for solving large sparse systems of linear equations.

As shown by Komzsik and Poschmann (1993), the linear system is solved with an iterative method by minimizing the error of the approximate solution in each step. In a step, the approximate solution leads to

$$\boldsymbol{b} - \boldsymbol{A}\boldsymbol{x} = \boldsymbol{r} \neq \mathbf{0}, \quad (2.92)$$

where \boldsymbol{r} is the residue. The conjugate gradient method minimizes the error function

$$\Phi(\boldsymbol{x}) = \frac{1}{2} \boldsymbol{x}^T \boldsymbol{A} \boldsymbol{x} - \boldsymbol{x}^T \boldsymbol{b}, \quad (2.93)$$

whose first derivative is given by the negative of residual of equation 2.92. The iterative problem consists in solving consecutive steps of the approximate solution as

$$\boldsymbol{x}_{k+1} = \boldsymbol{x}_k + \psi_k^s \boldsymbol{d}_k, \quad (2.94)$$

where \boldsymbol{d} is the search direction and ψ^s is the step, used in order to minimize the error function.

The direction can be found through a linear combination of the form

$$\boldsymbol{d}_k = -\boldsymbol{d}_{k-1} + \beta_{k-1}^s \boldsymbol{d}_{k-1} \quad (2.95)$$

where β^s is a scalar, who can be obtained by a

$$\beta_{k-1}^s = \frac{\boldsymbol{r}_{k-1}^T \boldsymbol{A} \boldsymbol{d}_{k-1}}{\boldsymbol{d}_{k-1}^T \boldsymbol{A} \boldsymbol{d}_{k-1}}. \quad (2.96)$$

The step can be found as

$$\psi_k^s = -\frac{\boldsymbol{r}_{k-1}^T \boldsymbol{d}_k}{\boldsymbol{d}_k^T \boldsymbol{A} \boldsymbol{d}_k}. \quad (2.97)$$

For the first iteration of the problem, the direction and the step can be found, respectively, by

$$\mathbf{d} = \mathbf{r} \quad (2.98)$$

and

$$\psi^s = \frac{\mathbf{r}^T \mathbf{r}}{\mathbf{r}^T \mathbf{A} \mathbf{r}}. \quad (2.99)$$

The convergence of the method is guaranteed in a number of iterations equal to the size of the linear system.

2.5.3.2 Diagonal Scaling

The condition number of a matrix can be defined as the ratio of its maximum singular value to its minimum singular value. The conjugate gradient method achieves a faster rate of convergence for smaller condition number. Thus, it is desirable to decrease the condition number of the coefficient matrix in order to improve the efficiency of the iterative method.

As shown by Pini and Gambolati (1990), the use of the simple and inexpensive diagonal scaling is superior to other methods in a wide range of problems. In the diagonal scaling, an auxiliary problem, in the form

$$\mathbf{D} \mathbf{A} \mathbf{D} \mathbf{x}' = \mathbf{D} \mathbf{b} \quad (2.100)$$

where \mathbf{D} is a diagonal matrix, chosen in order to reduce the condition number of \mathbf{A} and solved for \mathbf{x}' . The original variables are recovered as

$$\mathbf{x} = \mathbf{D}^{-1} \mathbf{x}'. \quad (2.101)$$

As shown by Takapoui and Javadi (2014), this can significantly decrease the number of iterations needed in order to achieve the convergence. The diagonal matrix is written such as

$$\mathbf{D} = \sqrt{\mathbf{A}_{ii}}, \quad (2.102)$$

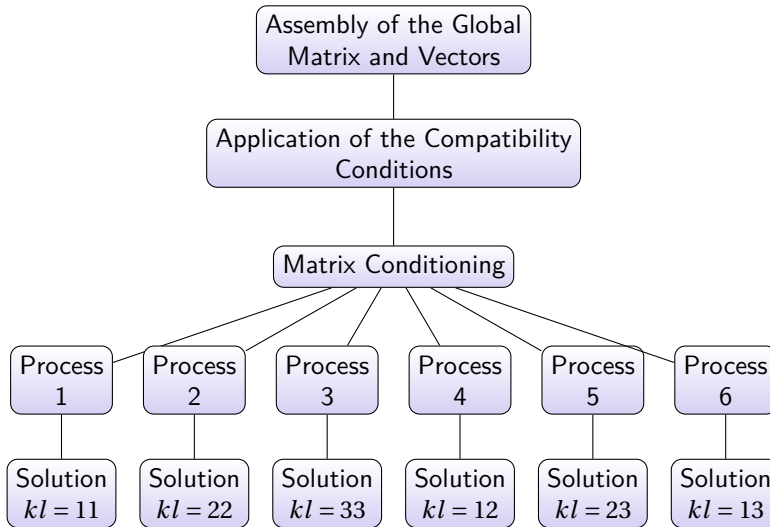
rendering the terms of the scaled matrix unitary.

2.5.3.3 Parallel Code

The solution of the linear systems for the mechanical case is the most demanding part of the algorithm. As the six linear system needed

to solve the mechanical homogenization system are independent on each other, a scheme of parallelization is adopted in order to solve each linear system in a different core. Figure 20 shows the scheme adopted. At first, the global matrix stiffness and the six global load vectors (one for each load case) are assembled, then the stiffness matrix is conditioned, and then each process receives one linear system to solve in parallel. The algorithm continues after all the linear systems are solved. The procedure of solution for the thermal case is equivalent, however, only three linear systems are solved in parallel.

Figure 20 – Solution of the linear systems



Source: Author's production, 2016

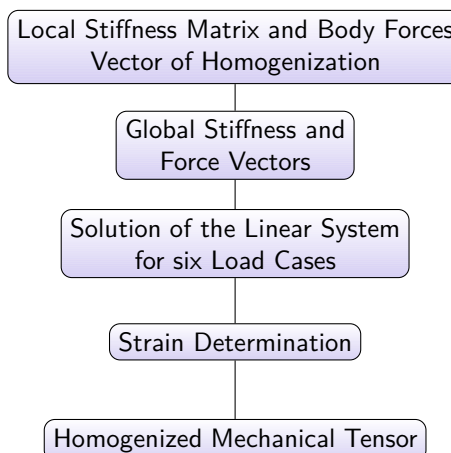
2.5.4 Mechanical Homogenized Coefficients

For the determination of the homogenized coefficients the data needed are the information of the coordinates of the nodes, connectivity of the elements, compatibility matrix, information of the boundary conditions, the properties of the base material (Young's Modulus and Poisson's Modulus) and the vector containing the densities of each element.

First, the local stiffness matrix for one element is determined. As all elements of the mesh have equal sizes, the local stiffness matrix is equal for all of them. The body forces follow the same principle. All elements have

the same body force vector, but it has to be regarded that six distinct local body forces must be determined, in order to solve the six load cases needed on the homogenization procedure. The assembly of the global stiffness matrix and the global body force vector follow the standard procedure, yet, the contribution of each element on the assemblies are weighted by the pseudo densities of each element (material interpolation). After this, the compatibility conditions are imposed upon the stiffness matrix and the body force vector and the six linear systems are solved, as the scheme of figure 20, in order to obtain the characteristic displacement fields of the base cell. The strain fields now can be obtained and finally the homogenized components of the fourth order elasticity tensor can be determined. A summary of the procedure to obtain the homogenized tensor is shown in figure 21.

Figure 21 – Mechanical homogenized coefficients



Source: Author's production, 2016

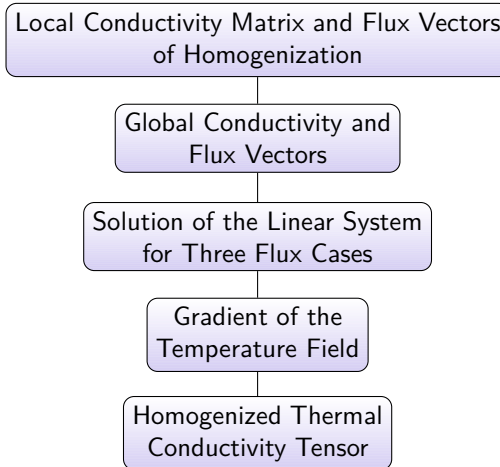
2.5.5 Thermal Homogenized Coefficients

The procedure is equivalent to the mechanical case. As data, it distinguish from the mechanical case only by the base material property, that now is the thermal conduction coefficient, and from the compatibility matrix, that now uses only one degree of freedom for node.

The thermal analysis is quite similar for the mechanical steps, but for this case, the stiffness matrix and the force vector are changed,

respectively, by the conductivity matrix and flux vector. It is sufficient to solve the linear system for three flux cases in order to determine the temperature field of the base cell and to obtain all the components of the homogenized thermal conductivity tensor. Figure 22 shows the summary of the steps for the determination of the homogenized tensor.

Figure 22 – Thermal homogenized coefficients



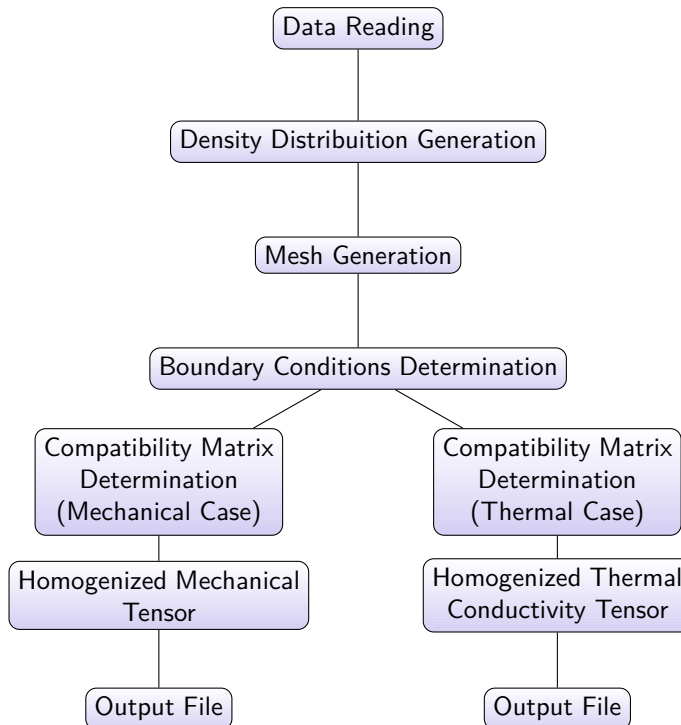
Source: Author's production, 2016

2.5.6 Analysis Problem

Figure 23 shows an summary of the whole analysis procedure. At first the data needed for both mechanical and thermal homogenization tensors determination is read. The distribution of densities and the mesh generation are made in the code itself.

The compatibility matrix are distinct between the mechanical and thermal cases, due to the fact that for the mechanical case each node has three associated degrees of freedom and for the thermal case, only one. Finally, the homogenized mechanical and thermal tensors can be determined through the procedures presented in figures 21 and 22, respectively. The algorithm ends by writing an output file containing the homogenized tensors.

Figure 23 – Algorithm of the analysis program



Source: Author's production, 2016

The validation of the implemented mechanical and thermal algorithms is shown in appendix C. This appendix uses simple geometries which allow to compare the results obtained with other mathematical procedures. Also, results found into literature for specific arrangements of micro structures are used as comparison.

3 OPTIMIZATION

In a brief way, optimization is a mathematical procedure used to obtain the best result for a problem under a certain set of constraints. Thus, the basic objective of optimization is to obtain the minimum (or the maximum) of a problem that can be written as a function of certain design variables.

This chapter presents the main concepts of optimization in a general context. At first a brief historical review is presented, then the basic optimization concepts and the types of optimization are shown.

3.1 HISTORICAL CONTEXT

According to Rao (2009), the existence of optimization methods may be traced back to Newton, Lagrange and Cauchy. The development of methods which use differential calculus are only suitable due to the contributions of Newton and Leibnitz in this area. The principles of variational methods, which deal with the minimization of functionals, were established by Bernoulli, Euler, Lagrange and Weierstrass. The development of optimization methods for constrained problems was first made by Lagrange, apud Rao (2009), and nowadays it is employed the so-called Lagrange Multiplier, which refers to a scalar used as a penalty in constrained optimization problems. Also it is worth to quote Cauchy, that made the first application of the Steepest Descent method for the solution of non constrained problems, and which is used until the present day.

Although the great initial effort, a small progress was made until the first half of the twentieth century, when the development of high-speed computers allowed the implementation of the optimization methods, encouraging the research on the optimization field.

Modern optimization methods and contributions were pioneered by the works of Courant (1943) upon penalty functions, Dantzig (1951) on the simplex method for linear programming and the works of Karush (1939) and Kuhn and Tucker (1951), who obtained the necessary and sufficient conditions for the achievement of the optimum in a constrained problem, known as the Karush-Kuhn-Tucker (KKT) conditions.

Thereafter, particularly in the sixties, several numerical methods to solve non-linear optimization problems were developed. For unconstrained optimization problems, it is worth mentioning the work of Fletcher and

Reeves (1964) on conjugate gradient method and, for constrained problems, the works of Rosen (1961) on gradient projection method and of Zoutendijk (1960) on the method of feasible directions.

In a concept of structural optimization applied to engineering problems, the solution of non-linear problems were pioneered by Schmit (1960). Also, early literature can be found from the early sixties by several authors, among it one can mention the works of Johnson (1961), Wilde and Beightler (1967) and Fox (1971).

In specific ways, several authors have added to this collection including books on specialized topics such as structural topology optimization, and at the scope of this work it worth mentioning the work of Bendsøe and Sigmund (2003) on topology optimization.

3.2 BASIC CONCEPTS

Representing a real optimization problem into a mathematical formulation is a decisive step in the solution of such problem. If the formulation is not quite appropriate as it should, possibly the solution will not be the optimum solution sought, or even the solution can be inappropriate. A special effort must be taken in order to transcribe correctly the real problem into a mathematical formulation. As shown by Arora (2007), any problem of optimization, or structural optimization, has three basic components (design variables, objective function and constraints):

- Design variables, designated by ρ : a set of scalars, or a vector, who describes the design of the structure. The design variables may represent geometrical parameters of the structure like an area or the length of a bar. They are changed during the optimization process in order to find the optimum design;
- Objective function, designated by $f(\rho)$: a function used to describe the parameter which it is intended to optimize and that gives, usually, a scalar measure of this parameter. In structural optimization, the objective function can play the role of the weight of the structure, the displacement of a certain point, its stiffness, among others;
- Equality and inequality constraints, designated, respectively, by $h(\rho)$ and $g(\rho)$: such as the objective function, the constraints are functions describing a certain parameter of the structure. The set of design variables must satisfy the constraints of the problem in order make

the problem feasible. In structural optimization, the constraints can represent a maximum volume for the structure, a maximum stress that can be applied in some part of the structure, among others;

- Side constraints, designated by $\underline{\rho}$ and $\bar{\rho}$: values imposed directly on the design variables that represent, respectively, its lower and upper bounds.

Therefore, an optimization problem can be written, on the standard minimization form, as

$$\begin{aligned} & \underset{\rho}{\text{Minimize}} && f(\rho) \\ & \text{Subject to} && g_j(\rho) \leq 0, \quad j = 1, \dots, n_g \\ & && h_k(\rho) = 0, \quad k = 1, \dots, n_h \\ & && \underline{\rho}_i \leq \rho_i \leq \bar{\rho}_i, \quad i = 1, \dots, n_d, \end{aligned} \tag{3.1}$$

where ρ is the vector of design variables, $g_j(\rho)$ is the j -th inequality constraint, $h_k(\rho)$ is the k -th equality constraint, $\underline{\rho}_i$ and $\bar{\rho}_i$ are, respectively, the inferior and superior bounds of the i -th design variable, n_d is the number of design variables, n_g is the number of inequality constraints and n_h is the number of equality constraints.

For a better understanding of an optimization problem, the concepts of necessary and sufficient conditions, regular point, Lagrange multipliers and KKT conditions must be presented.

3.2.1 Local and Global Minima

If the design variables, ρ , are within a feasible region, Ω_f , satisfying all the constraints, it is said that the function has a global minimum at ρ^* if

$$f(\rho^*) \leq f(\rho) \quad \forall \rho \in \Omega_f. \tag{3.2}$$

Likewise, a local minimum is defined as the lower value of the objective function within a small neighbourhood.

According to Belegundu and Chandrupatla (1999), when the objective function is convex (for a minimization problem) or concave (for a maximization problem) and the feasible set is a convex set, any local minimum is also a global minimum.

In structural optimization, most of the problems are not convex, consequently, the problems have several local minima. In a general way, when using gradient based methods, one can find different solutions when different initial points are chosen.

Also, it is not ensured that an optimization problem has a minimum. The existence of a minimum is ensured by the Weiestrass theorem, stating that if $f(\rho)$ is continuum in a closed and limited feasible region, then $f(\rho)$ has, at least, one global minimum in this region (ARORA, 2007).

3.2.2 Necessary and Sufficient Conditions

For the discussion of the local optimally conditions for an unconstrained problem, one must assume that the function $f(\rho)$ has a minimum at the point ρ^* . As shown by Arora (2007), it is necessary that the first derivatives of the function $f(\rho)$, at ρ^* , are equal to zero,

$$\frac{\partial f(\rho^*)}{\partial \rho_i} = 0; \quad i = 1 \dots n_d. \quad (3.3)$$

The sufficient condition for a local minimum, is that the Hessian matrix of the objective function, given by

$$\mathbf{H}(\rho^*) = \left[\frac{\partial^2 f}{\partial \rho_i \partial \rho_j} \right], \quad (3.4)$$

is positive definite at point ρ^* . Mathematically, a positive definite matrix is written as

$$\mathbf{a}^T \mathbf{H} \mathbf{a} > 0 \quad \forall \mathbf{a} \neq 0. \quad (3.5)$$

This condition ensures that the point ρ^* is a local minimum for the function $f(\rho)$.

3.2.3 Regular Point

The definition of a regular point is important to the derivation of the necessary and sufficient conditions on a constrained problem.

For a constrained problem, it is assumed that the function $f(\rho)$ has a minimum at the regular point ρ^* and the constraints $h_k(\rho)$ and $g_j(\rho)$ of the problem are differentiable functions. According to Belegundu

and Chandrupatla (1999), if the point ρ^* is a feasible point and if the gradients of the all equality constraints and all active inequalities are linearly independent at ρ^* , then the point is considered a regular point.

If a candidate minimum point is not a regular point, the necessary and sufficient conditions are not valid.

3.2.4 Lagrange Multipliers

Initially the necessary conditions are obtained for a problem with only equality constraints, and then generalized for a problem with equality and inequality constraints. Let the constrained optimization problem given by

$$\begin{aligned} & \underset{\rho}{\text{Minimize}} && f(\rho) \\ & \text{Subject to} && h_k(\rho) = 0, \quad k = 1, \dots, n_h. \end{aligned} \tag{3.6}$$

According to Arora (2007) there is a scalar associated with each constraint, called Lagrange Multiplier and, making an analogy, this scalar can be understood as the force required to impose this constraint to the problem. The Lagrangian Function is obtained adding a Lagrange Multiplier for each constraint of the problem, such that

$$L(\rho, \lambda) = f(\rho) + \sum_{k=1}^{n_h} \lambda_k h_k(\rho) = f(\rho) + \lambda^T h(\rho). \tag{3.7}$$

The condition for the minimum can be written as

$$\nabla L(\rho^*, \lambda^*) = 0. \tag{3.8}$$

If ρ^* is a regular point that minimizes the objective function, then there is an unique set of Lagrange Multipliers, λ^* , in which

$$\frac{\partial f(\rho^*)}{\partial \rho_i} + \sum_{k=1}^{n_h} \lambda_k^* \frac{\partial h_k(\rho^*)}{\partial \rho_i} = 0 \tag{3.9}$$

and

$$h_k(\rho^*) = 0. \tag{3.10}$$

Differentiating $L(\rho, \lambda)$ with respect to λ_k one can recover the equality constraints as

$$\frac{\partial L(\rho^*, \lambda^*)}{\partial \lambda_k} = 0 \Rightarrow h_k(\rho^*) = 0; \quad k = 1 \text{ to } n_h. \tag{3.11}$$

The gradient condition of equation 3.8 is stationary with respect to ρ and λ , consequently, the problem can now be treated as an unconstrained problem in the variables ρ and λ . For this case, the Lagrange multipliers can assume both positive and negative values.

A point that does not satisfy the conditions of the theorem can not be a local minimum point, but one can not conclude that a point who satisfies the conditions is a minimum point, being simply a candidate.

The presented concepts can be extended to a problem with equality and non equality constraints.

3.2.5 KKT Conditions

The necessary conditions of a general optimization problem are given by the Karush-Kuhn-Tucker (KKT) conditions. These conditions were obtained, separately, by Karush (1939) and Kuhn and Tucker (1951). One can see the necessary conditions of a general problem as an extension of the Lagrange Multiplier theorem, where the inequalities $g_j(\rho) \leq 0$ are considered. The general optimization problem is given by

$$\begin{aligned} & \underset{\rho}{\text{Minimize}} && f(\rho) \\ & \text{Subject to} && g_j(\rho) \leq 0, \quad j = 1, \dots, n_g \\ & && h_k(\rho) = 0, \quad k = 1, \dots, n_h. \end{aligned} \tag{3.12}$$

Having in mind that the values of the inequalities are either negative or zero, then a positive scalar can be added to each constraint in order to transform it in an equality constraint. This positive scalar, s_j , associated to each inequality constraint is called slack variable. Also, in order to avoid an extra constraint of the kind $s_j > 0$, one can write the slack variable as s_j^2 instead of s_j . Therefore, the inequality $g_j(\rho) \leq 0$ can be written as an equivalent equality constraint as

$$g_j(\rho) + s_j^2 = 0. \tag{3.13}$$

When the variable s_j has zero value, its corresponding inequality constraint is satisfied as an equality and called an active constraint.

For this case, besides the Lagrange Multipliers, λ , associated to the equality constraints, it is also considered the Kuhn-Tucker Multipliers, μ , associated to the inequality constraints. Hence, the Lagrangian Function

associated to the optimization problem of the equation 3.12 can be written as

$$\begin{aligned} L(\rho, \lambda, \mu, s) &= f(\rho) + \sum_{k=1}^{n_h} \lambda_k h_k(\rho) + \sum_{j=1}^{n_g} \mu_j (g_j(\rho) + s_j^2) \\ &= f(\rho) + \lambda^T h(\rho) + \mu^T (g(\rho) + s^2). \end{aligned} \quad (3.14)$$

According to Arora (2007), if ρ^* is a regular point of the feasible set that is a local minimum for the problem of equation 3.12, then there exists a set of multipliers λ^* and μ^* such that the Lagrangian function of equation 3.14 is stationary with respect to ρ , λ , μ and s at the regular point ρ^* .

The necessary conditions in regard to the general optimization problem posed in equation 3.12, according to Arora (2007) can be summarized as:

- Gradient conditions:

$$\frac{\partial L}{\partial \rho_i} = \frac{\partial f}{\partial \rho_i} + \sum_{k=1}^{n_h} \lambda_k^* \frac{\partial h_k}{\partial \rho_i} + \sum_{j=1}^{n_g} \mu_j^* \frac{\partial g_j}{\partial \rho_i} = 0, \quad (3.15)$$

$$\frac{\partial L}{\partial \lambda_k} = 0 \Rightarrow h_k(\rho^*) = 0 \quad (3.16)$$

and

$$\frac{\partial L}{\partial \mu_j} = 0 \Rightarrow (g_j(\rho^*) + s_j^2) = 0; \quad (3.17)$$

- Feasibility check for inequalities:

$$s_j^2 \geq 0; \quad (3.18)$$

- Switching conditions:

$$\frac{\partial L}{\partial s_j} = 0 \Rightarrow 2\mu_j^* s_j = 0; \quad (3.19)$$

- Non-negativity of Karush-Kuhn-Tucker Multipliers for inequalities:

$$\mu_j^* \geq 0; \quad (3.20)$$

- Regularity check: the gradients of the active constraints must be linearly independent.

It is worth mentioning some important points related to the KKT necessary conditions:

- The KKT conditions are not applicable if the minimum candidate point is not regular;
- If a point does not satisfy the KKT conditions it can not be a local minimum, unless it is an irregular point;
- The points satisfying the KKT conditions can be both constrained or unconstrained;
- If there are no inequality constraint active, and there are equality constraint on the problem, then the point is stationary, and it may be a minimum, a maximum or an inflection point.

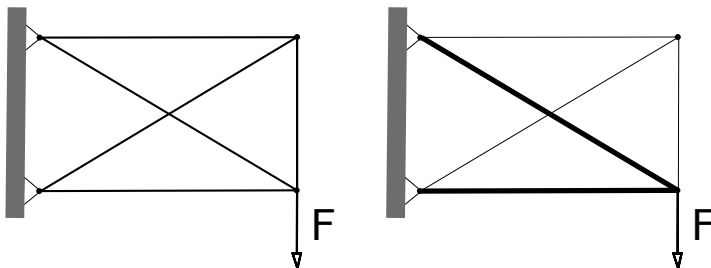
3.3 STRUCTURAL OPTIMIZATION

If the optimization problem is written such that it uses structural concepts, it is called structural optimization. Several criteria can be used to define the concept of optimum in a structural optimization. One can define a structural problem in order to minimize the weight of a structure without compromising its structural function, in order to maximize its stiffness for a pre determined volume of the structure, in order to avoid buckling phenomena among others. As shown by Christensen and Klarbring (2008), structural optimization can be divided into three distinct forms:

- Parametric Optimization: in this case, the design variables, ρ , are some sort of dimensions or parameters of the structure, as for example, an area of a cross section of a lattice bar or the thickness distribution on a plate. Figure 24 shows an example of Parametric Optimization;
- Shape Optimization: in this case, the design variables, ρ , represent the shape or boundary of some part of the structure. On a general way, the shape is written as a set of equations and the shape optimization consists in find the integration domain to satisfy the equilibrium problem in an optimum manner. Figure 25 shows an example of a shape optimization problem;

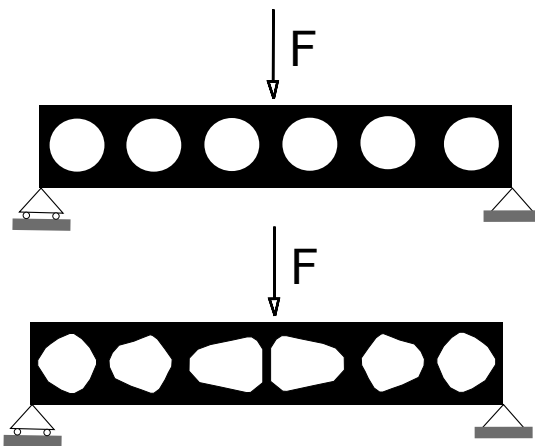
- Topology Optimization: is the most general form of structural optimization, allowing voids and new boundaries to be added to the structure. In this case, the design variables ρ represent the distribution of material on a given fixed domain. Figure 26 shows an example of topology optimization.

Figure 24 – Parametric optimization



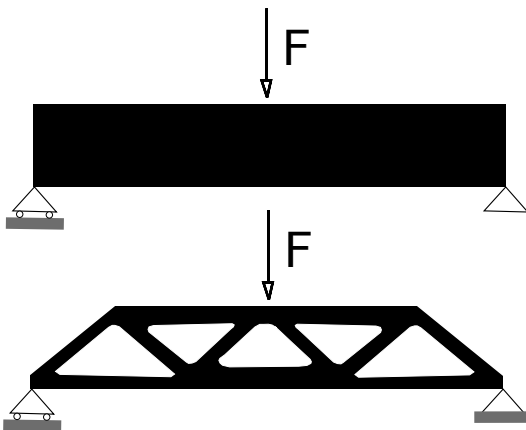
Source: Author's production, based on Christensen and Klarbring (2008)

Figure 25 – Shape optimization



Source: Author's production, based on Bendsøe and Sigmund (2003)

Figure 26 – Topology optimization



Source: Author's production, based on Bendsøe and Sigmund (2003)

4 TOPOLOGY OPTIMIZATION

The main purpose of topology optimization is to determine the distribution of a set of materials within a certain fixed region in order to extremize an objective function. In this work, it is required to find which points of domain should contain a base isotropic material and which points should be void. In a discrete form, it is required to find which elements of the finite element mesh should have material and which should not have material (BENDSØE; SIGMUND, 2003). Only the loads, the boundary conditions, the volume of the structure and possible additional constraints, such as prescribed holes or regions where there are, necessarily, material are known in advance.

This chapter addresses the main considerations about the topology optimization. At first, a brief historical review of the method is presented, than, important considerations, such as the material parameterization, the problems related to the method and filtering techniques are discussed. Finally, the solutions methods adopted to solve the problems in this work are presented.

4.1 HISTORICAL REVIEW

Several studies indicate that pioneer study on topology optimization is the work of Michell (1904). Based on the studies of Maxwell, apud Cardoso (2005), Michell searched for the minimum volume of a structure formed by bar elements, respecting the equilibrium relations and the stress constraints. For many decades, the work of Michell remained almost unknown, for being considered too academic and with no practical appeal, until the early sixties. Since this decade, its work was continued by several authors as Cox (1956), Hemp (1973), Prager (1974) and Owen (1975). Also, it is worth mentioning the work of Rozvany and Adidam (1972), that extended the work of Michell for beam elements.

The topology optimization of continuum mechanics was developed on the early eighties, using a relaxation method through the consideration of composites. Cheng and Olhoff (1981) presented a study on the maximization of the stiffness of thin plates considering the thickness as design variable. This work observed that as more refined the domain, more reinforcements appear, indicating one of the problems associated with topology optimization of continuum media, the mesh dependency. To avoid this issue, Cheng and Olhoff (1982) proposed an alternative parameterization of

the problem, using geometrical pre determined parameters of the reinforcements rather than the thickness of the place. Years later, Kohn and Strang (1986) generalized this approach for elasticity problems.

As an extension of these works, it was proposed the use of the homogenization theory, (BENDSØE; KIKUCHI, 1988), to describe the effective properties of a composite material. The homogenization theory allows a continuum and consistent parameterization of the material properties, ensuring a well posed problem. It is worth mentioning the works of Bendsøe and Kikuchi (1988), Guedes and Kikuchi (1990) and Sanchez-Hubert and Sanchez-Palencia (1992), in which the development of concepts and mathematics are established and also the works of Hassani and Hinton (1998a) and Hassani and Hinton (1998b) where a good review of the homogenization method is presented.

Simpler methods of parameterization, such as SIMP (Solid Isotropic Material with Penalization), (BENDSØE, 1989), that intends to relax the 0-1 parameterization are widely used until the present day. This parameterization uses an interpolation of the properties of the base material in order to obtain the effective properties of the media. An exponent n is used in order to adjust the interpolation degree. If the chosen exponent equals to 1, that is to say, a linear interpolation, structures with intermediate densities may occur, also known as region containing porous material. This was interpreted by Bendsøe and Sigmund (1999) as regions with isotropic microstructures.

According to Rozvany (2001), the SIMP parameterization requires a smaller number of parameters and it can be used in a general problem, which is not possible for another kinds of parameterizations. Conversely, according to Stolpe and Svanberg (2001), the SIMP parameterization depends on the exponent n and has no mathematical guaranty of convergence. Yet, another issue on account of the use of the SIMP parameterization, according to Bendsøe (1989), is the mesh dependency, indicating that the problem is not sufficiently relaxed.

In order to obtain a controlled complexity of the topology and a problem independent on the discretization of the domain, regularization methods were proposed. It is worth mentioning the works of Ambrosio and Buttazzo (1993), that proposes to restrict the solution space imposing a perimeter restriction, and Sigmund (1997), that uses a filtering scheme in order to avoid intrinsic problems of the parameterizations used on topology optimization

4.2 MATERIAL PARAMETERIZATION

In the topology optimization procedure, one can find the optimum distribution of isotropic material within a certain domain, in other words, one must find in which points of the domain there is material and in which points there is void. Being the design domain, Ω , and a sub domain, Ω^{mat} , where there is effectively material, it is desired to use the parameterization

$$\mathcal{P}(\mathbf{x}) = \kappa(\mathbf{x})\mathcal{P}(\mathbf{x})^0, \quad (4.1)$$

where $\mathcal{P}(\mathbf{x})^0$ is a property of the base material and $\kappa(\mathbf{x})$ is a discrete function, defined in every point, \mathbf{x} , of the domain Ω , such that

$$\kappa(\mathbf{x}) = \begin{cases} 1 & x \in \Omega^{mat} \\ 0 & x \in \Omega/\Omega^{mat} \end{cases}, \quad (4.2)$$

where Ω^{mat} is the region in which there is material and Ω/Ω^{mat} is the region in which there is no material. For this formulation, the effective property, $\mathcal{P}(\mathbf{x})$, can only assume the discrete values 0 and $\mathcal{P}(\mathbf{x})^0$ in every point of the domain.

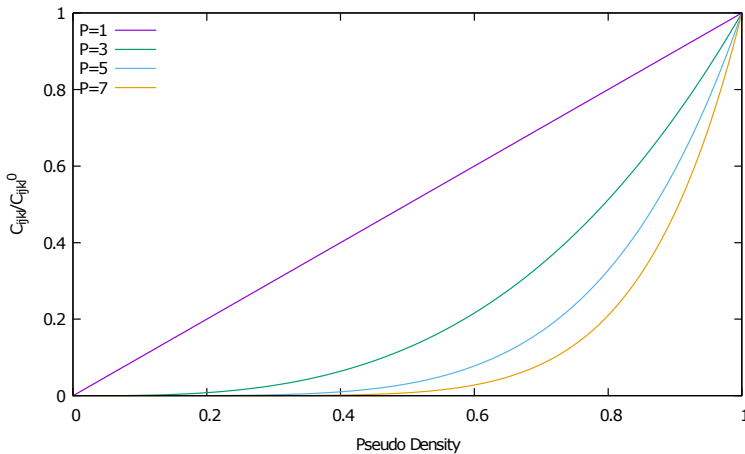
As shown by Kohn and Strang (1986), the discrete problem defined in equation 4.1 is ill-posed, leading to numerical issues due to the non existence of solution, besides being non-differentiable. Therefore, it is necessary a relaxation of the discrete problem (BENDSØE; KIKUCHI, 1988). This relaxation allows the design variables to assume intermediate values between 0 and 1. At first, these intermediate densities have no physical meaning, and one expects that at the end of optimization procedure only discrete values (0/1) remain.

The most popular way of addressing this kind problem is to replace the discrete variables with continuum variables and then to apply some sort of penalization, imposing the design variables to assume values 0 or 1. The well established SIMP (Solid Isotropic Material with Penalization) (BENDSØE; SIGMUND, 1999) has been widely used for these kind of problems, and, for the determination of the effective components of the constitutive tensor, it is set as

$$\begin{aligned} C_{ijkl}(\mathbf{x}) &= \rho(\mathbf{x})^p C_{ijkl}^0, & p > 1 \\ 0 \leq \rho(\mathbf{x}) &\leq 1, & x \in \Omega, \end{aligned} \quad (4.3)$$

where $\rho(\mathbf{x})$ is the vector containing the pseudo densities, or design variables, in every point of the domain Ω . The pseudo densities are interpolated

Figure 27 – SIMP



source: Author's production, 2016.

between $C_{ijkl}(p=0) = 0$ and $C_{ijkl}(p=1) = C_{ijkl}^0$, and it is required that, at the end of the procedure, all densities assume either 0 or 1 as its value.

At SIMP, one chooses as the penalization factor $p > 1$, so, intermediate density values become unfavourable, since the stiffness obtained is relatively small in comparison to the volume, or amount of material involved (BENDSØE; SIGMUND, 2003). Figure 27 shows the relation between a generic component of the constitutive tensor and the pseudo density with the variation of the penalization factor. One can see that for $p = 1$ there is a linear relation between the effective component of the tensor and the pseudo density, and for $p \rightarrow \infty$, the density becomes once again discrete, as the parameterization shown in equation 4.1.

As shown in Bendsøe and Sigmund (2003), the FEM can be used alongside SIMP in topology optimization problems. In this case, the domain Ω is divided into n finite elements, and the vector $p(x)$ contains the pseudo density of each element of the finite element mesh.

In the present work the domain is discretized by finite elements and it is assumed that every element's constitutive tensor has an effective

property

$$\mathbf{C}_e = \rho_e^p \mathbf{C}_e^0, \quad (4.4)$$

where ρ_e is the pseudo density of the e -th element, assumed as a constant within each element and \mathbf{C}_e^0 is the base material's fourth order elasticity tensor. In this way, one can write the effective stiffness matrix, for one element, as

$$\mathbf{K}_e = \int_{\Omega_e} \mathbf{B}^T \mathbf{C}_e \mathbf{B} d\Omega_e = \rho_e^p \int_{\Omega_e} \mathbf{B}^T \mathbf{C}_e^0 \mathbf{B} d\Omega_e = \rho_e^p \mathbf{K}_e^0, \quad (4.5)$$

where \mathbf{B} is the strain-displacement matrix and \mathbf{K}_e^0 is the stiffness matrix of the base material. The assembly of the global stiffness matrix is performed by the operator

$$\mathbf{K} = \bigoplus_{e=1}^n \mathbf{K}_e, \quad (4.6)$$

where n is the total number of elements of the mesh (BATHE, 2009). To avoid numerical issues due to a singular stiffness matrix, a minimum value for the pseudo density is assumed, such as $0 < \rho_{min} \leq \rho_e \leq 1$ (BENDSØE; SIGMUND, 1999). The minimum pseudo density also prevents that the derivatives of such element equals to zero.

4.3 PROBLEMS RELATED TO TOPOLOGY OPTIMIZATION

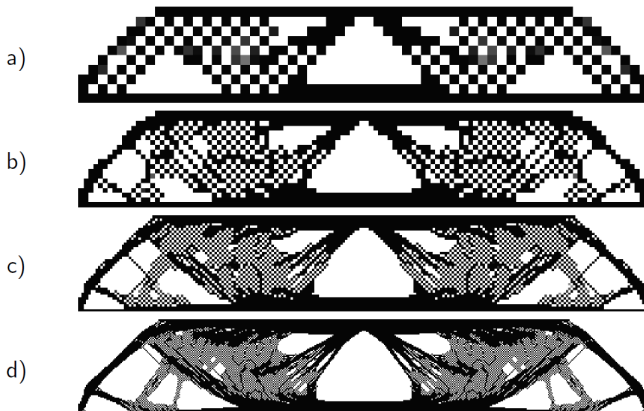
As shown by Sigmund (1994), two significant issues may occur with the material distribution obtained by the topology optimization. The first one is the appearance of patterns similar to a checkerboard, in which a region has, alternately, solid and void elements. The second one is the mesh-dependency of the results, in which different results are obtained for different mesh sizes. However, these problems can be avoided by using restriction methods.

4.3.1 Checkerboard

A problem related to the topology optimization is when alternating solid and void elements patterns, similar to a checkerboard, appear in certain regions of the domain. These patches of checkerboard patterns appear often in solutions obtained by a direct implementation of the material

distribution method that use the displacement based finite element method (BENDSØE; SIGMUND, 2003). The work of da Silva (2016) shows how the checkerboard patterns appear in a problem of compliance minimization for different sizes of finite element meshes (Figure 28).

Figure 28 – The checkerboard problem in a compliance minimization problem for several finite element mesh sizes. Mesh with a) 300 ; b) 1200 ; c) 4800; and d) 19200 finite elements.



source: (da Silva, 2016)

As shown by Diaz and Sigmund (1995), numerical approximations obtained by the finite element method may present the checkerboard issue due to the overestimate stiffness caused by this kind of pattern. In other words, the checkerboard pattern causes an artificially stronger material arrangement than any other possible arrangements with the same volume of material. This condition induces a preference on the use of checkerboard patterns on problems of stiffness maximization. As it is an artificially induced issue, this phenomenon can not be interpreted as an optimum solution.

4.3.2 Mesh dependency

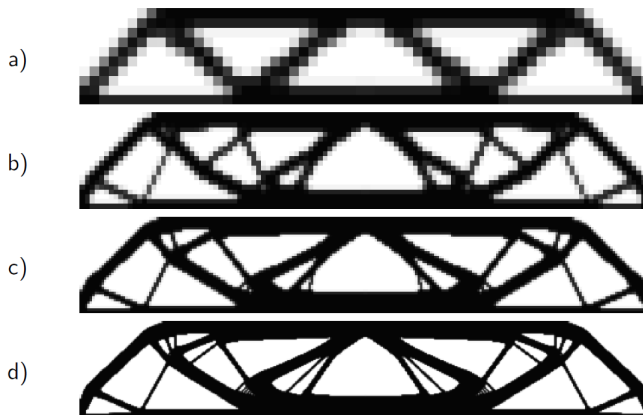
According to Bendsøe and Sigmund (2003), the 0-1 SIMP topology optimization lacks existence of solution in its continuum formulation. Basically, this happens due to the fact that, maintaining the volume, the introduction of new holes, or more reinforcements, will increase the effi-

ciency of a given structure. In the limit of the process, micro structures which increase the efficiency of the material appear. This microstructures are typically not isotropic and the initial description of only isotropic material of the problem can not be used.

In computational implementation, this effect can be understood as a numerical instability. In a finite element discretization, a more refined structure, with more reinforcements, appears when a finer finite element mesh is employed. As for the continuum approach, the limit induces the generation of microstructures.

The work of da Silva (2016) shows how different solutions can be obtained for different finite element meshes in a problem of compliance minimization (Figure 29).

Figure 29 – The mesh-dependency problem in a compliance minimization problem for several finite element mesh sizes. Mesh with a) 300 ; b) 1200 ; c) 4800; and d) 19200 finite elements



source: (da Silva, 2016)

4.3.3 Restriction Methods

To avoid the checkerboard and the mesh dependency problems, one can use the so called restriction methods. The main purpose of these methods is to restrict the solution space and the complexity of the topologies obtained, ensuring a mesh independence and the possibility of manufacturability in density-based topology.

According to Sigmund (2007), the restriction methods for density based topology optimization can be divided into three categories:

1. Mesh-independent filtering methods, which can be divided into density filters and sensibility filters. These are very popular approaches due to their efficiency and ease of implementation;
2. Constraint methods, such as perimeter control, global gradient control and local gradient control;
3. Other methods like wavelet parameterization and level-set.

Also, it is worth mentioning the existence of hibrid methods (CARDOSO; FONSECA, 2003) in which the box-constraints are changed due to a filtering scheme.

At this work, a filtering based on sensitivity method is used, in order to achieve the following results:

- Checkerboard-free solution;
- Reinforcement size control;
- Mesh-independent solution.

4.3.3.1 Filtering Methods

The filtering methods can be divided into density and sensitivity methods. According to Sigmund (2007), for the first case, the density of each element is changed as a weighted average of the densities inside of a predetermined neighbourhood, and than the finite element solver is called and the sensitivities are determinated. For the second case, the procedure is opposite. At first, the finite element problem is solved, than the sensitivities are determinated and finally they are heuristically modified as a weighted averages of the sensitivities of a predetermined neighbourhood. The sensitivities method is used in this work.

Sensitivity filtering can be found in the works of Sigmund (1994) and Sigmund and Petersson (1998). The basic idea is to apply the filter on the design sensitivities at each iteration of the algorithm. The filter makes the design sensitivity of a specific element on the finite element mesh dependent on a weighted average over the element itself and its

neighbours and, according to Sigmund and Petersson (1998), it is very efficient in removing checkerboards.

The neighbourhood of an element e , represented by N_e , is usually defined as the elements whose centroids are within a sphere (for the three-dimensional case) centred on the centroid of the element e with a radius R . Mathematically one can write

$$N_e = \{i, \|c_i - c_e\| \leq R\}, \quad (4.7)$$

where c_i is the centroid of the element i and c_e is the centroid of the element e .

It follows that the filtering method can be understood as an operator applied to the sensitivity in the form

$$\frac{\widehat{\partial f}}{\partial \rho_e} = \frac{\sum_{i \in N_e} w_e(c_i) \frac{\partial f}{\partial \rho_i}}{\sum_{i \in N_e} w_e(c_i)}, \quad (4.8)$$

where f is the objective function, ρ_e is the pseudo density of the element subjected to the filtering, ρ_i is the pseudo density of a neighbour element, $\frac{\partial f}{\partial \rho_e}$ is the modified sensibility of the element e and $w_e(c_i)$ is usually a linear weight function associated to the element e , which can be written as

$$w_e(c_i) = \frac{R - D_{ie}}{R}, \quad (4.9)$$

where D_{ie} is the Euclidean distance between the filtered element and its neighbours.

4.4 SOLUTION OF THE TOPOLOGY OPTIMIZATION PROBLEM

Several methods can be used in order to solve a topology optimization problem. The simplest method is the Optimality Criteria, but it can be used only in particular situations. Here, besides the Optimality Criteria, two other methods to solve the topology optimization problems are presented: the Sequential Linear Programming (SLP) and the Method of Moving Asymptotes (MMA).

4.4.1 Optimality Criteria

The first approach used in this work to solve the topology optimization problem is the Optimality Criteria (OC). Let the minimization

problem given by

$$\begin{aligned} & \underset{\rho}{\text{Minimize}} \quad \Phi(\rho) \\ & \text{Subject to} \quad V \leq V_f, \end{aligned} \quad (4.10)$$

where Φ is the objective function, ρ is the vector containing the pseudo densities of the elements, V is the total volume of the structure and V_f is the admissible volume. The volume of the structure can be found as

$$V = \sum_e^n V_e \rho_e, \quad (4.11)$$

where V_e and ρ_e are the volume and pseudo-density of the element e of the mesh. This method is based in Bendsøe and Sigmund (2003), and it upgrades the pseudo densities of each element such as

$$\rho_e^{k+1} = \rho_e^k \beta_e^\eta \quad (4.12)$$

respecting the limits

$$\rho_e^{k+1} \in [\rho_e^k - d_e, \rho_e^k + d_e] \quad (4.13)$$

$$\rho_e^{k+1} \in [\rho_{min}, 1.0], \quad (4.14)$$

where d_e is a positive moving limit of the e -th element, ρ_{min} is the minimum admissible pseudo density, η is a relaxation parameter and β_e is the update parameter, given by

$$\beta_e = \frac{\max\left(0, -\frac{d\Phi(\rho)}{d\rho_e}\right)}{\lambda \frac{dV(\rho)}{d\rho_e}}, \quad (4.15)$$

where λ is the Kuhn Tucker Multiplier that can be obtained by a bisection algorithm. The Optimality Criteria can be summarized as follows:

1. Set the initial parameters of bisection, generally

$$\lambda_1 = 0 \quad (4.16)$$

and

$$\lambda_2 = \Lambda, \quad (4.17)$$

where Λ is a large number, the tolerance for the stop criteria, tol , and the structure's admissible volume, V_f ;

2. Find λ as

$$\lambda = \frac{\lambda_1 + \lambda_2}{2}; \quad (4.18)$$

3. For each element in the finite element mesh, find β_e , using equation 4.15 and update its pseudo density through equation 4.12, respecting the imposed limits;
4. Find the structure's volume, equation 4.11, and update the bisection limits as:
 - if $V > V_f$ then $\lambda_1 = \lambda$;
 - if $V < V_f$ then $\lambda_2 = \lambda$.
5. Test the tolerance as:
 - if $tol < \lambda_2 - \lambda_1$ back to step 2;
 - if $tol > \lambda_2 - \lambda_1$ the algorithm ends.

The Optimality Criteria was chosen due to its simplicity, low computational cost and speed. Although it can be used only with restricted problems, and only with volume restriction, it can handle very well proposed problems.

4.4.2 Sequential Linear Programming

The Sequential Linear Programming (SLP) is a method used to solve non-linear problems and consists in the use of series of linear approximations. Each linear problem is generated by approximating the objective function and the constraints using a first order Taylor series expansion about the current design point ρ . According to Rao (2009), the SLP algorithm can be posed as follows:

1. Start with an initial design vector ρ . Iteration $k = 1$;
2. Linearize the objective function and the constraints using a first order Taylor series, about the initial point as

$$\Phi(\rho) \approx \Phi(\rho_i) + \nabla \Phi(\rho_i)^T (\rho - \rho_i), \quad (4.19)$$

$$g(\rho) \approx g(\rho_i) + \nabla g(\rho_i)^T (\rho - \rho_i), \quad (4.20)$$

$$h(\rho) \approx h(\rho_i) + \nabla h(\rho_i)^T (\rho - \rho_i); \quad (4.21)$$

3. State a standard optimization problem using the linearized objective function and constraints;
4. Select the proper moving limits;
5. Solve the linearized problem in order to obtain the design variables, ρ_{k+1} ;
6. Evaluate the original constraint at the point ρ_{k+1} and verify if they are satisfied within a small tolerance. If all the constraints are satisfied, than the procedure is stopped and

$$\rho_{opt} \simeq \rho_{k+1}. \quad (4.22)$$

If some of the constraints are not within the small tolerance neighbourhood, than set the design variable vector as $\rho_k = \rho_{k+1}$, iteration as $k = k + 1$ and back to item 2.

This method is an efficient technique for solving convex problems with nearly linear objective and constraint functions, since each iteration provides a linear problem, which can be solved with a certain efficiency. According to Arora (2007), some observations to highlight some features and limitations of the SLP method are:

1. The selection of moving limits is one trial and error and can be best achieved using an interactive procedure;
2. The method may not converge to the precise minimum, since no descent function is used, and a line search is not performed;
3. The method can cycle between two points if the optimum solution is not a vertex of the feasible set;
4. The method is quite simple conceptually and numerically. Though the method may not be used to reach a precise minimum, it can be used in some practical problems.

This method was used in order to handle more general problems, as for example, problems with symmetry constraints in the components of the homogenized tensors.

For the implementation, an external library, Hanson and Hirbert (1981), is used.

4.4.3 Method of Moving Asymptotes

The method of moving asymptotes (MMA) is a non-linear iterative method used in structural optimization, and is based on a convex approximation.

According to Svanberg (1987), the solution of an optimization problem, defined by Ψ^0 , set as

$$\begin{aligned} & \underset{\rho}{\text{Minimize}} \quad \Phi(\rho) \\ & \text{Subject to} \quad g_j(\rho) \leq \hat{g}_j, \quad j = 1, \dots, n_g \\ & \quad \underline{\rho}_i \leq \rho_i \leq \bar{\rho}_i, \quad i = 1, \dots, n_d, \end{aligned} \quad (4.23)$$

where \hat{g}_j is a scalar associated to the j -th constraint, n_g is the number of constraints and n_d is the number of design variables, can be summarized as follows:

1. Set an initial point, ρ^0 , and set the iteration as $k = 0$;
2. For the iteration k , find the values of the objective function and the constraints, as well as their derivatives;
3. Generate a sub-problem, Ψ^k , to replace to original problem, by replacing the original objective function, Φ and the constraints by explicit functions given, respectively by Φ^k and g_j^k ;
4. Solve the sub-problem Ψ^k and let the optimal solution of this problem be the next iteration point, ρ^{k+1} . Set the iteration as $k = k + 1$ and go to step 2.

The process is interrupted when some convergence criterium is fulfilled.

In a brief way, the functions Φ^k and g_j^k are obtained by the linearization of the original functions in variables of the form

$$\frac{1}{\rho_i - L_i} \quad (4.24)$$

and

$$\frac{1}{U_i - \rho_i}, \quad (4.25)$$

where L_i and U_i are known as moving asymptotes. The moving asymptotes parameters are chosen, at the iteration k , such that

$$L_i^k < \rho_i^k < U_i^k \quad i = 1, \dots, n_d. \quad (4.26)$$

Now, the sub problem, Ψ^k , is defined as

$$\begin{aligned} \text{Minimize}_{\rho} \quad & \sum_{i=1}^{n_d} \left(\frac{p_{oi}^k}{U_i^k - \rho_i} + \frac{q_{oi}^k}{\rho_i - L_i^k} \right) + r_o^k \\ \text{Subject to} \quad & \sum_{i=1}^{n_d} \left(\frac{p_{ji}^k}{U_i^k - \rho_i} + \frac{q_{ji}^k}{\rho_i - L_i^k} \right) + r_j^k \leq \hat{g}_j, \quad j = 1, \dots, n_g \\ & \max \left\{ \underline{\rho}_i, \alpha_i^k \right\} \leq \rho_i \leq \min \left\{ \bar{\rho}_i, \beta_i^k \right\}, \quad i = 1, \dots, n_d, \end{aligned} \quad (4.27)$$

where the functions p , q and r are dependent on the value of the original functions at the current design point, its derivatives and on the value of the moving asymptotes. In addition, the index 0 refers on the objective function and the index j refers to the constraints. The parameters α_i^k and β_i^k are move limits and are generally chosen such that

$$L_i^k < \alpha_i^k < \rho_i^k < \beta_i^k < U_i^k \quad (4.28)$$

and the moving asymptotes are heuristically chosen.

A detailed review of the method can be found in Svanberg (1987), Bruyneel, Duysinx and Fleury (2001) and Svanberg (2007).

5 FORMULATION

This chapter shows the formulation used in the optimization problems proposed in this work and the models used in the analysis problem.

As the possibility of production of a porous media became possible with the rapid prototyping methods, the tailoring of the properties of the porous media became a very interesting study field. This procedure is called inverse analysis, and intends to find the topology of the base cell of the porous media who better fits a macroscopic requirement of the porous media.

With regard to the concepts of topology optimization within the homogenization context, two distinct problems are proposed. The first one consists in the maximization of a linear combination of the components of the homogenized constitutive tensor. This intends to find the topology of the base cell who maximizes certain components of the homogenized tensor, rendering the porous media to be specialized in some sort of application and with a pre-determined volume of material.

The second one consists in the approximation of the homogenized constitutive tensor based on a given constitutive tensor. This approach enables the tailoring of a material with a predetermined property, allowing a wide range of applications in several areas. In this work, the mechanical constitutive tensor of the human bone is used as the target tensor, and as base material for the porous media, it is used a bio-compatible titanium alloy. This application becomes very important in medical applications, specially in the area of bone implants.

Besides the optimization procedure, this chapter addresses an analysis procedure. The proposal is to study the behaviour of two distinct hollow sphere materials. The effective homogenized elasticity and thermal conductivity tensors are evaluated and a relation between the geometrical parameters of the RVE and the effective properties are investigated.

According to Öchsner, Hosseini and Merkel (2009), hollow sphere structures are novel lightweight material in the group of cellular materials which can provide to the material a combination of very specific characteristics, such as the ability to absorb high amounts of energy, potential for noise control, vibration damping and thermal insulation. Also, according to Sanders and Gibson (2003), hollow sphere structures can be manufactured from a broad range of materials and assembled in a periodic structure with relatively small number of imperfections. These factors show that this kind

of structures can play a significant role in technology and render this an important study subject.

5.1 OPTIMIZATION PROBLEMS

5.1.1 Linear Combination of the Components of the Homogenized Constitutive Tensor

The objective function, Φ , is given by the linear combination of the homogenized constitutive tensor, thus, one can write

$$\Phi = \sum_{i=1}^{21} \alpha_i C_i^H, \quad (5.1)$$

where α_i is an arbitrary scalar and C_i is the i -th component of the homogenized constitutive tensor. Accordingly, the optimization problem can be written as

$$\begin{aligned} & \underset{\rho}{\text{Maximize}} \quad \Phi(\rho) \\ & \text{Subject to} \quad \sum_{e=1}^n \rho_e v_e \leq V_f \\ & \quad \rho_{min} \leq \rho_e \leq 1, \end{aligned} \quad (5.2)$$

where ρ_e and v_e are, respectively, the pseudo density and the volume of the e -th element of the mesh and V_f is an admissible volume for the structure.

As the objective function is a linear combination, its derivatives are a linear combination as well. So, taking the derivatives of equation 5.1 with regard to the pseudo density of an element q of the finite element mesh, one can write

$$\frac{\partial \Phi}{\partial \rho_q} = \sum_{i=1}^{21} \alpha_i \frac{\partial C_i^H}{\partial \rho_q}. \quad (5.3)$$

At this point it becomes clear that to evaluate the derivative of the objective function, the derivatives of every component of the homogenized constitutive tensor must be obtained.

5.1.2 Target Tensor

The objective function Φ , for this case, is given by the L2 norm of the difference between the components of a given tensor and the homogenized tensor. Mathematically, one can write

$$\Phi = \|\mathbf{C}^H(\rho) - \mathbf{C}^*\|_2. \quad (5.4)$$

For the three-dimensional case, the equation 5.4 is written as

$$\Phi = \sqrt{\left(C_{ijkl}^H - C_{ijkl}^* \right)^2}, \quad (5.5)$$

where $i, j, k, l = 1, 2, 3$. Thus, the optimization problem can be defined as

$$\begin{aligned} & \text{Minimize}_{\rho} \quad \Phi(\rho) \\ & \text{Subject to} \quad \sum_{e=1}^n \rho_e v_e \leq V_f \\ & \quad \rho_{min} \leq \rho_e \leq 1. \end{aligned} \quad (5.6)$$

Throughout the chain rule is possible to find the derivatives of the objective function with regard to the pseudo-density of an element q of the mesh as

$$\frac{\partial \Phi}{\partial \rho_q} = \frac{1}{2 \sqrt{\left(C_{ijkl}^H - C_{ijkl}^* \right)^2}} 2 \left(C_{ijkl}^H - C_{ijkl}^* \right) \frac{\partial C_{ijkl}^H}{\partial \rho_q}. \quad (5.7)$$

Yet, using the equations 5.5 and 5.7, one obtains

$$\frac{\partial \Phi}{\partial \rho_q} = \frac{1}{\Phi} \left(C_{ijkl}^H - C_{ijkl}^* \right) \frac{\partial C_{ijkl}^H}{\partial \rho_q}. \quad (5.8)$$

As for the previous case, the evaluation of the derivatives of the homogenized components of the constitutive tensor with regard to the pseudo densities of the elements of the mesh is needed.

5.2 SENSITIVITY ANALYSIS

In order to find the derivatives of the objective function, one must find the derivatives of all components of the homogenized constitutive tensor with respect of the pseudo-density of each element of the mesh. From

the integral equation 2.24, the generic component C_{ijkl}^H of the homogenized tensor is given by

$$C_{ijkl}^H = \frac{1}{|Y|} \int_Y \left(C_{ijkl} - c_{ij}^T \partial \chi^{kl} \right) dY, \quad (5.9)$$

where c_{ij} is the column related to the indexes ij of the base material constitutive tensor and $\partial \chi^{kl}$ is the strain field of the unit cell in regard to the load case kl . Numerically, the equation 5.9 becomes

$$C_{ijkl}^H = \frac{1}{|Y|} \sum_{e=1}^n \sum_{m=1}^{ng} \left[\left(C_{ijkl} - c_{ij}^T \partial \chi_e^{kl} \right) W_m J_m \right], \quad (5.10)$$

where W_m is the quadrature weight, J_m is the determinant of Jacobian matrix, n is the number of elements used for the discretization of the domain and ng is the number of points used for the numerical integration. Using the SIMP to evaluate the effective properties of an element,

$$C = \rho_e^p C^0, \quad (5.11)$$

equation 5.10 becomes

$$C_{ijkl}^H = \frac{1}{|Y|} \sum_{e=1}^n \sum_{m=1}^{ng} \left[\left(\rho_e^p C_{ijkl}^0 - \rho_e^p (c_{ij}^0)^T \partial \chi_e^{kl} \right) W_m J_m \right]. \quad (5.12)$$

Writing the strain field, $\partial \chi_e^{kl}$, as

$$\partial \chi_e^{kl} = B_{em} \chi_e^{kl}, \quad (5.13)$$

where B_{em} is the strain-displacement matrix, which contains the derivatives of the shape functions of the e -th element in the m -th Gauss point, and a localization matrix H_e , which does the mapping between the global and local vectors as

$$\chi_e = H_e \chi, \quad (5.14)$$

one can write equation 5.12 as

$$C_{ijkl}^H = \frac{1}{|Y|} \sum_{e=1}^n \sum_{m=1}^{ng} \left[\left(\rho_e^p C_{ijkl}^0 - \rho_e^p (c_{ij}^0)^T B_{em} H_e \chi^{kl} \right) W_m J_m \right]. \quad (5.15)$$

As the displacement field χ^{kl} is a function of the elements pseudo-densities, the derivatives of the equation 5.15 contain the derivatives of the

displacement field with respect to the pseudo-densities. To avoid a costly evaluation of these derivatives, the adjoint method is used.

This method consists in adding a null therm to the equation, in this case, the equilibrium problem, given by

$$\mathbf{f}^{kl} = \mathbf{K}\chi^{kl} \Rightarrow \mathbf{K}\chi^{kl} - \mathbf{f}^{kl} = 0, \quad (5.16)$$

where \mathbf{K} is the global stiffness matrix and \mathbf{f}^{kl} is the global force vector, in order to obtain an auxiliary problem able to avoid the calculation of the derivatives of the displacement field. Adding the equilibrium problem to equation 5.15, one gets

$$\begin{aligned} C_{ijkl}^H &= \frac{1}{|Y|} \sum_{e=1}^n \sum_{m=1}^{ng} \left[\left(\rho_e^P C_{ijkl}^0 - \rho_e^P (c_{ij}^0)^T \mathbf{B}_{em} \mathbf{H}_e \chi^{kl} \right) W_m J_m \right] \\ &+ \lambda_{ij}^T [\mathbf{K}\chi^{kl} - \mathbf{f}^{kl}], \end{aligned} \quad (5.17)$$

where the λ_{ij} is the adjoint vector, that can be chosen as any vector, since the added therm has zero as value. The force global vector can be obtained through

$$\mathbf{f}^{kl} = \biguplus_{e=1}^n \mathbf{f}_e^{kl}, \quad (5.18)$$

where \mathbf{f}_e^{kl} is the force vector for the e -th element, given by

$$\mathbf{f}_e^{kl} = \frac{1}{|Y|} \int_Y \mathbf{B}_e^T c_{kl} dY. \quad (5.19)$$

The numerical solution of equation 5.19, using the SIMP for the effective properties, is

$$\mathbf{f}_e^{kl} = \frac{1}{|Y|} \sum_{m=1}^{ng} [\mathbf{B}_{em}^T \rho_e^P c_{kl} W_m J_m]. \quad (5.20)$$

Using the localization matrix, \mathbf{H}_e , equation 5.18 can be written as

$$\mathbf{f}^{kl} = \sum_{e=1}^n \mathbf{H}_e^T \mathbf{f}_e^{kl}, \quad (5.21)$$

and global force vector as

$$\mathbf{f}^{kl} = \frac{1}{|Y|} \sum_{e=1}^n \sum_{m=1}^{ng} [\mathbf{H}^T \mathbf{B}_{em}^T \rho_e^P c_{kl} W_m J_m]. \quad (5.22)$$

Finally, the homogenized component of the tensor, is given by

$$\begin{aligned} C_{ijkl}^H &= \frac{1}{|Y|} \sum_{e=1}^n \sum_{m=1}^{ng} \left[\left(\rho_e^P C_{ijkl}^0 - \rho_e^P (c_{ij}^0)^T B_{em} H_e \chi^{kl} \right) W_m J_m \right] \\ &\quad + \lambda_{ij}^T \left[K \chi^{kl} - \frac{1}{|Y|} \sum_{e=1}^n \sum_{m=1}^{ng} (H_e B_{em}^T \rho_e^P c_{kl}) W_m J_m \right]. \end{aligned} \quad (5.23)$$

The derivatives of the equation 5.23, with respect to the pseudo density of an element q of the mesh, are given by

$$\begin{aligned} \frac{\partial C_{ijkl}^H}{\partial \rho_q} &= \frac{1}{|Y|} \sum_{e=1}^n \sum_{m=1}^{ng} \left[\left(\frac{\partial \rho_e^P}{\partial \rho_q} C_{ijkl}^0 - \frac{\partial \rho_e^P}{\partial \rho_q} (c_{ij}^0)^T B_{em} H_e \chi^{kl} \right. \right. \\ &\quad \left. \left. - \rho_e^P (c_{ij}^0)^T B_{em} H_e \frac{\partial \chi^{kl}}{\partial \rho_q} \right) W_m J_m \right] + \lambda_{ij}^T \frac{\partial K}{\partial \rho_q} \chi^{kl} + \lambda_{ij}^T K \frac{\partial \chi^{kl}}{\partial \rho_q} \\ &\quad - \lambda_{ij}^T \frac{1}{|Y|} \sum_{e=1}^n \sum_{m=1}^{ng} \left[H_e^T B_{em}^T \frac{\partial \rho_e^P}{\partial \rho_q} c_{kl}^0 W_m J_m \right]. \end{aligned} \quad (5.24)$$

Collecting the terms that are dependent of the derivatives of the displacement field, one finds

$$\begin{aligned} \frac{\partial C_{ijkl}^H}{\partial \rho_q} &= \frac{1}{|Y|} \sum_{e=1}^n \sum_{m=1}^{ng} \left[\left(\frac{\partial \rho_e^P}{\partial \rho_q} C_{ijkl}^0 - \frac{\partial \rho_e^P}{\partial \rho_q} (c_{ij}^0)^T B_{em} H_e \chi^{kl} \right) W_m J_m \right] \\ &\quad + \lambda_{ij}^T \frac{\partial K}{\partial \rho_q} \chi^{kl} - \lambda_{ij}^T \frac{1}{|Y|} \sum_{e=1}^n \sum_{m=1}^{ng} \left[H_e^T B_{em}^T \frac{\partial \rho_e^P}{\partial \rho_q} c_{kl}^0 W_m J_m \right] \\ &\quad + \left(\lambda_{ij}^T K - \frac{1}{|Y|} \sum_{e=1}^n \sum_{m=1}^{ng} \rho_e^P (c_{ij}^0)^T B_{em} H_e W_m J_m \right) \frac{\partial \chi^{kl}}{\partial \rho_q}. \end{aligned} \quad (5.25)$$

As λ_{ij} is an arbitrary vector, it can be chosen in order to enforce to zero the therms multiplying the derivatives of the displacement field with regard to the pseudo densities (last line of equation 5.25). By doing so, one obtains an auxiliary problem, given by

$$\lambda_{ij}^T K = \frac{1}{|Y|} \sum_{e=1}^n \sum_{m=1}^{ng} \left[\rho_e^P (c_{ij}^0)^T B_{em} H_e W_m J_m \right], \quad (5.26)$$

which is used to find the derivatives of the homogenized constitutive tensor,

given by

$$\begin{aligned} \frac{\partial C_{ijkl}^H}{\partial p_q} &= \frac{1}{|Y|} \sum_{e=1}^n \sum_{m=1}^{ng} \left[\left(\frac{\partial p_e^P}{\partial p_q} C_{ijkl}^0 - \frac{\partial p_e^P}{\partial p_q} (c_{ij}^0)^T B_{em} H_e \chi^{kl} \right) W_m J_m \right] \\ &- \lambda_{ij}^T \frac{1}{|Y|} \sum_{e=1}^n \sum_{m=1}^{ng} \left[H_e^T B_{em}^T \frac{\partial p_e^P}{\partial p_q} c_{kl}^0 W_m J_m \right] \\ &+ \lambda_{ij}^T \frac{\partial K}{\partial p_q} \chi^{kl}. \end{aligned} \quad (5.27)$$

Using the Kronecker delta, defined as

$$\delta_{eq} = \begin{cases} 1 & \text{if } e = q \\ 0 & \text{if } e \neq q \end{cases}, \quad (5.28)$$

one can write

$$\frac{\partial p_e^P}{\partial p_q} = \delta_{eq} (P p_e^{P-1}). \quad (5.29)$$

The assembly of the global stiffness matrix is made by the operator

$$K = \biguplus_{e=1}^n p_e^P K_e, \quad (5.30)$$

and its derivatives are given by

$$\frac{\partial K}{\partial p_q} = \biguplus_{e=1}^n \frac{\partial p_e^P}{\partial p_q} K_e. \quad (5.31)$$

Finally, using the Kronecker delta, one can write equation 5.31 as

$$\frac{\partial K}{\partial p_q} = \biguplus_{e=1}^n \delta_{eq} P p_e^{P-1} K_e^0. \quad (5.32)$$

In summary, the auxiliary problem of equation 5.26 must be solved in order to obtain the derivatives of a component of the homogenized tensor with respect to an element of the mesh using equation 5.27. Equations 5.29 and 5.32 are used as auxiliary expressions.

Appendix D shows the validation of the sensitivity analysis by means of the central difference method.

5.3 ALGORITHM DESCRIPTION

This section describes an optimization problem involving porous materials. First, the data needed for the problem, in addition to the data used to find the homogenized coefficients, is shown, and then an algorithm is presented. All codes were written in the free Language Julia and the output files containing the topologies are written in order to be displayed in the free software Gmsh.

5.3.1 Data

Besides the data needed to determine the homogenized mechanical tensor, the optimization problem needs extra information for the procedure.

In relation to SIMP, the penalization factor, P , must be informed, as well as the relaxation parameter, η and the limits for the bisection algorithm. For the filtering scheme, the filtering radius, which indicates the size of the neighbourhood of an element, must be informed.

As two distinct optimization problems were suggested, one has to chose between the maximization of a linear combination of the components of the homogenized constitutive tensor and the approximation of a target constitutive tensor.

Also, one among three distinct optimization procedures must be chosen: the Optimum Criteria, the Sequential Linear Programming and the Method of Moving Asymptotes.

Finally, two distinct constraints can be used in the program. The first one is the volume constraint, in which a maximum volume for the RVE is adopted and the second one is a constraints that imposes that two components of the homogenized tensor have equal numerical values.

5.3.2 Optimization Problem

Figure 30 shows a summary of the topology algorithm developed, which takes the requirements for the macroscopic media and gives the distribution of densities of the base cell that better fits these requirements.

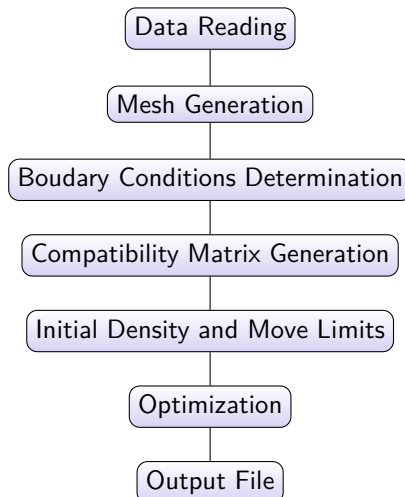
At first, the algorithm reads the data provided by the user, such as geometrical and material parameters and the requirements for the op-

timization procedure. The pre-processing consists in the mesh generation and the specification of the boundary conditions, the compatibility matrix for the periodicity consideration and the vectors containing the initial pseudo density and the move limits of each element of the mesh.

The optimization procedure follows figure 31, and it stops when a certain number of iterations is reached. At first the homogenized mechanical tensor is calculated, then the sensitivity analysis is made, that is to say, the gradient of the objective function and the gradient of the constraints are computed. The filtering method is applied in the gradient of the objective function and then the optimization procedure is called. Three optimization methods were implemented for solving the problem, the Optimum Criteria (OC), the Sequential Linear Programming (SLP) and the Method of Moving Asymptotes (MMA), and the user can choose between one of these methods to solve the problem. The vector of densities and the vector of moving limits are updated and the optimization procedure returns to the beginning.

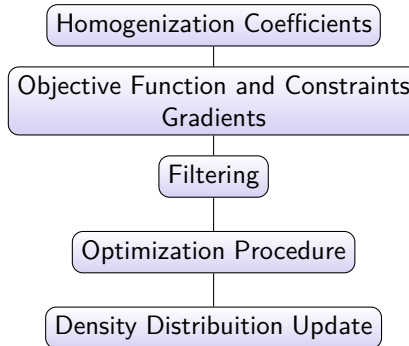
When the number of iterations is reached, the optimization procedure is ended and then the densities distribution is written in a text format, compatible with the software Gmsh, in order to visualize the RVE obtained topology.

Figure 30 – Algorithm of the optimization program



Source: Author's production, 2016.

Figure 31 – Algorithm of the optimization procedure



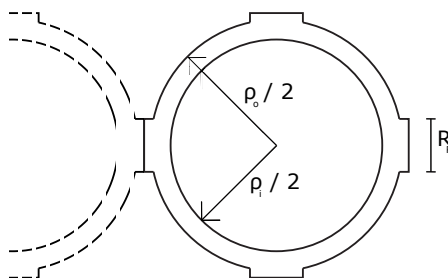
Source: Author's production, 2016.

5.4 ANALYSIS PROBLEM

The cellular materials chosen to be studied are the so called hollow sphere structures (HSS). Two different topologies are proposed and the homogenization method is used in order to evaluate the effective mechanical and thermal properties of this kind of structure.

The first model is shown in figure 32, where a RVE is represented in two dimensions for sake of simplicity. For a media formed by this kind of structure, two adjacent base cells are connected by a flat reinforcement. The domain is considered unitary and the geometry is described by three geometrical parameters, the internal diameter, ρ_i , the outer diameter ρ_o and the diameter of the reinforcement, R_R .

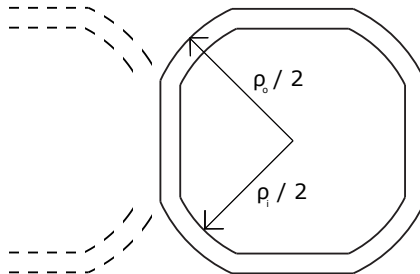
Figure 32 – Hollow sphere - model 1



Source: Author's production, 2016.

Figure 33 shows the base cell of the second case analysed. For this case, two adjacent spheres are connected by a flat area. Again, the domain is considered unitary. This model has two geometrical parameters, the outer diameter, ρ_o and the inside diameter, ρ_i and the flat area is a function of both parameters.

Figure 33 – Hollow sphere - model 2



Source: Author's production, 2016.

By varying the geometrical parameters of both base cells, and obtaining the homogenized mechanical and thermal properties of the media, one can generate a set of equations relating the geometrical parameters of the RVE and the effective properties of the media. Thus, a point cloud, relating the geometrical properties of the base cell and the effective properties, can be generated and the least square method can be used in order to approximate an equation for the properties.

5.4.1 Least Square Method

In order to find the homogenized components of the tensors in intermediate configurations, the least square method is used to adjust a surface based on the data given by the simulations. Using the Least Square Function, given by,

$$\Phi = \sqrt{\sum_{i=1}^{n_p} (f(\rho) - V_i)^2}, \quad (5.33)$$

where n_p is the number of simulations made, ρ is the vector containing the design variables and V_i is the value of a component of the tensor at the i -th simulation, it is possible to adjust the coefficients of the function

that better fit the simulations for some of the coefficients of the tensor. The optimal set of parameters is found when

$$\nabla_{\alpha} \Phi = \mathbf{0}, \quad (5.34)$$

where α is the vector containing the coefficients of the function f . When the gradient goes to zero, the minimum of the function is achieved, indicating that the coefficients which better fit the simulation points for that function were achieved.

6 RESULTS

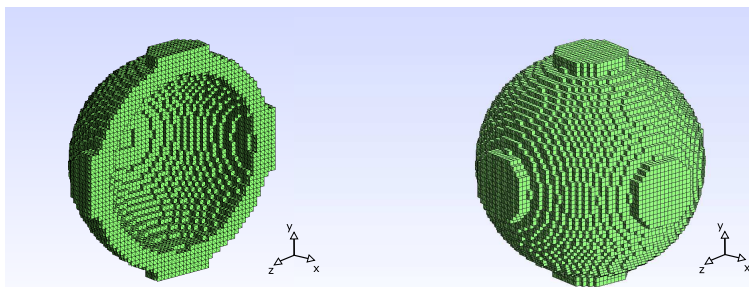
This chapter is divided in three main sections. The first one shows the results for the analysis case, in which the variation of the properties of a media formed by hollow spheres base cells in relation to the geometrical parameters of the base cell is investigated. The second section shows the results obtained for the maximization of a linear combination of the components of the mechanical homogenized tensor. The third section shows the topology of the base cells obtained that provides a better approximation for a given constitutive tensor.

6.1 EFFECTIVE PROPERTIES OF HOLLOW SPHERE STRUCTURES (HSS)

This section shows the results obtained for the analysis of two hollow spheres cellular material models. It is intended to show how the effective elasticity and thermal conductivity properties vary in terms of the geometrical parameters of the RVE.

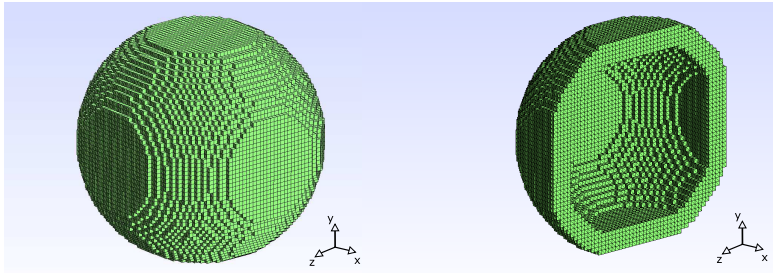
The discretization into finite elements of both geometries studied can be seen in figures 34 and 35, showing the distribution of material on the base cell and its cross-section for each case. The domain is an unit cube and is discretized by $50 \times 50 \times 50$ elements in all cases. The data used is shown in table 1, where the base material plays the role of an aluminium alloy.

Figure 34 – Hollow sphere structure - Case 1



Source: Author's production, 2016

Figure 35 – Hollow sphere structure - case 2



Source: Author's production, 2016

Table 1 – Simulation data

Young Modulus (E) [GPa]	70.0
Poisson (ν)	0.3
Thermal Conductivity (K_t) [$\text{Wm}^{-1}\text{K}^{-1}$]	237.0
Void Density (ρ_{min})	10^{-9}

6.1.1 Numerical Results

For both cases studied, the mechanical homogenized tensor has the form

$$C^h = \begin{bmatrix} C_{1111}^H & C_{1122}^H & C_{1133}^H & 0 & 0 & 0 \\ & C_{2222}^H & C_{2233}^H & 0 & 0 & 0 \\ & & C_{3333}^H & 0 & 0 & 0 \\ & & & C_{1212}^H & 0 & 0 \\ & & & & C_{2323}^H & 0 \\ & & & & & C_{1313}^H \end{bmatrix}, \quad (6.1)$$

sym.

in which $C_{1111}^H = C_{2222}^H = C_{3333}^H$, $C_{1122}^H = C_{1133}^H = C_{2233}^H$ and $C_{1212}^H = C_{2323}^H = C_{1313}^H$. The equalities on the components of the tensor indicate a cubic symmetry on the homogenized tensor, since the normal components in the three principal directions are equal to each other, and so are the three shear components, although, the shear components cannot be related with the normal and coupled normal components. The thermal conductivity tensor,

for both topologies, has the form

$$\mathbf{Kt}^H = \begin{bmatrix} kt_{11}^H & 0 & 0 \\ 0 & kt_{22}^H & 0 \\ 0 & 0 & kt_{33}^H \end{bmatrix}, \quad (6.2)$$

in which $kt_{11}^H = kt_{22}^H = kt_{33}^H$.

6.1.1.1 First Hollow Sphere Model

This section shows the results for the hollow sphere case where two adjacent spheres are joined together by a reinforcement. The finite model used is shown in figure 34 and the internal, external and reinforcement diameters are used as design variables, as shown in figure 32.

Figures 36, 37 and 38 show the variation of the components C_{1111}^H , C_{1122}^H and C_{1212}^H of the homogenized mechanical tensor, respectively. In all figures, one can see the variation of components as a function of the internal and external diameters of the hollow sphere and for four distinct values of reinforcements, R_R .

Figure 36 – C_{1111}^H values obtained for the first model

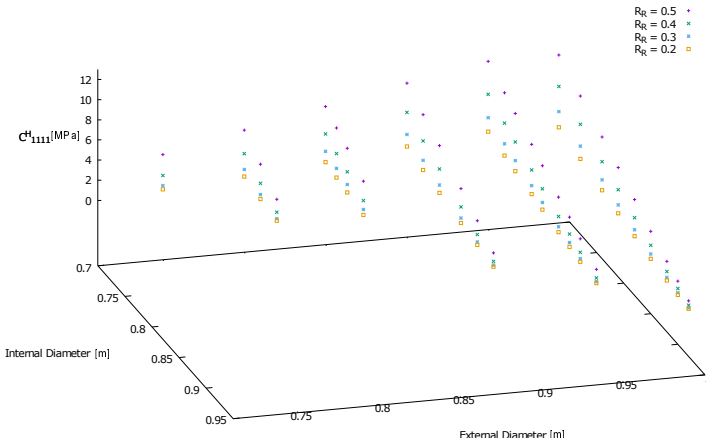
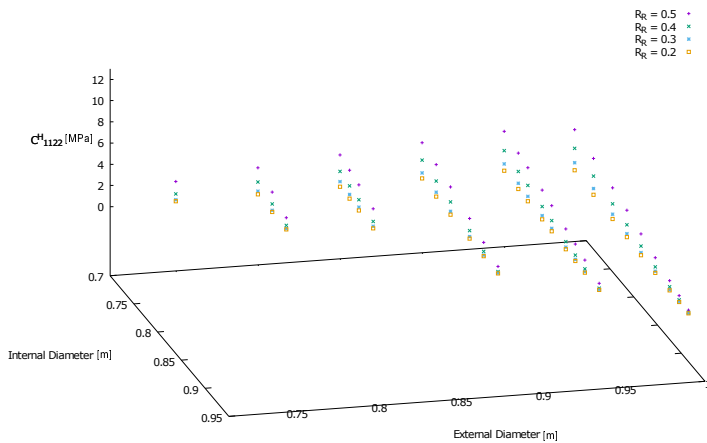
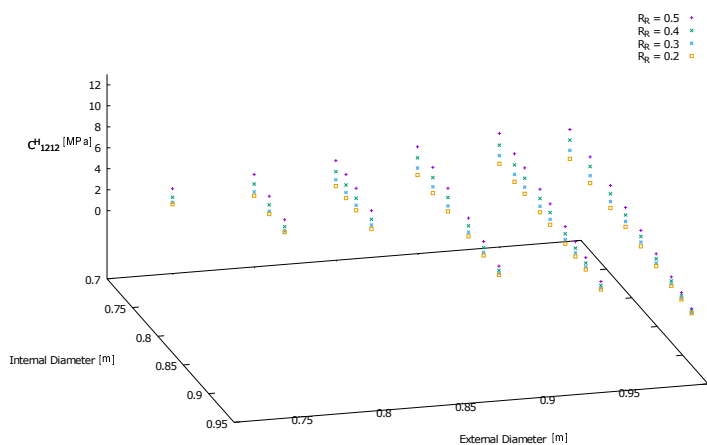


Figure 37 – C_{1122}^H values obtained for the first model



Source: Author's production, 2016

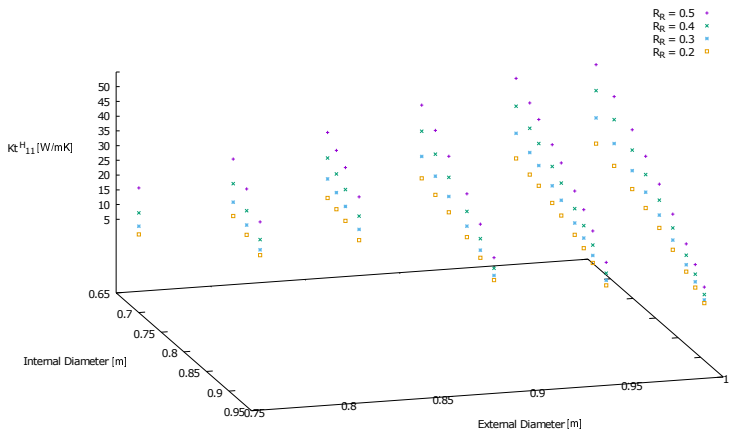
Figure 38 – C_{1212}^H values obtained for the first model



Source: Author's production, 2016

Figure 39 shows the component of the homogenized thermal conductivity tensor, as a function of the same variables as for the mechanical case.

Figure 39 – Kt_{11}^H values obtained for the first model



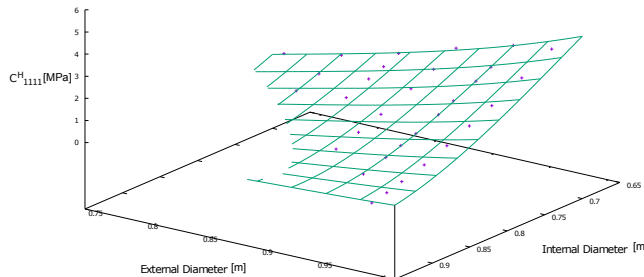
Source: Author's production, 2016

For this case, the inner diameter, the outer diameter and the reinforcement diameter are used to adjust an equation for each component of the tensors. It is presented a surface for each component and for each value of reinforcement, although a single equation for each component is obtained. The surfaces obtained are valid only if the internal diameter is smaller than the external diameter and in the regions where there are sampled points.

A complete third degree polynomial surface is used in order to avoid numerical ill behaviour that may be caused for an high order polynomial surface, expected for the big number of simulated points used for the approximation.

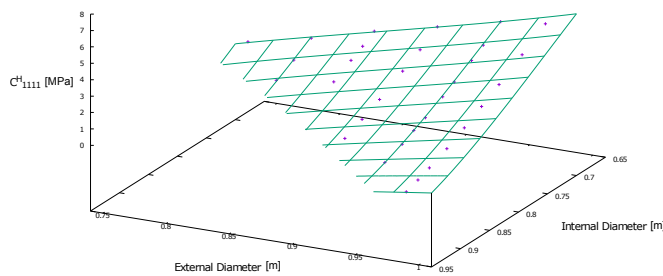
Figures 40, 41, 42 and 43 show the surfaces obtained to adjust the component C_{1111}^H of the homogenized elastic tensor for reinforcements of, respectively, $R_R = 0.2$, $R_R = 0.3$, $R_R = 0.4$ and $R_R = 0.5$.

Figure 40 – Surface and simulated points for the C_{1111}^H component, reinforcement of $R_R = 0.2$



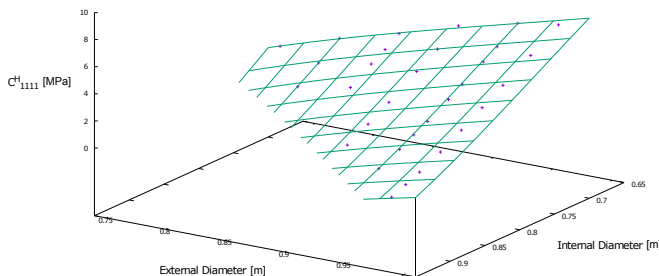
Source: Author's production, 2016

Figure 41 – Surface and simulated points for the C_{1111}^H component, reinforcement of $R_R = 0.3$



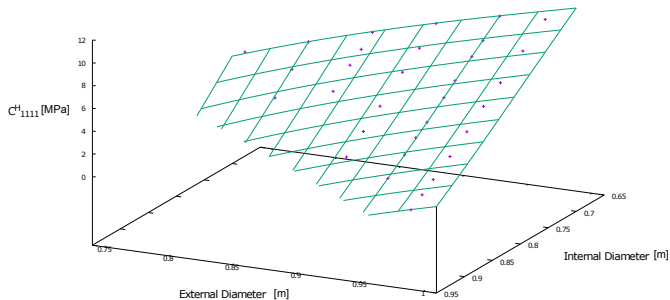
Source: Author's production, 2016

Figure 42 – Surface and simulated points for the C_{1111}^H component, reinforcement of $R_R = 0.4$



Source: Author's production, 2016

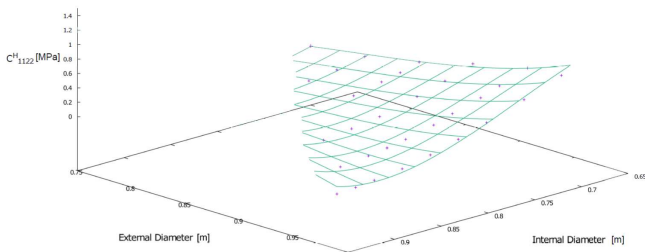
Figure 43 – Surface and simulated points for the C_{1111}^H component, reinforcement of $R_R = 0.5$



Source: Author's production, 2016

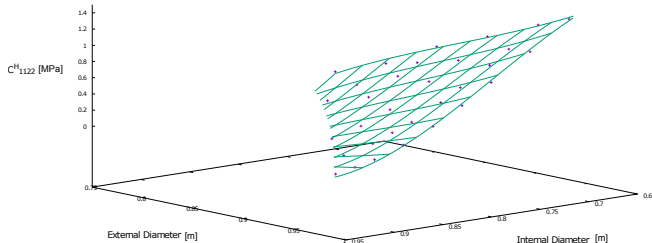
Figures 44, 45, 46 and 47 show the surfaces obtained to adjust the component C_{1122}^H of the homogenized elastic tensor for reinforcements of, respectively, $R_R = 0.2$, $R_R = 0.3$, $R_R = 0.4$ and $R_R = 0.5$.

Figure 44 – Surface and simulated points for the C_{1122}^H component, reinforcement of $R_R = 0.2$



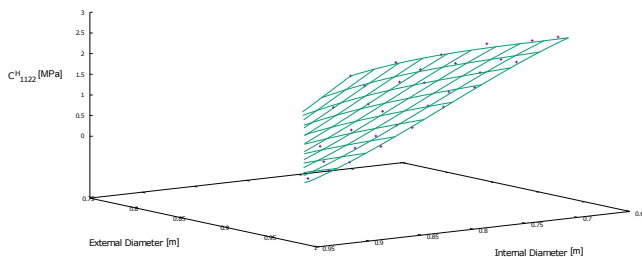
Source: Author's production, 2016

Figure 45 – Surface and simulated points for the C_{1122}^H component, reinforcement of $R_R = 0.3$



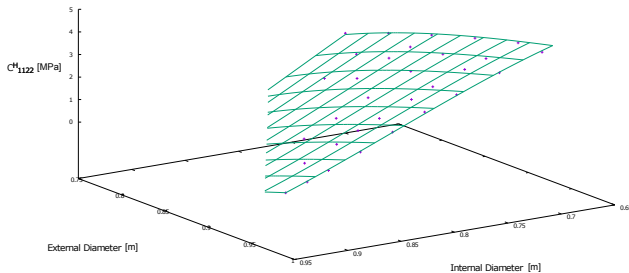
Source: Author's production, 2016

Figure 46 – Surface and simulated points for the C_{1122}^H component, reinforcement of $R_R = 0.4$



Source: Author's production, 2016

Figure 47 – Surface and simulated points for the C_{1122}^H component, reinforcement of $R_R = 0.5$

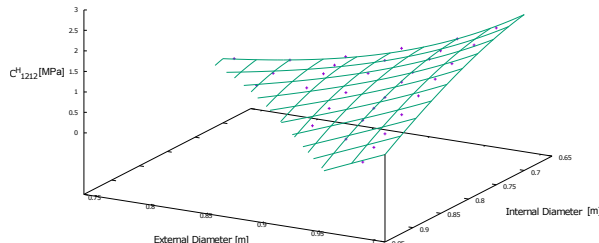


Source: Author's production, 2016

Figures 48, 49, 50 and 51 show the surfaces obtained to adjust

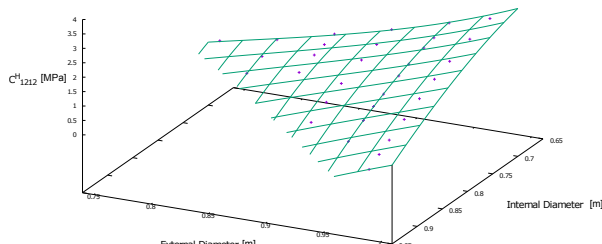
the component C_{1212}^H of the homogenized elastic tensor for reinforcements of, respectively, $R_R = 0.2$, $R_R = 0.3$, $R_R = 0.4$ and $R_R = 0.5$.

Figure 48 – Surface and simulated points for the C_{1212}^H component, reinforcement of $R_R = 0.2$



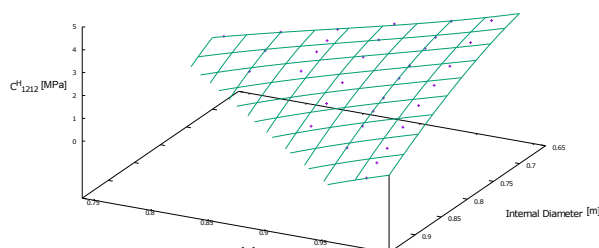
Source: Author's production, 2016

Figure 49 – Surface and simulated points for the C_{1212}^H component, reinforcement of $R_R = 0.3$



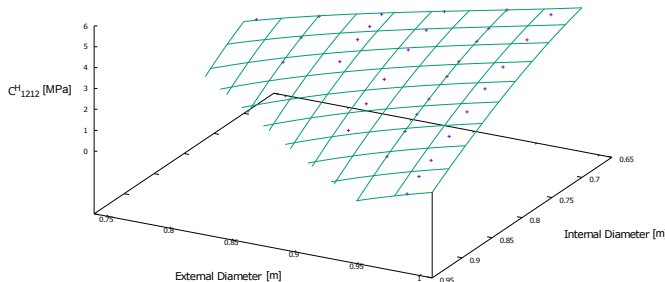
Source: Author's production, 2016

Figure 50 – Surface and simulated points for the C_{1212}^H component, reinforcement of $R_R = 0.4$



Source: Author's production, 2016

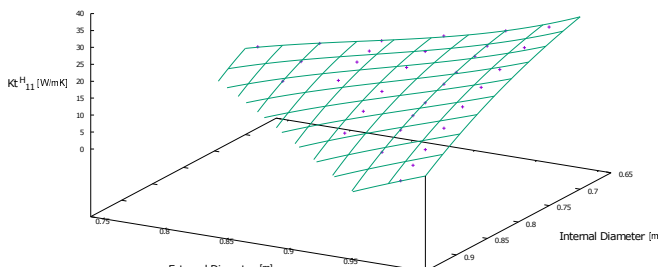
Figure 51 – Surface and simulated points for the C_{1212}^H component, reinforcement of $R_R = 0.5$



Source: Author's production, 2016

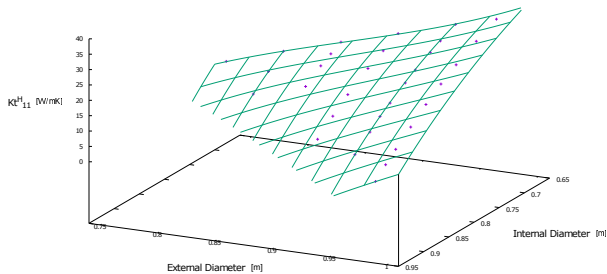
Figures 52, 53, 54 and 55 show the surfaces obtained to adjust the component Kt_{11}^H of the homogenized conductivity thermal tensor for reinforcements of, respectively, $R_R = 0.2$, $R_R = 0.3$, $R_R = 0.4$ and $R_R = 0.5$.

Figure 52 – Surface and simulated points for the Kt_{11}^H component, reinforcement of $R_R = 0.2$



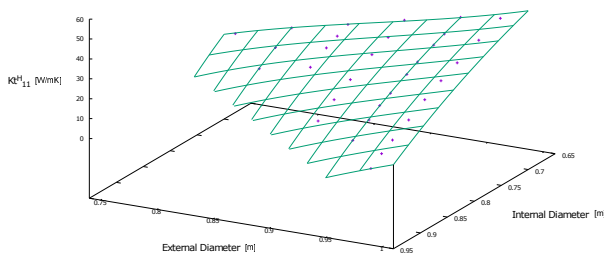
Source: Author's production, 2016

Figure 53 – Surface and simulated points for the Kt_{11}^H component, reinforcement of $R_R = 0.3$



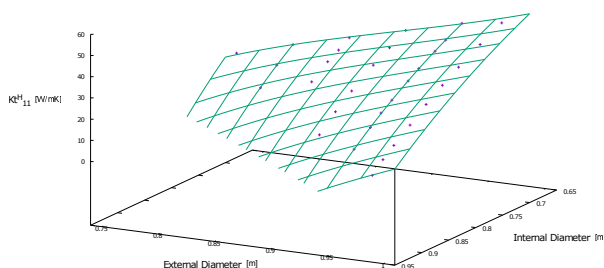
Source: Author's production, 2016

Figure 54 – Surface and simulated points for the Kt_{11}^H component, reinforcement of $R_R = 0.4$



Source: Author's production, 2016

Figure 55 – Surface and simulated points for the Kt_{11}^H component, reinforcement of $R_R = 0.5$



Source: Author's production, 2016

The components of the mechanical and thermal homogenized tensors can be determinated by the equations,

$$\begin{aligned} C_{1111}^H &= 26.06R_R^3 + 44.12\rho_o R_R^2 - 146.90\rho_i R_R^2 + 81.59R_R^2 \\ &- 131.27\rho_o^2 R_R + 251.15\rho_i \rho_o R_R + 77.64\rho_o R_R - 68.30\rho_i^2 R_R \\ &- 121.68\rho_i R_R - 4.90R_R + 42.85\rho_o^3 - 84.52\rho_i \rho_o^2 \\ &- 11.34\rho_o^2 - 101.70\rho_i^2 \rho_o + 219.93\rho_i \rho_o - 71.65\rho_o \\ &+ 84.37\rho_i^3 - 65.94\rho_i^2 - 45.15\rho_i + 33.45 \quad [\text{MPa}], \end{aligned}$$

$$\begin{aligned} C_{1122}^H &= 10.10R_R^3 + 23.55\rho_o R_R^2 - 51.50\rho_i R_R^2 + 33.70R_R^2 \\ &- 82.60\rho_o^2 R_R + 205.59\rho_i \rho_o R_R + 11.25\rho_o R_R - 158.84\rho_i^2 R_R \\ &+ 37.26\rho_i R_R - 26.78R_R + 43.66\rho_o^3 - 84.24\rho_i \rho_o^2 \\ &- 29.24\rho_o^2 - 77.04\rho_i^2 \rho_o + 205.43\rho_i \rho_o - 52.06\rho_o \\ &+ 121.32\rho_i^3 - 156.14\rho_i^2 + 18.81\rho_i + 13.545 \quad [\text{MPa}], \end{aligned}$$

$$\begin{aligned} C_{1212}^H &= -5.03R_R^3 - 38.53\rho_o R_R^2 - 9.64\rho_i R_R^2 + 56.47R_R^2 \\ &- 104.34\rho_o^2 R_R + 86.13\rho_i \rho_o R_R + 168.32\rho_o R_R - 42.90\rho_i^2 R_R \\ &- 41.77\rho_i R_R - 70.30R_R + 60.63\rho_o^3 - 200.20\rho_i \rho_o^2 \\ &+ 27.35\rho_o^2 + 103.43\rho_i^2 \rho_o + 194.80\rho_i \rho_o - 129.43\rho_o \\ &+ 18.26\rho_i^3 - 153.24\rho_i^2 + 49.29\rho_i + 29.85 \quad [\text{MPa}], \end{aligned}$$

$$\begin{aligned} Kt_{11}^H &= 22.18R_R^3 - 478.80\rho_o R_R^2 + 163.70\rho_i R_R^2 + 336.33R_R^2 \\ &- 490.54\rho_o^2 R_R + 805.19\rho_i \rho_o R_R + 799.87\rho_o R_R - 140.194\rho_i^2 R_R \\ &- 976.21\rho_i R_R - 16.88R_R + 810.61\rho_o^3 - 1964.54\rho_i \rho_o^2 \\ &- 553.47\rho_o^2 + 1001.49\rho_i^2 \rho_o + 2079.92\rho_i \rho_o - 435.75\rho_o \\ &- 137.13\rho_i^3 - 815.66\rho_i^2 - 156.49\rho_i + 172.95 \quad [\text{Wm}^{-1}\text{K}^{-1}], \end{aligned}$$

where R_R is the diameter of the reinforcement, ρ_i and ρ_o are, respectively, the inner and the outer diameters of the hollow sphere.

6.1.1.2 Second Hollow Sphere Model

For the case in which two adjacent spheres are connected by a flat area, as shown in figure 33, the components of the mechanical and thermal conductivity homogenized tensor are shown as a function of the external and internal diameters of the hollow sphere. The flat area is determined as a function of the both diameters, enforcing that the whole sphere has the same thickness. The finite element model is shown in figure 35.

Figures 56, 57, 58 and 59 show the variation of components C_{1111}^H , C_{1212}^H and C_{1122}^H of the homogenized elasticity tensor and Kt_{11}^H of the homogenized thermal, respectively.

Figure 56 – C_{1111}^H values obtained for the second model

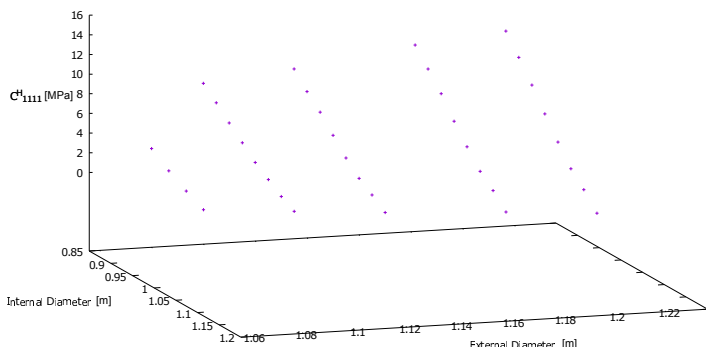
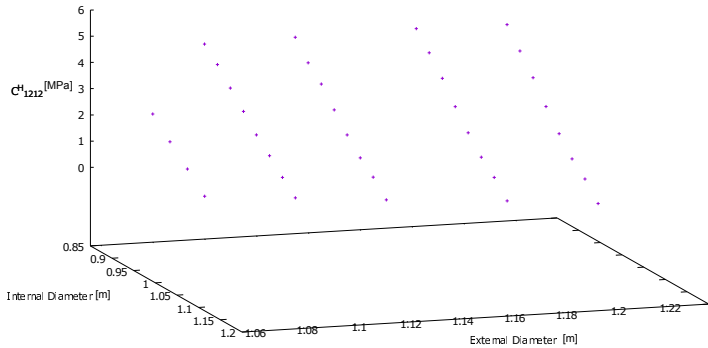
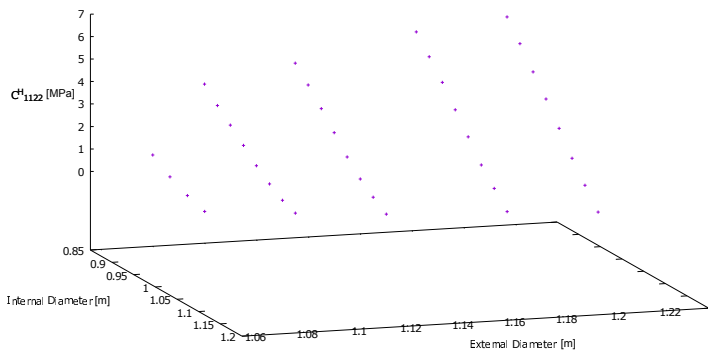


Figure 57 – C_{1212}^H values obtained for the second model

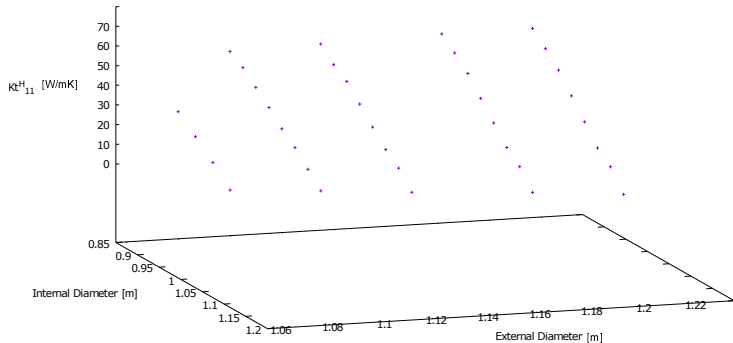


Source: Author's production, 2016

Figure 58 – C_{1122}^H values obtained for the second model



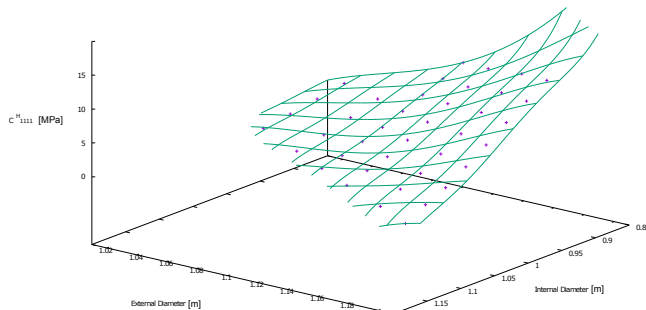
Source: Author's production, 2016

Figure 59 – Kt_{11}^H values obtained for the second model

Source: Author's production, 2016

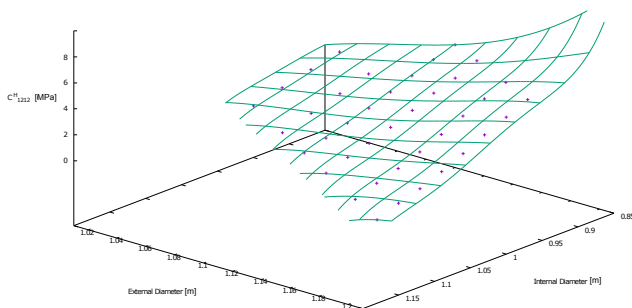
For this case, the inner and outer diameters of the hollow sphere are used to adjust a fifth order polynomial surface to the simulated data. Numerical bad behaviour were observed for higher orders on the adjustment of the surfaces. As for the previous case, the surfaces obtained are valid when the internal diameter is smaller than the external diameter and where there are sampled points.

Figures 60, 61, 62 and 63 show the surfaces obtained for the components C_{1111}^H , C_{1212}^H and C_{1122}^H of the homogenized elasticity tensor and Kt_{11}^H of the homogenized thermal, respectively.

Figure 60 – Surface and simulated points for C_{1111}^H 

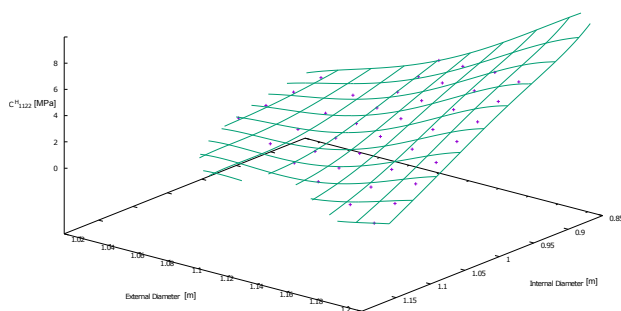
Source: Author's production, 2016

Figure 61 – Surface and simulated points for C_{1212}^H



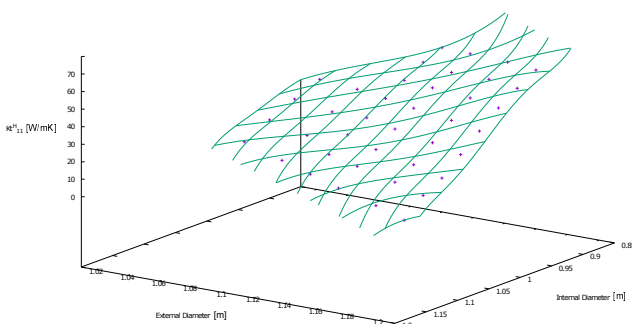
Source: Author's production, 2016

Figure 62 – Surface and simulated points for C_{1112}^H



Source: Author's production, 2016

Figure 63 – Surface and simulated points for Kt_{11}^H



Source: Author's production, 2016

The components of the tensors can be obtained by

$$\begin{aligned} C_{1111}^H &= -36851.09\rho_o^5 - 143951.33\rho_i\rho_o^4 + 319371.33\rho_o^4 + 445271.42\rho_i^2\rho_o^3 \\ &- 203868.68\rho_i\rho_o^3 - 564869.50\rho_o^3 - 553081.38\rho_i^3\rho_o^2 + 102800.87\rho_i^2\rho_o^2 \\ &+ 230403.45\rho_i\rho_o^2 + 504778.69\rho_o^2 + 347902.52\rho_i^4\rho_o - 110446.77\rho_i^3\rho_o \\ &+ 52830.71\rho_i^2\rho_o - 201584.61\rho_i\rho_o - 205423.15\rho_o - 84237.18\rho_i^5 \\ &+ 20030.83\rho_i^4 + 22039.32\rho_i^3 - 42914.18\rho_i^2 + 76875.36\rho_i \\ &+ 24921.40 \quad [\text{MPa}], \end{aligned}$$

$$\begin{aligned} C_{1122}^H &= -1560.00\rho_o^5 - 18751.25\rho_i\rho_o^4 + 11531.95\rho_o^4 + 62594.92\rho_i^2\rho_o^3 \\ &- 35324.86\rho_i\rho_o^3 + 23523.66\rho_o^3 - 64338.91\rho_i^3\rho_o^2 - 18434.66\rho_i^2\rho_o^2 \\ &+ 70668.90\rho_i\rho_o^2 - 81965.11\rho_o^2 + 41798.35\rho_i^4\rho_o - 22445.51\rho_i^3\rho_o \\ &+ 53199.48\rho_i^2\rho_o - 82681.88\rho_i\rho_o + 82582.43\rho_o - 11526.87\rho_i^5 \\ &+ 10285.98\rho_i^4 - 6854.88\rho_i^3 - 13581.88\rho_i^2 + 28768.71\rho_i \\ &- 27488.29 \quad [\text{MPa}], \end{aligned}$$

$$\begin{aligned} C_{1212}^H &= -11729.13\rho_o^5 - 28798.39\rho_i\rho_o^4 + 87755.58\rho_o^4 + 141984.66\rho_i^2\rho_o^3 \\ &- 140792.10\rho_i\rho_o^3 - 118017.64\rho_o^3 - 200614.77\rho_i^3\rho_o^2 + 99462.67\rho_i^2\rho_o^2 \\ &+ 138420.48\rho_i\rho_o^2 + 76426.99\rho_o^2 + 132996.72\rho_i^4\rho_o - 64118.51\rho_i^3\rho_o \\ &- 14873.43\rho_i^2\rho_o - 94516.34\rho_i\rho_o - 13548.79\rho_o - 32937.03\rho_i^5 \\ &+ 10527.23\rho_i^4 + 15146.01\rho_i^3 - 10106.84\rho_i^2 + 32067.81\rho_i \\ &- 4735.81 \quad [\text{MPa}], \end{aligned}$$

$$\begin{aligned} Kt_{11}^H &= -187634.72\rho_o^5 - 616855.47\rho_i\rho_o^4 + 1579529.74\rho_o^4 + 2887243.37\rho_i^2\rho_o^3 \\ &- 2762467.12\rho_i\rho_o^3 - 2081219.45\rho_o^3 - 4186231.64\rho_i^3\rho_o^2 + 2403743.13\rho_i^2\rho_o^2 \\ &+ 2274302.55\rho_i\rho_o^2 + 1473847.44\rho_o^2 + 2704782.61\rho_i^4\rho_o - 1105834.82\rho_i^3\rho_o \\ &- 1036963.33\rho_i^2\rho_o - 1029394.96\rho_i\rho_o - 506587.66\rho_o - 647953.96\rho_i^5 \\ &+ 117296.50\rho_i^4 + 387351.16\rho_i^3 - 2820.61\rho_i^2 + 297022.48\rho_i \\ &+ 38836.78 \quad \left[\text{Wm}^{-1}\text{K}^{-1} \right], \end{aligned}$$

where ρ_i and ρ_o are, respectively, the inner and outer diameters of the hollow sphere.

6.1.2 Summary

In this section an analysis problem regarding porous materials was shown. The properties of two distinct hollow spheres models, with respect to the geometrical parameters of the RVE, were obtained. The interpolation approach, used to evaluate the effective properties, and the finite element structured mesh, were chosen in order to make the analysis problem compatible with a topology optimization problem.

The validation of the algorithm, presented in appendix C, shows that the homogenization by asymptotic expansion method provides good results for the determination of effective properties of a porous media in comparison with results of the literature. Thus, the present work can be used with a good accuracy within its limitations.

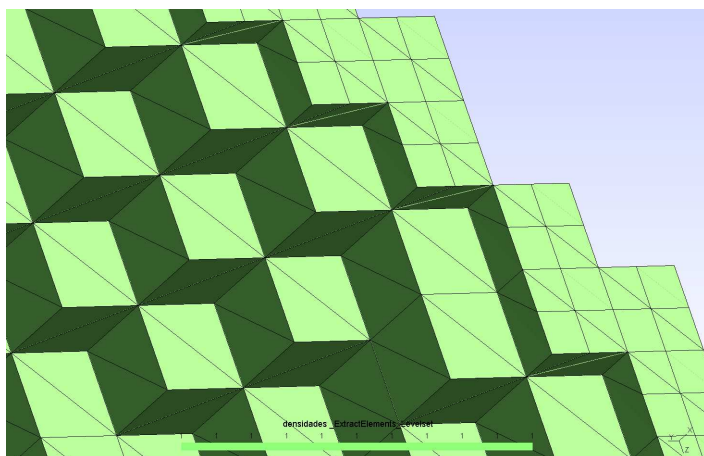
The expressions obtained for the determination of the effective properties of the media open a wide range of possibilities concerning the manufacturing of these materials. Several combinations of the geometrical parameters of the hollow spheres were analysed, thus, the designer can chose the material bearing in mind its manufacturing limitations.

Also, with the equations obtained is possible to design a macroscopic structure. For instance, it is possible to use these equations alongside an optimization procedure in order to find the best distribution of hollow spheres in the domain that extremizes some requirement of the structure.

In all surfaces analysed, the points whose inner and outer diameters of the hollow sphere are near to each other, in other words, the thickness of the hollow sphere is small, the behaviour of the surface is not regular, and at these points the error presented is higher than in other regions of the surface. This behaviour is due, basically, to the discretization of the domain. It is not possible to represent the thin thickness with a good accuracy with the finite element mesh used. Figure 64 shows a cross section of a hollow sphere with the smallest thickness evaluated. One can see a region where two elements are connected only by the edges. This fact induces the domain to have a smaller stiffness, behaviour that was observed in the simulated points in comparison with the surface obtained.

If these points are removed from the approximation, the results improve substantially. The maximum relative errors between the surface and the simulated points, for the first and second cases are shown, respectively, in tables 2 and 3. As one can see, the larger errors occur in the C_{1122}^H component of the mechanical tensor.

Figure 64 – Mesh detail



Source: Author's production, 2016

Table 2 – Maximum error - Case 1

Component	Maximum Error (%)
C_{1111}^H	10.85
C_{1212}^H	7.48
C_{1122}^H	12.16
Kt_{11}^H	3.68

Table 3 – Maximum error - Case 2

Component	Maximum Error (%)
C_{1111}^H	4.94
C_{1212}^H	3.19
C_{1122}^H	6.32
Kt_{11}^H	3.76

Also, it is noted that for the first case the errors were considerably larger than for the second case. This can be explained by the amount of

points in each case. For the first case, three design variables were used, instead of the two for the second case, which induces a greater number of points used to adjust an equation for all the simulated points. As the least square method is sensitive to the number of sampled points, larger errors may be achieved for the case with three design variables.

Furthermore, it is interesting to consider the symmetry of the domain, that induces to analyse only an eighth of the domain, increasing the refinement of the mesh. This approach is not possible with the homogenization method used, due to the fact that the displacement, or temperature, field on opposite faces of the RVE must have the same shape. With the symmetry consideration, this consideration can not be imposed, rendering the problem not suitable.

The best way to improve the results for small thickness of the hollow sphere is a refinement of the mesh. The main issue associated with this, is the computational effort. For the presented problem a $50 \times 50 \times 50$ element mesh is used, leading to the maximum computational effort of the equipment used. In comparison, five distinct finite element meshes were used in order to obtain the homogenized properties of a random media. The processing time and the computational effort were obtained, and table 4 shows the results.

Table 4 – Computational effort

Mesh	time (s)	RAM (Gb)
$10 \times 10 \times 10$	15.5	1.7
$20 \times 20 \times 20$	38.4	2.4
$30 \times 30 \times 30$	199.9	3.2
$40 \times 40 \times 40$	244.5	4.7
$50 \times 50 \times 50$	602.0	7.9

6.2 MAXIMIZATION OF THE COMPONENTS OF THE HOMOGENIZED TENSOR

This section shows the results obtained for the maximization of a linear combination of the components of the homogenized fourth order elasticity tensor. Three distinct problems are addressed. The first one is the linear combination of the components C_{1111}^H and C_{2323}^H . The second one is the linear combination of C_{1212}^H , C_{2323}^H and C_{1313}^H , and the third one

is the linear combination of C_{1111}^H , C_{2222}^H and C_{3333}^H . The first case aims at showing how the topology obtained is dependent on the initial topology, the second case aims to show the variation of the obtained topologies with the volume fraction variation and the third one aims to show the influence of the finite element mesh discretization. An unit RVE is used in all cases and table 5 shows the data used in all the simulations, where the base material chosen plays the role of an steel alloy.

Table 5 – Simulation data

Young's Modulus (E) [GPa]	200.0
Poisson's Modulus (v)	0.3
Minimum Density (ρ_{min})	10^{-3}
Penalization (P)	3.0
Filtering Radius (R)[m]	0.07

6.2.1 Maximization of the Linear Combination of the Components 1111 and 2323 of the Homogenized Tensor

The first case studied is the maximization of the linear combination

$$C_{1111}^H + C_{2323}^H,$$

meaning that is required the maximization of the normal stiffness on the x direction and the shear stiffness on yz plane. The domain is discretized by $40 \times 40 \times 40$ elements and the admissible volume of the structure, V_f , is constant and equals to 55% of the RVE's total volume.

The optimization problem can be set as

$$\begin{aligned} & \text{Maximize}_{\rho} \quad C_{1111}^H + C_{2323}^H \\ & \text{Subject to} \quad V \leq V_f, \end{aligned} \tag{6.3}$$

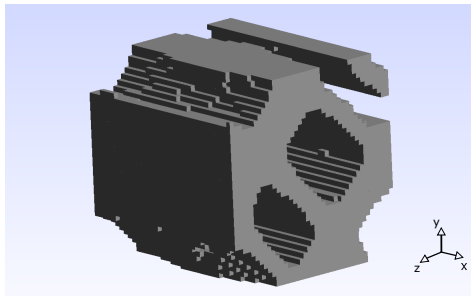
where V is the volume of the structure. The optimization procedure adopted is the Optimum Criteria.

Three distinct initial topologies are used for this case. The first one is an initial cell with a completely random distribution of pseudo-densities. The second one is an initial cell with a reinforcement in each principal

plane, namely, one reinforcement on xy plane, one on yz plane and one on xz plane of the RVE. The third initial topology is a RVE which a sphere is removed from its centre.

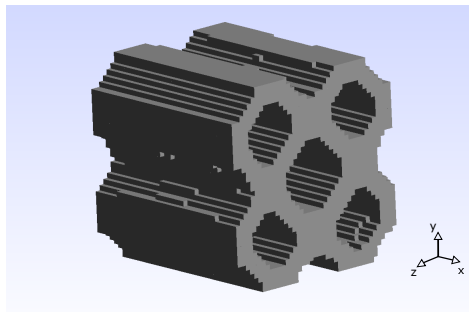
Figures 65, 66 and 67 show the final topologies obtained for the three initial density distributions, respectively.

Figure 65 – Maximization of $C_{1111}^H + C_{2323}^H$, topology obtained for the first initial material distribution



Source: Author's production, 2016.

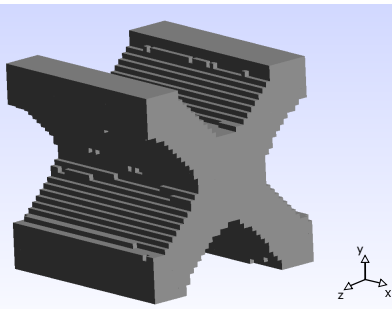
Figure 66 – Maximization of $C_{1111}^H + C_{2323}^H$, topology obtained for the second initial material distribution



Source: Author's production, 2016.

The numerical results obtained are shown in table 6. The topologies and the numerical results show that this problem does not have an unique solution. The result obtained for the first initial topology clearly differs from the other two. As an initial random distribution of material was used, it is not possible to guarantee a symmetry of the RVE. Also, it can be seen in the first topology obtained that there is no contact in

Figure 67 – Maximization of $C_{1111}^H + C_{2323}^H$, topology obtained for the third initial material distribution



Source: Author's production, 2016.

one section of the figure. This is physically impossible, but mathematically the topology obtained is possible, since that this part contributes to the normal stiffness on x direction.

The results obtained from the second and third initial topologies are very similar, as well as its topologies, when the porous media is considered. The slightly difference is the complete symmetry of the unit cell, present on the third case but not on the second, due to the fact that this topology have different hole sizes.

Nevertheless, one can notice, for all topologies obtained, that there are reinforcements with 45° in yz plane, associated with the shear stiffness, and normal reinforcements on x direction, associated with the normal stiffness, as expected.

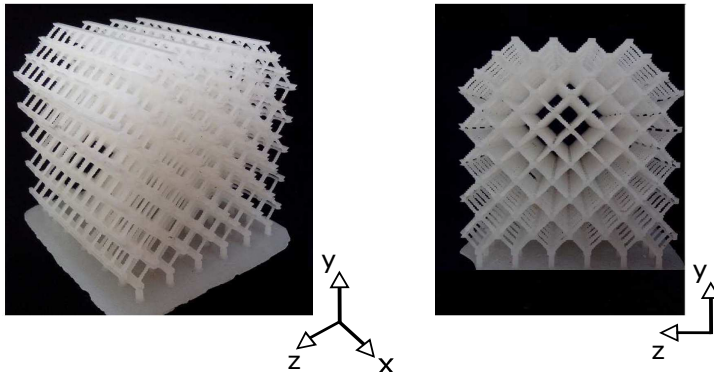
Table 6 – Components 1111 and 2323 of the homogenized tensor

	C_{1111}^H [GPa]	C_{2323}^H [GPa]
Initial Topology 1	123.59	30.21
Initial Topology 2	126.38	31.00
Initial Topology 3	126.80	31.96

Finally, a case with a different bound of relative volume, 10%, is performed in order to manufacture the media relative to the obtained RVE. Figure 68 shows the media formed by the repetition of six base cells

in each direction, that was printed using a Projet 3D 1000 printer. One can see the reinforcements on the x direction and the 45° reinforcements in yz plane in the global domain.

Figure 68 – Maximization of the components 1111 e 2323



Source: Author's production, 2016.

6.2.2 Maximization of the Linear Combination of the Components 1212, 2323 and 1313 of the Homogenized Tensor

For this case, it is required the maximization of the linear combination

$$C_{1212}^H + C_{2323}^H + C_{1313}^H, \quad (6.4)$$

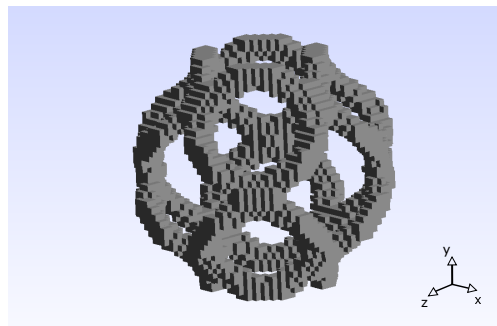
meaning that the maximization of the shear stiffness on the three planes simultaneously is required. Several volumes for the structure are used, and restrictions of equality among the three shear components of the homogenized tensor are imposed. The RVE is discretized by $40 \times 40 \times 40$ elements and, for all cases, the initial material distribution is the same. The optimization problem can be set as

$$\begin{aligned} & \text{Maximize}_{\rho} \quad C_{1212}^H + C_{2323}^H + C_{1313}^H \\ & \text{Subject to} \quad V \leq V_f \\ & \quad |C_{1212}^H - C_{1313}^H| \leq tol \\ & \quad |C_{2323}^H - C_{1313}^H| \leq tol \\ & \quad |C_{1212}^H - C_{2323}^H| \leq tol, \end{aligned} \quad (6.5)$$

where tol is a small scalar adopted to ensure that the constrained components have close values. As more constraints are used besides the volume constraint, the optimum criteria can not be used. Due to this fact, the Sequential Linear Programming is used as optimization procedure.

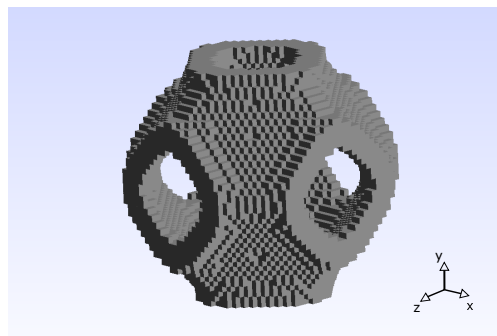
Figures 69, 70, 71 and 72 show the topologies obtained for the base cell with relative volumes of 10%, 20%, 30% and 40%, respectively, and table 7 shows the numerical results.

Figure 69 – Maximization of $C_{1212}^H + C_{2323}^H + C_{1313}^H$, $V_f = 0.1$



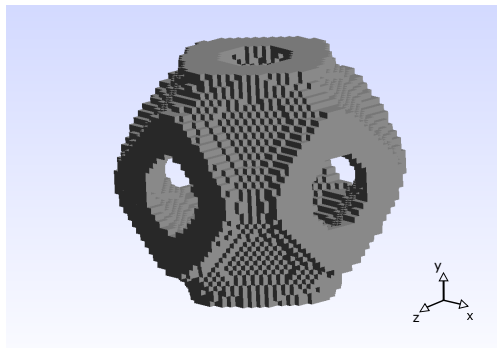
Source: Author's production, 2016.

Figure 70 – Maximization of $C_{1212}^H + C_{2323}^H + C_{1313}^H$, $V_f = 0.2$



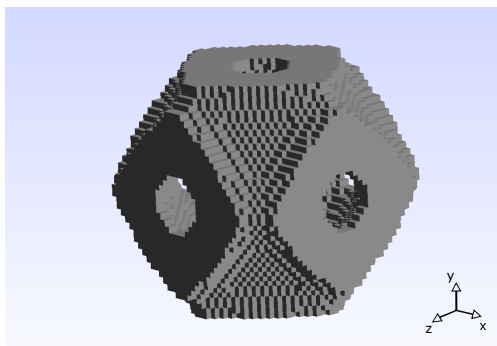
Source: Author's production, 2016.

Figure 71 – Maximization of $C_{1212}^H + C_{2323}^H + C_{1313}^H$, $V_f = 0.3$



Source: Author's production, 2016.

Figure 72 – Maximization of $C_{1212}^H + C_{2323}^H + C_{1313}^H$, $V_f = 0.4$



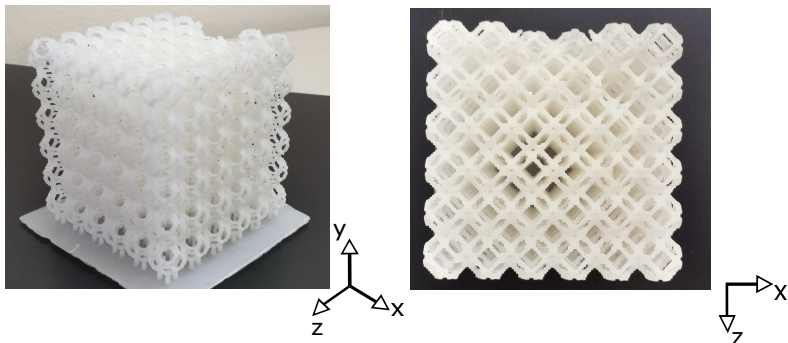
Source: Author's production, 2016.

Table 7 – Shear components of the homogenized tensor

Volume Fraction	$C_{1212}^H, C_{2323}^H, C_{1313}^H$ [GPa]
0.1	2.74
0.2	7.95
0.3	12.88
0.4	18.75

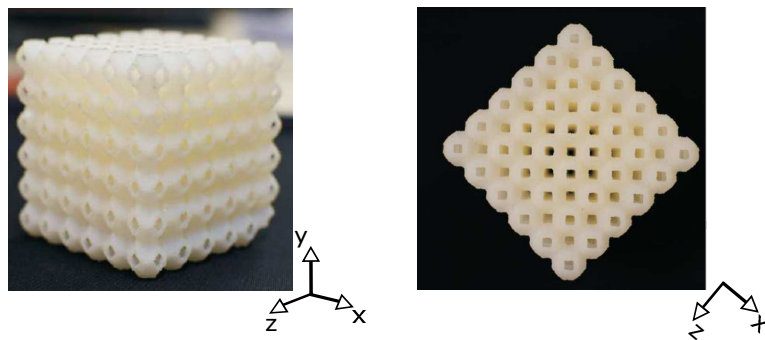
As can be seen in all topologies, there are 45° reinforcements in the three planes. As a way of enlightenment, two prototypes were printed using the Projet 1000 3D printer, the first using the base cell of figure 69 and the second using the base cell of figure 70. The prototypes are shown in figures 73 and 74, in which it becomes clear the reinforcements of 45° in all planes, condition expected for the increasing of the shear stiffness on the three planes of the media.

Figure 73 – Maximization of $C_{1212}^H + C_{2323}^H + C_{1313}^H$, media with $V_f = 0.1$



Source: Author's production, 2016.

Figure 74 – Maximization of $C_{1212}^H + C_{2323}^H + C_{1313}^H$, media with $V_f = 0.2$



Source: Author's production, 2016.

6.2.3 Maximization of the Linear Combination of the Components 1111, 2222 and 3333 of the Homogenized Tensor

This cases addresses the maximization of the linear combination

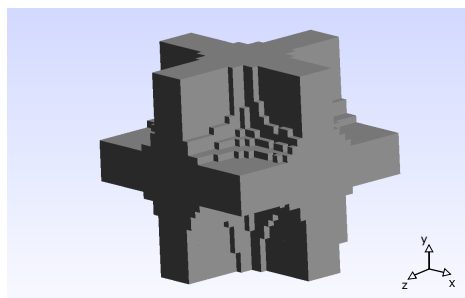
$$C_{1111}^H + C_{2222}^H + C_{3333}^H, \quad (6.6)$$

meaning that is required the maximization of normal stiffness in the three principal directions and, again, it is imposed the equality restrictions on the components of the tensor. Two different meshes were used, the first one with $30 \times 30 \times 30$ elements and the second one with $40 \times 40 \times 40$ elements in order to investigate the influence of the discretization on the results. The initial material distribution is equal for both cases. The optimization problem can be set as

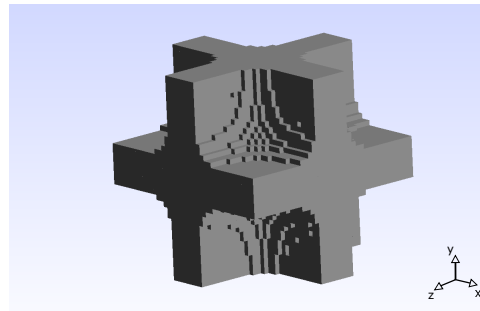
$$\begin{aligned} & \text{Maximize}_{\rho} \quad C_{1111}^H + C_{2222}^H + C_{3333}^H \\ & \text{Subject to} \quad V \leq V_f \\ & \quad |C_{1111}^H - C_{2222}^H| \leq tol \\ & \quad |C_{2222}^H - C_{3333}^H| \leq tol \\ & \quad |C_{1111}^H - C_{3333}^H| \leq tol. \end{aligned} \quad (6.7)$$

For this case, as an alternative, the method of moving asymptotes is used as optimization procedure. Figure 75 and 76 show the topologies obtained for both cases.

Figure 75 – Maximization of $C_{1111}^H + C_{2222}^H + C_{3333}^H$, mesh of $30 \times 30 \times 30$ elements



Source: Author's production, 2016.

Figure 76 – Maximization of $C_{1111}^H + C_{2222}^H + C_{3333}^H$, mesh of $40 \times 40 \times 40$ elements

Source: Author's production, 2016.

The results for both meshes are shown in table 8. These results show that the filter used makes the problem mesh independent, since the topologies obtained for both cases are equal. In addition, both topologies present reinforcements on the three principal directions, behaviour expected to increase the normal stiffness.

Table 8 – Normal components of the homogenized tensor

Mesh	$C_{1111}^H, C_{2222}^H, C_{3333}^H$ [GPa]
$30 \times 30 \times 30$	99.68
$40 \times 40 \times 40$	100.26

6.2.4 Summary

It has been shown that the topology optimization combined with homogenization method provides a powerful tool to design lightweight materials. The results presented in this section show, in a general way, how a linear combination of the components of the elastic tensor of a porous media can be maximized. The topologies obtained seem to be consistent with the expected results.

It may be regarded that several aspects of an optimization problem can be analysed with this approach. It has been shown the influence of the mesh and the initial material distribution in these kind of problems. Also, it has been shown that several optimization procedures can be

used in order to achieve the optimum design of a porous material. The optimum criteria was the simplest approach used. This is a fast and easy to implement method, although, it can be used only in specific problems, and does not allow to include extra constraints to the problem. The other possibilities, were the sequential linear programming and the method of moving asymptotes, which allow to address more general problems and include extra constraints to the problem. Nevertheless, these methods are considerably more complex than the optimum criteria, being more difficult to implement and requiring a greater computational effort.

The most important aspect is the range of possibilities, in the context of structural optimization, that this approach offers. It is clear that this tool provides to the designer the possibility of tailoring a material in a very specific way. For example, structures subjected to a particular loading condition can be designed in order to improve the efficiency of this material in regard to this solicitation, having as a key target, for instance, mass reduction.

Finally, even if only three distinct cases of linear combination were studied, many other cases can be addressed, as for example, the design of a porous media which maximizes a coupled component of the mechanical tensor. Also, this approach can be extended in order to evaluate the engineering constants of the material, by looking, for example, the maximization of the Young's Modulus in a given direction or the minimization of the Poisson's Coefficient in a particular plane.

6.3 TAILORING OF MECHANICAL PROPERTIES

This section shows the results obtained for the problem of approximating a given fourth order elasticity tensor. Five different initial material distributions are chosen in order to obtain the topologies of the RVE that match the properties of a human bone.

In the work of Yoon and Katz (1976), the authors use an ultrasonic wave propagation in order to obtain the elastic tensor of dry human cortical bone. The fourth order tensor obtained is

$$C^* = \begin{bmatrix} 23.4 & 9.06 & 9.11 & 0 & 0 & 0 \\ & 23.4 & 9.11 & 0 & 0 & 0 \\ & & 32.5 & 0 & 0 & 0 \\ & & & 7.17 & 0 & 0 \\ & & & & 8.71 & 0 \\ & & & & & 8.71 \end{bmatrix} [\text{GPa}], \quad (6.8)$$

sym.

which is the tensor used for the approximation in this work.

The simulation input data is shown in table 9, where the base material plays the role of a biocompatible titanium alloy, chosen in order to aim a medical application. Furthermore, a mesh of $40 \times 40 \times 40$ elements, an unit RVE and the Optimum Criteria as optimization procedure, are used in all cases.

Table 9 – Simulations properties

Young's Modulus (E) [GPa]	113.8
Poisson's Coefficient (ν)	0.342
Minimum Density (ρ_{min})	10^{-3}
Penalization (P)	3.0
Filtering Radius (R) [m]	0.07

The optimization problem can be set as

$$\begin{aligned} & \underset{\rho}{\text{Minimize}} \quad ||\mathbf{C}^* - \mathbf{C}^H||_2 \\ & \text{Subject to} \quad V \leq V_f, \end{aligned} \tag{6.9}$$

where \mathbf{C}^* is the target tensor, \mathbf{C}^H is the homogenized tensor, V is the volume of the structure and V_f is the admissible volume.

As shown before, the topology optimization is dependent on the initial densities distribution. Thereby, five distinct initial material distributions are used in order to find possible different minima for the problem and to investigate the non uniqueness of solution of the problem.

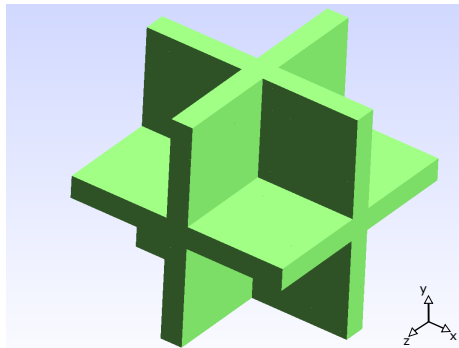
6.3.1 Topologies

The initial material distribution for the first case is shown in figure 77, and the mechanical tensor for this initial distribution is

$$\mathbf{C}^H = \begin{bmatrix} 25.45 & 5.86 & 5.86 & 0 & 0 & 0 \\ 25.45 & 5.86 & 0 & 0 & 0 & 0 \\ & 25.45 & 0 & 0 & 0 & 0 \\ & & 4.61 & 0 & 0 & 0 \\ & & & 4.61 & 0 & 0 \\ & & & & 4.61 & 0 \end{bmatrix} [\text{GPa}]. \tag{6.10}$$

sym.

Figure 77 – Initial material distribution - Case 1



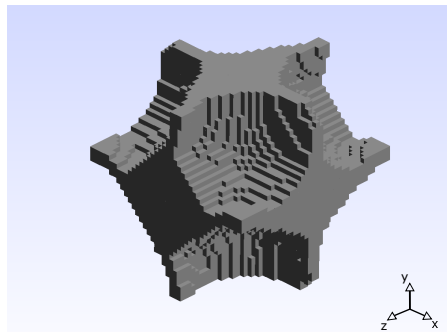
Source: Author's production, 2016.

The optimization procedure results in the base cell's topology shown in figure 78, and the mechanical tensor for the media formed by the repetition of this base cell is

$$C^H = \begin{bmatrix} 23.38 & 9.15 & 9.28 & 0 & 0 & 0 \\ & 23.38 & 9.29 & 0 & 0 & 0 \\ & & 32.52 & 0 & 0 & 0 \\ & & & 6.89 & 0 & 0 \\ & & & & 8.27 & 0 \\ & & & & & 8.27 \end{bmatrix} [\text{GPa}]. \quad (6.11)$$

sym.

Figure 78 – Final material distribution - Case 1



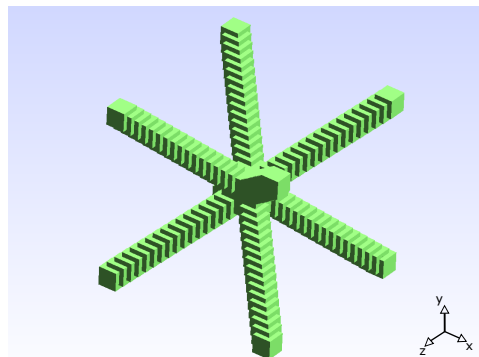
Source: Author's production, 2016.

The initial topology used for the second case is shown in figure 79, whose homogenized tensor is given by

$$C^H = \begin{bmatrix} 1.44 & 1.35 & 1.35 & 0 & 0 & 0 \\ & 1.44 & 1.35 & 0 & 0 & 0 \\ & & 1.44 & 0 & 0 & 0 \\ & & & 1.23 & 0 & 0 \\ & & & & 1.23 & 0 \\ & & & & & 1.23 \end{bmatrix} [\text{GPa}]. \quad (6.12)$$

sym.

Figure 79 – Initial material distribution - Case 2



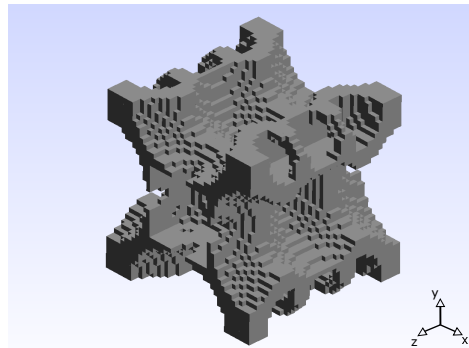
Source: Author's production, 2016.

The topology obtained for this case is shown in figure 80, whose mechanical tensor is

$$C^H = \begin{bmatrix} 23.28 & 9.38 & 9.14 & 0 & 0 & 0 \\ & 23.28 & 9.14 & 0 & 0 & 0 \\ & & 32.38 & 0 & 0 & 0 \\ & & & 6.15 & 0 & 0 \\ & & & & 8.50 & 0 \\ & & & & & 8.50 \end{bmatrix} [\text{GPa}]. \quad (6.13)$$

sym.

Figure 80 – Final material distribution - Case 2

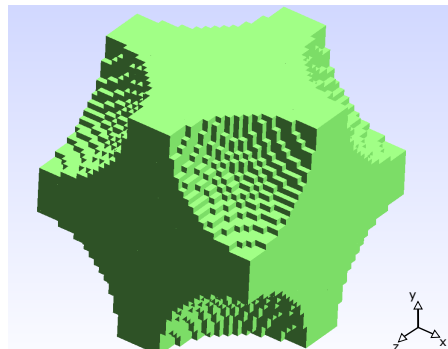


Source: Author's production, 2016.

The third case studied starts with the topology shown in figure 81, whose homogenized tensor is given by

$$\mathbf{C}^H = \begin{bmatrix} 39.23 & 16.75 & 16.75 & 0 & 0 & 0 \\ 39.23 & 16.75 & 0 & 0 & 0 & 0 \\ & 39.23 & 0 & 0 & 0 & 0 \\ & & 11.64 & 0 & 0 & 0 \\ & & & 11.64 & 0 & 0 \\ & & & & 11.64 & 0 \\ sym. & & & & & 11.64 \end{bmatrix} [\text{GPa}]. \quad (6.14)$$

Figure 81 – Initial material distribution - Case 3



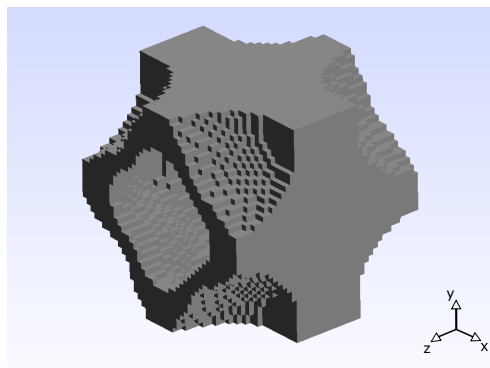
Source: Author's production, 2016.

Figure 82 shows the topology obtained. The homogenized tensor, for this case, is given by

$$\mathbf{C}^H = \begin{bmatrix} 23.35 & 9.21 & 9.20 & 0 & 0 & 0 \\ & 23.34 & 9.20 & 0 & 0 & 0 \\ & & 32.47 & 0 & 0 & 0 \\ & & & 7.00 & 0 & 0 \\ & & & & 8.51 & 0 \\ & & & & & 8.51 \end{bmatrix} [\text{GPa}]. \quad (6.15)$$

sym.

Figure 82 – Final material distribution - Case 3



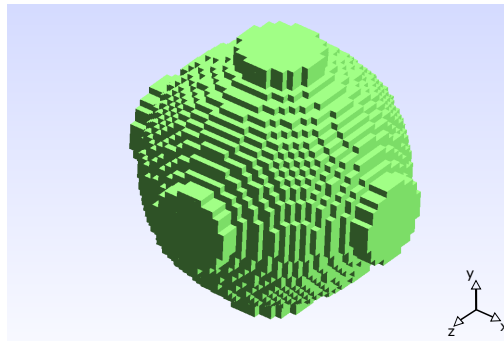
Source: Author's production, 2016.

The fourth case uses, as the initial topology, the RVE shown in figure 83, whose homogenized tensor is

$$\mathbf{C}^H = \begin{bmatrix} 6.27 & 1.84 & 1.84 & 0 & 0 & 0 \\ & 6.27 & 1.84 & 0 & 0 & 0 \\ & & 6.27 & 0 & 0 & 0 \\ & & & 2.85 & 0 & 0 \\ & & & & 2.85 & 0 \\ & & & & & 2.85 \end{bmatrix} [\text{GPa}]. \quad (6.16)$$

sym.

Figure 83 – Initial material distribution - Case 4



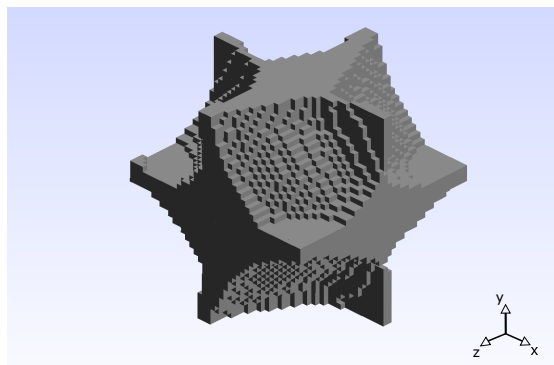
Source: Author's production, 2016.

Figure 84 shows the RVE obtained, whose homogenized tensor is

$$C^H = \begin{bmatrix} 23.35 & 9.20 & 9.31 & 0 & 0 & 0 \\ 23.36 & 9.31 & 0 & 0 & 0 & 0 \\ & 32.48 & 0 & 0 & 0 & 0 \\ & & 6.97 & 0 & 0 & 0 \\ & & & 8.35 & 0 & 0 \\ & & & & 8.34 & \end{bmatrix} [\text{GPa}]. \quad (6.17)$$

sym.

Figure 84 – Final material distribution - Case 4



Source: Author's production, 2016.

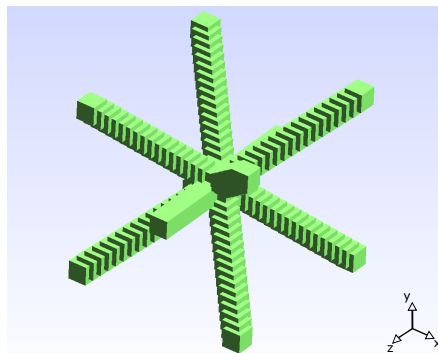
The last case studied uses as the initial material distribution the

RVE shown in figure 85, whose homogenized tensor is

$$\begin{bmatrix} 1.46 & 1.37 & 1.36 & 0 & 0 & 0 \\ & 1.46 & 1.36 & 0 & 0 & 0 \\ & & 2.80 & 0 & 0 & 0 \\ & & & 1.26 & 0 & 0 \\ & & & & 1.24 & 0 \\ & & & & & 1.24 \end{bmatrix} [\text{GPa}]. \quad (6.18)$$

sym.

Figure 85 – Initial material distribution - Case 5



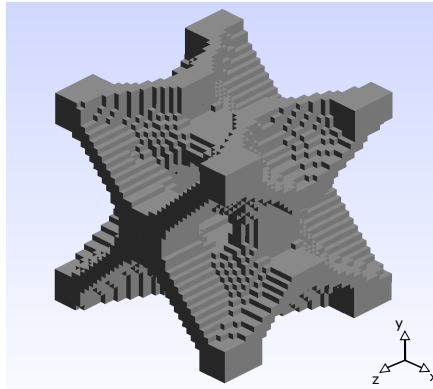
Source: Author's production, 2016.

As the result of the optimization, the RVE of figure 86 is obtained and its homogenized tensor is given by

$$C^H = \begin{bmatrix} 23.28 & 9.33 & 9.41 & 0 & 0 & 0 \\ & 23.29 & 9.42 & 0 & 0 & 0 \\ & & 32.46 & 0 & 0 & 0 \\ & & & 6.84 & 0 & 0 \\ & & & & 8.26 & 0 \\ & & & & & 8.28 \end{bmatrix} [\text{GPa}]. \quad (6.19)$$

sym.

Figure 86 – Final material distribution - Case 5



Source: Author's production, 2016.

6.3.2 Summary

In all cases, the topologies of the RVE are different, indicating the non uniqueness of the solution, although the numerical results are very similar to each other. The fourth order elasticity tensor obtained for all cases approximates the target tensor with a certain accuracy. It can be seen that the normal components of the tensor, in all cases, are very well approximated. The shear and the coupled components have a better or a worst approximation depending on the topology obtained. Also, it can be seen that even for very different initial material distributions and, consequently, initial homogenized tensors, the procedure leads to good results.

The value of the objective function, given by the norm of the difference of the target tensor and the homogenized tensor, for each case, is shown in table 10. As one can see, the third case has the lowest value of the objective function and the second the highest, showing that the third RVE gives a better approximation to the target tensor.

Other comparison is the relative error, set as

$$EC_{ijkl}^H = \frac{|C_{ijkl}^* - C_{ijkl}^H|}{C_{ijkl}^*} 100\%. \quad (6.20)$$

Table 11 shows the relative error of the homogenized components of all topologies. Again, it can be seen that the result obtained for the third case

Table 10 – Objective function value

Topology	$\Phi = C^* - C^H _2$
1	0.7293
2	1.1314
3	0.3977
4	0.6473
5	0.8898

gives a better estimative for the target tensor, where the largest error is smaller than 3%.

Table 11 – Relative error

	1	2	3	4	5
$EC_{1111}^H (\%)$	0.09	0.51	0.04	0.21	0.51
$EC_{3333}^H (\%)$	0.06	0.37	0.09	0.06	0.12
$EC_{1122}^H (\%)$	0.99	3.53	1.65	1.54	2.98
$EC_{1133}^H (\%)$	1.87	0.33	0.99	2.96	3.29
$EC_{1212}^H (\%)$	3.91	14.23	2.37	2.79	4.60
$EC_{2323}^H (\%)$	5.05	2.41	2.29	4.13	5.17

It is important to consider that:

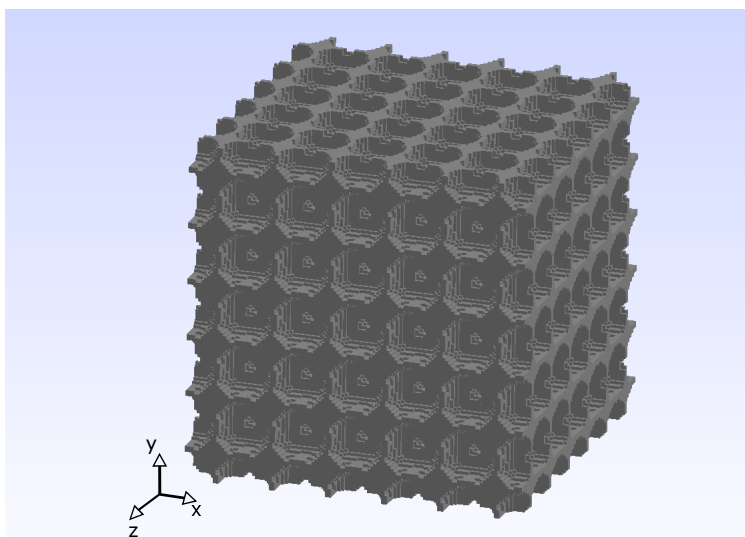
- The properties of a human bone may vary substantially due to several factors;
- Only one target tensor was analysed, as well as one base material;
- The biocompatible titanium alloy has a higher stiffness than the bone, what can result in an inappropriate prosthesis manufactured with the raw material.
- The main objective of such problem is to obtain an artificial material, with properties in the same order of magnitude of the properties of the bone, in order to substitute a damaged tissue.

Thus, one can conclude that the results obtained were very satisfactory. If errors smaller than 5% in every component of the homogenized tensor

with respect to the target tensor may be achieved, then when a range of properties is considered, this result becomes more acceptable. Also, only the mechanical properties of one kind of alloy were used. If another kind of base material is used, it may be found a better result. A prosthesis made of these microstructures would provide a better approximation of the bone properties than one with a raw material, rendering this a very useful material.

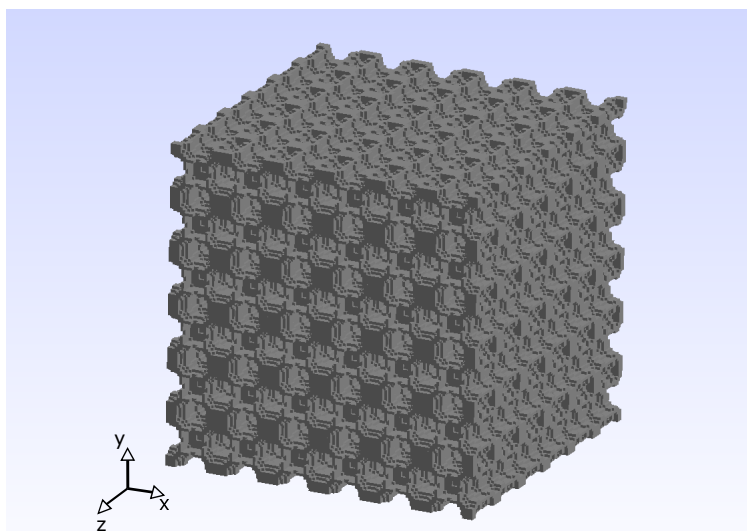
Finally, as a summary of all results, figures 87, 88, 89, 90 and 91 show the media formed by each of the topologies obtained and figure 92 shows graphically the numerical results for all topologies, in which the components of the target tensor are shown in the full lines and the components of the homogenized tensors are shown in the discrete points.

Figure 87 – Media for the mechanical tailoring - case 1



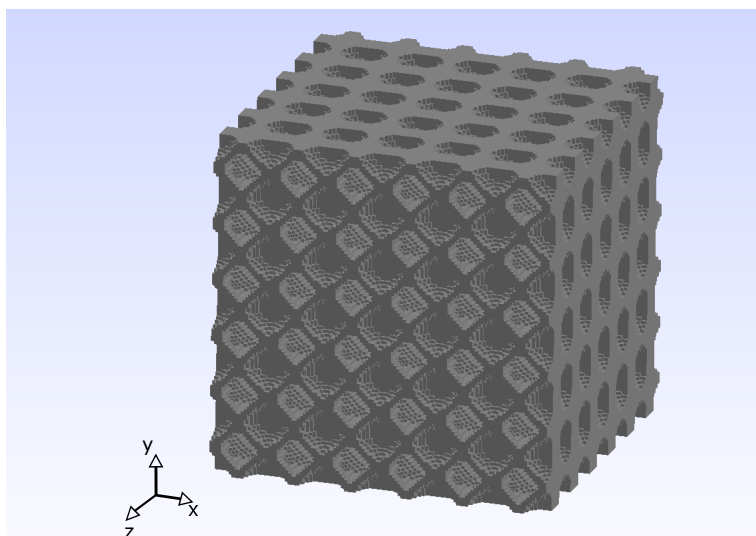
Source: Author's production, 2016.

Figure 88 – Media for the mechanical tailoring - case 2



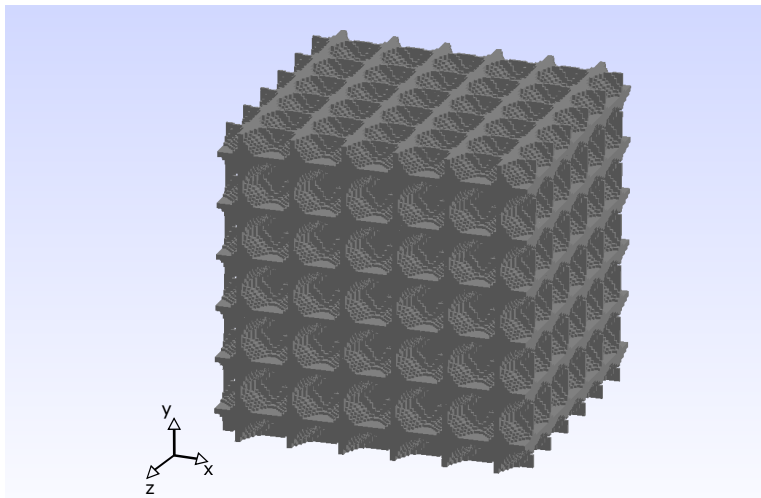
Source: Author's production, 2016.

Figure 89 – Media for the mechanical tailoring - case 3



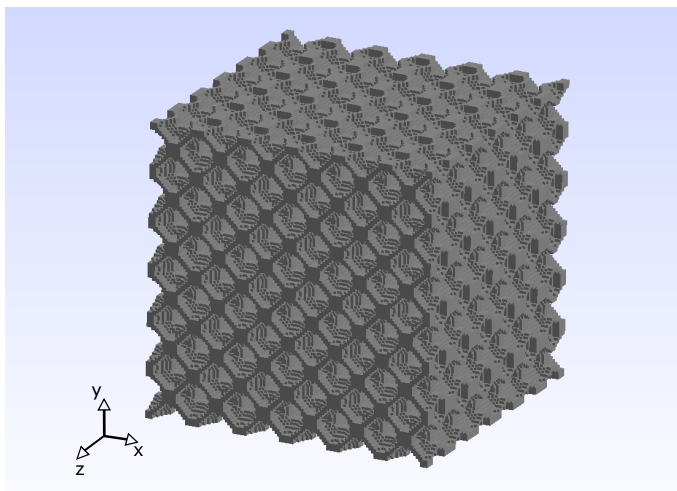
Source: Author's production, 2016.

Figure 90 – Media for the mechanical tailoring - case 4



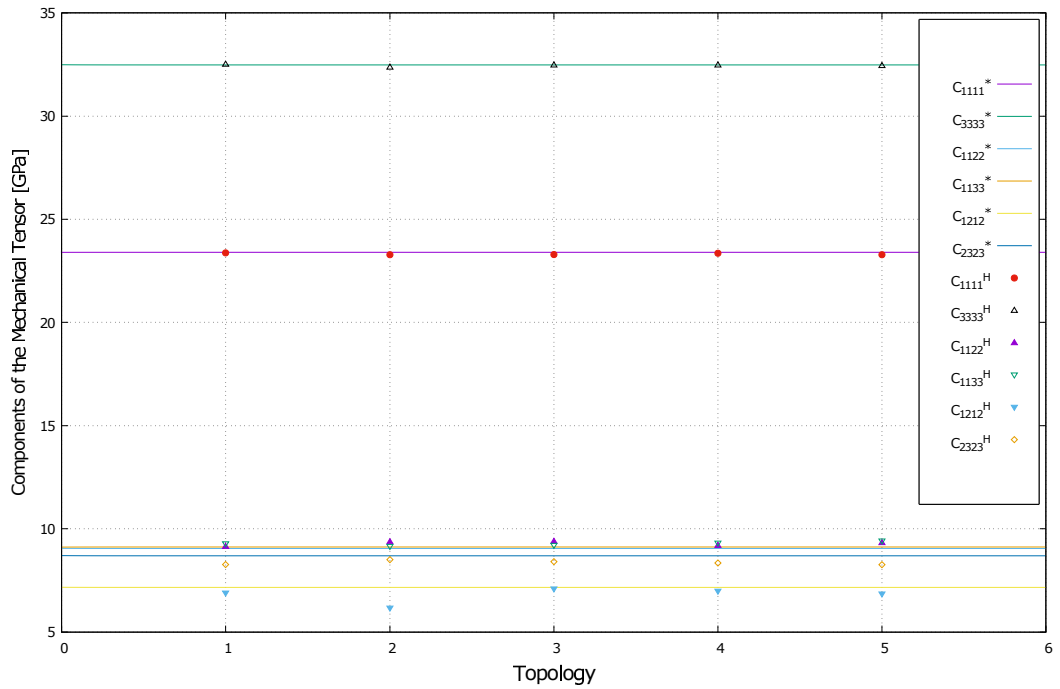
Source: Author's production, 2016.

Figure 91 – Media for the mechanical tailoring - case 5



Source: Author's production, 2016.

Figure 92 – Final results



Source: Author's p. 2016.

7 CONCLUSION

In the present work numerical simulations regarding to the porous materials behaviour are studied. The linear elastic tensor and the thermal conductivity tensor are evaluated using the homogenization by asymptotic expansion and the equilibrium problems are solved using the finite element method. Also, the topology optimization is used in order to find the geometry of the base cell of a porous media regarding two distinct problems. The first one is the maximization of a linear combination of the homogenized mechanical tensor of the porous media and the second one is to approximate a target tensor.

Regarding the analysis problem, it has been found that:

- The homogenization by asymptotic expansion method, implemented in this work is efficient due to the fact that several models are used as reference and are compared with the results obtained with the implemented method, providing good results;
- The homogenization method can be used in order to predict the effective properties of either porous media or composites, described by an RVE.

In regard to the optimization problems, the following conclusions are considered:

- Several optimization methods can be used. The simplest is the optimum criteria. Even though this method is very fast in comparison to other consolidated methods, its application is very limited, being restricted to some kind of problems. The SLP and MMA can be used in a more general way, however, the computational effort associated to these methods is considerably higher than that needed for the optimum criteria;
- The initial material distribution influences the final topology and the numerical results. This fact was observed in this work and shows that the problems is not convex, rendering the global minimum not guaranteed;
- The application of the topology optimization in order to maximize a linear combination of the components of the homogenized tensor presents satisfactory results. Since the evaluation of properties and

the derivatives of the problem were both validated, the results obtained are reliable. Also, the topologies obtained, when the macroscopic media is considered, show expected reinforcements for the given applications, for instance, when it is required the maximization of a normal component of the fourth order elasticity tensor, reinforcements in this particular principal direction appear in the optimization procedure. In addition, if it is required the maximization of a shear component, 45° reinforcements appear in that particular plane;

- It has been shown that it is possible to find the topology of a base cell whose homogenized tensor approximates the properties of a target tensor, in the case of this work, the human bone mechanical tensor. The results showed that an excellent accuracy may be achieved. As mentioned before, the problem is not convex, leading to several local minima, fact that leads to the finding of more than one topology for the approximation. For the best result achieved, the error in every component is less than 3%;
- An artificial biocompatible alloy has mechanical properties in a higher order of magnitude as those of the human bone. Thus, the main purpose of this kind of approach is the use of biocompatible base material properties in order to render the properties of the porous media in the same order of magnitude as those the human bone, what has been achieved in this work. Also, considering that the properties of a natural tissue varies in a wide range, the errors achieved may be acceptable.

As final remarks, it has been shown that the three well established tools in the computational mechanics used at this work, the finite element method, the homogenization by asymptotic expansion and the topology optimization, when used combined can handle several kinds of problems. Cellular materials can be used as specialized materials, and this may be achieved by the use of the methods presented at this work, which enable rendering the requirements and properties of the media. Finally, this kind of material opens a wide range of practical applications, making this an interesting subject of research.

7.1 SUGGESTIONS FOR FURTHER WORKS

Several aspects can be used in order to enrich this work:

- The computational effort is a limitation of this work. If a more powerful computer is used, it would be possible to use a more refined mesh, increasing the accuracy of the results and improving the RVE topologies details;
 - The use of different kinds of finite elements could provide a better approximation for the geometries used. A shell element, for instance, can be used in order to approximate a hollow sphere RVE;
 - The use of a post processing, such as a shape optimization, can be used in order to obtain a continuous geometry;
 - The use of the rapid prototyping processes, which allow the manufacture of this kind of material, enabling an experimental analysis and comparison with the numerical results;
 - The use of the homogenization method to evaluate other equivalent properties, such as the electrical conductivity on a composite.
-

BIBLIOGRAPHY

- AMBROSIO, L.; BUTTAZZO, G. An optimal design problem with perimeter penalization. *Calc. Var.*, n. 1, p. 55–69, 1993. Cited on page 92.
- ARORA, J. S. *Optimization of Structural and Mechanical Systems*. [S.I.]: World Scientific, 2007. Cited 5 times on pages 82, 84, 85, 87, and 102.
- BANHART, J. Manufacture, characterisation and application of cellular metals and metal foams. *Progress in Materials Science*, v. 46, p. 559–632, 2000. Cited on page 35.
- BATHE, K.-J. *Finite Element Procedures*. [S.I.]: Prentice-Hall, Inc., 2009. Cited 3 times on pages 57, 73, and 95.
- BELEGUNDU, A. D.; CHANDRUPATLA, T. R. *Optimization Concepts and Applications in Engineering*. [S.I.]: Prentice Hall, 1999. Cited 2 times on pages 83 and 85.
- BENDSØE, M. Optimal shape design as a material distribution problem. *Structural Optimization*, n. 1, p. 193–202, 1989. Cited on page 92.
- BENDSØE, M. P.; KIKUCHI, N. Generating optimal topologies in structural design using a homogenization method. *Computer Methods in Applied Mechanics and Engineering*, v. 71, p. 197–224, 1988. Cited 3 times on pages 38, 92, and 93.
- BENDSØE, M. P.; SIGMUND, O. Material interpolation schemes in topology optimization. *Archive of Applied Mechanics*, n. 69, p. 635–654, 1999. Cited 3 times on pages 92, 93, and 95.
- BENDSØE, M. P.; SIGMUND, O. *Topology Optimization - Theory, Methods and Applications*. [S.I.]: Springer, 2003. Cited 7 times on pages 82, 89, 90, 91, 94, 96, and 100.
- BENSSOUSAN, A.; LIONS, J.; PAPANICOLAU, G. Asymptotic analysis for periodic structures. 1978. Cited on page 45.
- BEZANSON, J.; KARPINSKI, S.; SHAH, V. B.; EDELMAN, A. Julia: A fast dynamic language for technical computing. September 2012. Cited on page 42.
- BRUYNEEL, M.; DUYNSINX, P.; FLEURY, C. A family of mma approximations for structural optimization. *ASMO UK ISSMO*, 2001. Cited on page 104.

- CAPRA, S. C.; CANALE, R. P. *Métodos Numéricos para Engenharia*. [S.I.]: McGraw Hill, 2008. Cited on page 74.
- CARDOSO, E. L. *Otimização Topológica de Transdutores Piezelétricos Considerando Não-Linearidade Geométrica*. Tese (Tese de Doutorado) — Universidade Federal do Rio Grande do Sul - UFRGS, 2005. Cited on page 91.
- CARDOSO, E. L.; FONSECA, J. S. O. Complexity control in the topology optimization of continuum structures. *Journal of the Brazilian Society of Mechanical Sciences and Engineering*, v. 25, n. 3, p. 293–301, 2003. Cited on page 98.
- CARNIEL, T. A. Análise e otimização de células periódicas de "lattice block materials" visando aplicações termo-mecânicas. *Departamento de Engenharia Mecânica. UDESC. Joinville. 2009. Relatório Interno*, 2009. Cited on page 39.
- CHENG, K.-T.; OLHOFF, N. An investigation concerning optimal design of solid elastic plates. *Int. J. Solids Structures*, v. 17, p. 305–323, 1981. Cited on page 91.
- CHENG, K.-T.; OLHOFF, N. Regularized formulation for optimal design of axisymmetric plates. *Int. J. Solids Structures*, v. 18, p. 153–169, 1982. Cited on page 91.
- CHRISTENSEN, P. W.; KLARBRING, A. *An Introduction to Structural Optimization*. [S.I.]: Springer, 2008. Cited 2 times on pages 88 and 89.
- CHRISTENSEN, R. M. Mechanics of cellular and other low-density materials. *International Journal of Solids and Structures*, n. 37, p. 93–104, 2000. Cited on page 35.
- ÖCHSNER, A.; HOSSEINI, S. M.; MERKEL, M. Numerical simulation of sintered perforated hollow sphere structures (phss) to investigate thermal conductivity. *Proceedings of the International MultiConference of Engineers and Computer Scientists*, v. 2, 2009. Cited on page 105.
- CIARANESCU, D.; PAULIN, D. Homogenization in opens sets with holes. *Journal of Mathematical Analysis and Applications*, v. 71, p. 590–607, 1979. Cited on page 45.
- COOK, R. D. *Finite Element Modeling for Stress Analysis*. [S.I.]: John Wiley and Sons, Inc., 1995. Cited 2 times on pages 73 and 182.

- COURANT, R. Variational methods for the solution of problems of equilibrium and vibrations. *Bulletin of the American Mathematical Society*, n. 49, p. 2165–2187, 1943. Cited on page 81.
- COX, H. The design of structures of least weight. *Pergamon London*, 1956. Cited on page 91.
- da Silva, G. A. *Otimização Topológica de Estruturas Contínuas Considerando Incertezas*. Dissertação (Dissertação de Mestrado) — Universidade do Estado de Santa Catarina, 2016. Cited 2 times on pages 96 and 97.
- DANTZIG, G. Maximization of a linear function of variables subject to linear inequalities. 1951. Cited on page 81.
- DIAZ, A.; SIGMUND, O. Checkerboard patterns in layout optimization. *Structural Optimization*, v. 10, p. 40–45, 1995. Cited on page 96.
- FANG, Z.; SUN, W.; TZENG, J. T. Asymptotic homogenization and numerical implementation to predict the effective mechanical properties for electromagnetic composite conductor. *Journal of Composite Materials*, v. 38, n. 16, p. 1371–1385, 2004. Cited on page 54.
- FLETCHER, R.; REEVES, C. Function minimization by conjugate gradients. *The Computer Journal*, p. 149–154, 1964. Cited on page 82.
- FOX, R. L. Optimization methods for engineering design. *Addison-Wesley, Boston, MA*, 1971. Cited on page 82.
- FRANCO, M. D. *Otimização Topológica Aplicada ao Projeto de Microestruturas Osteocompatíveis*. Dissertação (Dissertação de Mestrado) — Universidade do Estado de Santa Catarina, 2014. Cited 2 times on pages 40 and 41.
- GEUZAINÉ, C.; REMACLE, J.-F. Gmsh: a three-dimensional finite element mesh generator with built-in pre- and post-processing facilities. *International Journal for Numerical Methods in Engineering*, p. 1–24, 2009. Cited on page 42.
- GIBSON, L. J.; ASHBY, M. F. *Cellular solids - Structure and properties*. [S.l.]: Cambridge: Cambridge University Press, 1997. Cited 3 times on pages 33, 34, and 35.
- GRENSTEDT, J. L. Effective elastic behavior of some models for 'perfect' cellular solids. *International Journal of Solids and Structures*, n. 36, p. 1471–1501, 1999. Cited 2 times on pages 33 and 35.

GUEDES, J. M.; KIKUCHI, N. Preprocessing and postprocessing for materials based on the homogenization method with adaptive finite element methods. *Computer methods in applied mechanics and engineering*, v. 83, p. 143–198, 1990. Cited 3 times on pages 45, 53, and 92.

GUTH, D. C. *Otimização de Materiais Constituídos de células Treliçadas com Restrições de Isotropia para Aplicações Termomecânicas*. Dissertação (Dissertação de Mestrado) — Universidade do Estado de Santa Catarina, 2012. Cited on page 40.

GUTH, D. C.; LUERSEN, M. A.; MUÑOZ-ROJAS, P. A. Optimization of periodic truss materials including constitutive symmetry constraints. *Materialwissenschaft und Werkstofftechnik*, v. 43, n. 5, p. 447–456, 2012. Cited 2 times on pages 41 and 42.

HALPIN, J. C. Effects on environmental factors on composite materials. *AFML-TR*, 1969. Cited on page 197.

HALPIN, J. C.; TSAI, S. W. Effects of environmental factors on composite materials. *AFNL-RT*, 1969. Cited on page 36.

HANSON, R. J.; HIRBERT, K. L. A sparse linear programming subprogram. *Report SAND81-0297, Sandia National Laboratories*, 1981. Cited on page 102.

HASHIN, Z. The elastic moduli of heterogeneous materials. *Journal of Applied Mechanics*, p. 143–150, 1962. Cited on page 36.

HASHIN, Z. A variational approach to the theory of elastic behavior of multiphase materials. *Journal of Mechanics and Physics of Solids*, p. 127–140, 1963. Cited on page 36.

HASSANI, B.; HINTON, E. A review of homogenization and topology optimization i-homogenization theory for media with periodic structure. *Computers and Structures*, v. 69, p. 707–717, 1998. Cited 5 times on pages 48, 52, 53, 92, and 175.

HASSANI, B.; HINTON, E. A review of homogenization and topology optimization ii-analytical and numerical solutions of homogenization equations. *Computers and Structures*, v. 69, p. 719–738, 1998. Cited 2 times on pages 54 and 92.

HEMP, W. Optimum structures. *Clarendon, Oxford*, 1973. Cited on page 91.

- HILL, R. Theory of mechanical properties of fibre-strengthened materials: self-consistent model. *Journal of Mechanics and Physics of Solids*, n. 189, 1965. Cited on page 36.
- HOLLISTER, S. J.; KIKUCHI, N. A comparison of homogenization and standard mechanics analyses for periodic porous composites. *Computational Mechanics*, v. 10, p. 73–95, 1992. Cited 2 times on pages 46 and 175.
- HOLLISTER, S. J.; KIKUCHI, N. Homogenization theory and digital imaging: A basis for studying the mechanics and design principles of bone tissue. *Biotechnology and Bioengineering*, p. 586–594, 1994. Cited 3 times on pages 36, 37, and 46.
- HUGHES, J. R. *The Finite Element Method - Linear Static and Dynamic Finite Element Analysis*. [S.I.]: Dover Publications, Inc., 2000. Cited 4 times on pages 73, 181, 182, and 183.
- JOHNSON, R. C. Optimum design of mechanical elements. *Wiley-Interscience, New York*, 1961. Cited on page 82.
- JONES, R. M. *Mechanics of Composite Materials*. [S.I.]: Taylor and Francis Inc, 1999. Cited on page 36.
- KARUSH, W. *Minima of functions of several variables with inequalities as side conditions*. Dissertação (Master Thesis) — University of Chicago, 1939. Cited 2 times on pages 81 and 86.
- KELLER, J. B. Effective behaviour of heterogeneous media. *Proc. Symposium on Statistical Mechanics and Statistical Methods*, p. 631–644, 1977. Cited 2 times on pages 36 and 45.
- KOHN, R.; STRANG, G. Optimal design and relaxation of variational problems, i. *Communications on Pure and Applied Mathematics, Wiley Subscription Services, Inc., A Wiley Company*, v. 39, n. 1, p. 113–137, 1986. Cited 2 times on pages 92 and 93.
- KOMZSIK, L.; POSCHMANN, P. Iterative solution techniques for finite element applications. *Finite Elements in Analysis and Design*, v. 14, n. 1, p. 373–379, 1993. Cited on page 74.
- KRISHNAN, S.; GARIMELLA, S. V.; MURTHY, J. Y. Thermal characterization of open-celled metal foams by direct simulation. *Cellular and Porous Materials: Thermal Properties Simulation and Prediction*, p. 267–289, 2008. Cited on page 201.

- KUHN, H.; TUCKER, A. W. Nonlinear programming. *Proceedings of the Second Berkeley Symposium on Mathematical Statistics and Probability*, p. 481–492, 1951. Cited 2 times on pages 81 and 86.
- LARSEN, E. W. Neutron transport and diffusion in inhomogeneous media. *Int. J. Math. Phys.*, n. 16, p. 1421–1427, 1975. Cited on page 45.
- LESAINT, P. On the convergence of wilson's nonconforming element for solving the elastic problems. *Computer Methods in Applied Mechanics and Engineering*, n. 7, p. 1–16, 1976. Cited on page 185.
- LIN, C. Y.; KIKUCHI, N.; HOLLISTER, S. J. A novel method for biomaterial scaffold internal architecture design to match bone elastic properties with desired porosity. *Journal of Biomechanics*, v. 37, p. 623–636, 2004. Cited on page 38.
- LÉNÉ, F.; LEGUILLOON, D. Homogenized constitutive law for a partially cohesive composite material. *International Journal of Solids and Structures*, v. 18, p. 443–458, 1982. Cited on page 45.
- LUXNER, M. H. *Modeling and Simulation of Highly Porous Open Cell Structures - Elasto-Plasticity and Localization versus Disorder and Defects*. [S.I.]: VDI Verlag, 2006. Cited 2 times on pages 34 and 35.
- LUXNER, M. H.; STAMPFL, J.; PETTERMANN, H. E. Finite element modeling concepts and linear analyses of 3d regular open cell structures. *Journal of Materials Science*, n. 40, p. 5859–5866, 2005. Cited on page 36.
- MENDONÇA, P. de T. R. *Materiais Compostos e Estruturas-Sanduíche*. [S.I.]: Manole, 2005. Cited 3 times on pages 33, 188, and 198.
- MICHELL, A. The limits of economy in frame structures. *Phil. Mag.*, v. 8, p. 589–597, 1904. Cited on page 91.
- MUÑOZ-ROJAS, P. A.; CARNIEL, E. C. N. S. T. A.; ÖCHSNER, A. *Optimization of a Unit Periodic Cell in Lattice Block Materials Aimed at Thermo-Mechanical Applications*. [S.I.]: Springer, 2011. Cited 3 times on pages 39, 53, and 65.
- MUÑOZ-ROJAS, P. A.; LUERSEN, M. A.; CARNIEL, T. A.; BERTOTTI, E. A design of multifunctional truss-like periodic materials using a global-local optimization method. *Defect and Diffusion Forum*, p. 1073–1078, 2011. Cited 2 times on pages 39 and 40.

- MUÑOZ-ROJAS, P. A.; SILVA, E. C. N.; CARDOSO, E. L.; JUNIOR, M. V. *On the Application of Optimization Techniques to Heat Transfer in Cellular Materials.* [S.I.]: Wiley-VCH, 2008. Cited 2 times on pages 41 and 65.
- MUSKHELISHVILI, N. I. *Some Basic Problems of the Mathematical Theory of Elasticity.* [S.I.]: Springer Netherlands, 2010. Cited on page 36.
- NEVES, M. M.; RODRIGUES, H.; GUEDES, J. M. Optimal design of periodic linear elastic microstructures. *Computers and Structures*, v. 76, p. 421–429, 2000. Cited 2 times on pages 37 and 38.
- OWEN, J. The analysis and design if light structures. *Edward Arnold, London*, 1975. Cited on page 91.
- PAUL, B. . prediction of elastic constants of multiphase materials. *Transactions of the Metallurgical Society of AIME*, p. 36–41, 1960. Cited on page 36.
- PINI, G.; GAMBOLATI, G. Is a simple diagonal scaling the best preconditioner for conjugate gradients on supercomputers? *Advanced Water Resources*, v. 13, n. 3, p. 147–153, 1990. Cited on page 75.
- PRAGER, W. A note on discretized michell structures. *Comp. Meth. Appl. Mech. Eng*, v. 3, p. 349–355, 1974. Cited on page 91.
- RAO, S. S. *Engineering Optimization.* [S.I.]: John Wiley and Sons, 2009. Cited 2 times on pages 81 and 101.
- ROSEN, J. The gradient projection method for nonlinear programming. *Journal of the Society for Industrial and Applied Mathematics*, p. 514–532, 1961. Cited on page 82.
- ROZVANY, G. Aims, scope, methods, history and unified terminologu of computer-aided topology optimization in structural mechanics. *Struct. Multidisc. Optim.*, n. 21, p. 90–108, 2001. Cited on page 92.
- ROZVANY, G.; ADIDAM, S. J. *Eng. Mch. ASCE*, v. 98, n. Rectangular Grillages of Least Weight, p. 1337–1352, 1972. Cited on page 91.
- SANCHEZ-HUBERT, J.; SANCHEZ-PALENCIA, E. *Introduction aux Méthodes Asymptotiques et à l'homogénéisation.* [S.I.]: Masson, 1992. Cited 2 times on pages 36 and 92.

- SANCHEZ-PALENCIA, E. Comportemens local et macroscopique d'un type de milieux physiques heterogenes. *Int. J. Eng. Sci.*, n. 12, p. 331–351, 1974. Cited on page 45.
- SANCHEZ-PALENCIA, E. Non-homogeneous media and vibration theory. *Lect Notes Phys.*, 1980. Cited 2 times on pages 36 and 45.
- SANCHEZ-PALENCIA, E. Homogenization in mechanics - a survey of solved and open problems. *Rend. Sem. Mat. Univers. Politecn. Torino*, v. 44, p. 143–198, 1986. Cited 2 times on pages 49 and 52.
- SANDERS, W.; GIBSON, L. Mechanics of bcc and fcc hollow-sphere foams. *Materials Science and Engineering*, n. 352, p. 150–161, 2003. Cited 2 times on pages 36 and 105.
- SCHMIT, L. A. Structural design by systematic synthesis. *Proceedings of the 2nd Conference on Electronic Computation*, p. 105–122, 1960. Cited on page 82.
- SEGURADO, J.; LLORCA, J. A numerical approximation to the elastic properties of sphere-reinforced composites. *Journal of the Mechanics and Physics of Solids*, v. 50, p. 2107–2121, 2002. Cited 2 times on pages 194 and 199.
- SIGMUND, O. *Design of Material Structures Using Topology Optimization*. Tese (Tese de Doutorado) — Department of Solid Mechanics, Technical University of Denmark, Denmark, 1994. Cited 3 times on pages 47, 95, and 98.
- SIGMUND, O. On the design of compliant mechanisms using topology optimization. *Mech. Struct. Mach.*, n. 25, p. 495–526, 1997. Cited on page 92.
- SIGMUND, O. Morphology-based black and white filters for topology optimization. *Structural and Multidisciplinary Optimization*, v. 33, p. 401–424, 2007. Cited on page 98.
- SIGMUND, O.; PETERSSON, J. Numerical instabilities in topology optimization: A survey on procedures dealing with checkerboards, mesh-dependencies and local minima. *Structural Optimization*, n. 16, p. 68–75, 1998. Cited 2 times on pages 98 and 99.
- SMITH, M.; GUAN, Z.; CANTWELL, W. J. Finite element modelling of the compressive response of lattice structures manufactures using the selective laser melting. *International Journal of Mechanical Sciences*, v. 67, p. 28–41, 2013. Cited on page 35.

- STOLPE, M.; SVANBERG, K. On the trajectories of the epsilon-relaxation approach for stress-constrained truss topology optimization. *Struct. Multidisc. Optim.*, v. 21, p. 140–151, 2001. Cited on page 92.
- SVANBERG, K. The method of moving asymptotes - a new method for structural optimization. *International Journal for Numerical Methods in Engineering*, v. 24, p. 359–373, 1987. Cited 2 times on pages 103 and 104.
- SVANBERG, K. Mma and gcmma, versions september 2007. *Optimization and Systems Theory*, 2007. Cited on page 104.
- TAKAPOUI, R.; JAVADI, H. Preconditioning via diagonal scaling. 2014. Cited on page 75.
- WANG, H. V. A Unit Cell Approach for Lightweight Structure and Compliant Mechanism. Tese (Tese de Doutorado) — Georgia Institute of Technology, 2005. Cited on page 35.
- WEIHONG, Z.; FENGWEN, W.; GAOMING, D.; SHIPING, S. Topology optimization design of material microstructures using strain energy-based method. *Chinese Journal of Aeronautics*, v. 20, p. 320–326, 2007. Cited on page 38.
- WHITNEY, J. M. Elastic moduli of unidirectional composites with anisotropic fibers. *Journal of Composite Materials*, p. 188–193, 1967. Cited on page 36.
- WILDE, D. J.; BEIGHTLER, C. S. Foundations of optimization. *Englewood Cliffs, NJ*, 1967. Cited on page 82.
- YANG, Q.-S.; BECKER, W. Numerical investigation for stress, strain and energy homogenization of orthotropic composite with periodic microstructure and non-symmetric inclusions. *Computational Materials Science*, n. 31, p. 169–180, 2004. Cited on page 67.
- YOON, H. S.; KATZ, L. Ultrasonic wave propagation in human cortical bone - ii measurements of elastic properties and microhardness. *Journal of Biomechanics*, v. 9, p. 459–464, 1976. Cited on page 146.
- ZHU, H. X.; HOBDELL, J.; WINDLE, A. H. Effects of cell irregularity on the elastic properties of open-cell foams. *Acta Materialia*, n. 48, p. 4893–4900, 2000. Cited on page 35.
- ZIENKIEWICZ, O. C.; TAYLOR, R. L. *The Finite Element Method*. [S.I.]: Butterworth Heinemann, 2000. Cited 2 times on pages 58 and 73.

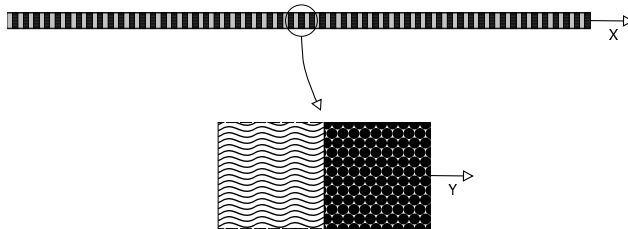
ZOUTENDIJK, G. Methods of feasible directions. 1960. Cited on page 82.

APPENDIX A – UNIDIMENSIONAL HOMOGENIZATION

As a way to enlightenment the homogenization method, this appendix shows the determination of the longitudinal stress in a heterogeneous bar. The mathematical development and the concepts herein presented are based on the works of Hassani and Hinton (1998a) and Hollister and Kikuchi (1992).

In accordance with the theory, it is assumed that the material has a periodic micro structure, as shown in figure 93, in which each highlighted section has a distinct Young's Modulus.

Figure 93 – Unidimensional media



Source: Author's production, 2016, based on (HASSANI; HINTON, 1998a)

The governing equations of an unidimensional linear elastic problem, are the Hooke's law, given by

$$\sigma^\epsilon = E^\epsilon \frac{\partial u^\epsilon}{\partial x} \quad (\text{A.1})$$

and the first Cauchy's law for the motion, given by

$$\frac{\partial \sigma^\epsilon}{\partial x} + \gamma^\epsilon = 0, \quad (\text{A.2})$$

where σ is the axial stress on the bar, u is the displacement, E is the Young's Modulus, x is the spatial coordinate into the macroscopic scale and γ is the specific weight. The ϵ index at equations A.1 and A.2 denote the dependency of the variables in regard to the non linearity of the problem.

Also, it is considered that E^ϵ and γ^ϵ are macroscopically uniform in the domain and vary only microscopically, so, one can write

$$E^\epsilon(x, x/\epsilon) = E^\epsilon(x/\epsilon) = E(y) \quad (\text{A.3})$$

and

$$\gamma^\epsilon(x, x/\epsilon) = \gamma^\epsilon(x/\epsilon) = \gamma(y), \quad (\text{A.4})$$

where y is the spatial coordinates into the microscopic scale. Using the periodic expansion, equation 2.6, the expressions for displacement and stress become

$$u^\epsilon(x) = u^0(x, y) + \epsilon u^1(x, y) + \epsilon^2 u^2(x, y) + \dots \quad (\text{A.5})$$

and

$$\sigma^\epsilon(x) = \sigma^0(x, y) + \epsilon \sigma^1(x, y) + \epsilon^2 \sigma^2(x, y) + \dots, \quad (\text{A.6})$$

where u^i and σ^i , for $i = 1, 2, \dots$, are periodic in y and the length of the period is Y .

Reminding that:

- The derivatives of a periodic function are also periodic;
- The integral of the derivative of a periodic function over the domain is zero;
- If $\Phi = \Phi(x, y)$ and y depends on x , so

$$\frac{d\Phi}{dx} = \frac{\partial\Phi}{\partial x} + \frac{\partial\Phi}{\partial y} \frac{dy}{dx} \quad (\text{A.7})$$

and using equation 2.2, one can write

$$\frac{d\Phi}{dx} = \frac{\partial\Phi}{\partial x} + \frac{1}{\epsilon} \frac{\partial\Phi}{\partial y}. \quad (\text{A.8})$$

Replacing the expression of displacement and stress, equations A.5 and A.6, into the elasticity expression, equation A.1, and into the equilibrium expression, equation A.2, and taking in consideration the mathematical relations for a periodic function, one can get the relations

$$\begin{aligned} \sigma^0 &+ \epsilon \sigma^1 + \epsilon^2 \sigma^2 + \dots \\ &= E(y) \left[\frac{\partial u^0}{\partial x} + \frac{1}{\epsilon} \frac{\partial u^0}{\partial y} + \epsilon \frac{\partial u^1}{\partial x} + \frac{\partial u^1}{\partial y} + \right. \\ &\quad \left. + \epsilon^2 \frac{\partial u^1}{\partial x} + \epsilon \frac{\partial u^2}{\partial y} + \dots \right] \end{aligned} \quad (\text{A.9})$$

and

$$\frac{\partial \sigma^0}{\partial x} + \frac{1}{\epsilon} \frac{\partial \sigma^0}{\partial y} + \epsilon \frac{\partial \sigma^1}{\partial x} + \frac{\partial \sigma^1}{\partial y} + \dots + \gamma(y) = 0. \quad (\text{A.10})$$

Collecting the terms that have the same ϵ exponent at equation A.9, one can obtain

$$\sigma^0 = E(y) \left[\frac{\partial u^0}{\partial x} + \frac{\partial u^1}{\partial y} \right], \quad (\text{A.11})$$

$$0 = E(y) \frac{\partial u^0}{\partial y}, \quad (\text{A.12})$$

and

$$\sigma^1 = E(y) \left[\frac{\partial u^1}{\partial x} + \frac{\partial u^2}{\partial y} \right]. \quad (\text{A.13})$$

In a similar way, with the equilibrium expression, equation A.10,

$$\frac{\partial \sigma^0}{\partial x} + \frac{\partial \sigma^1}{\partial y} + \gamma(y) = 0 \quad (\text{A.14})$$

and

$$\frac{\partial \sigma^0}{\partial y} = 0. \quad (\text{A.15})$$

From an analysis of equations A.12 and A.15 one can conclude that u^0 and σ^0 have a dependency only on the variable x , in other words, $u^0 = u^0(x)$ and $\sigma^0 = \sigma^0(x)$. This fact shows that the properties mentioned are dependent only on the macroscopic scale, being independent on the microscopic scale. Thereby, equation A.11 can written as

$$\sigma^0(x) = E(y) \left[\frac{du^0(x)}{dx} + \frac{\partial u^1(x, y)}{\partial y} \right]. \quad (\text{A.16})$$

Dividing both sides of equation A.16 by $E(y)$ and taking its integral on the period Y ,

$$\int_Y \frac{\sigma^0(x)}{E(y)} dy = \int_Y \frac{du^0(x)}{dx} dy + \int_Y \frac{\partial u^1(x, y)}{\partial y} dy. \quad (\text{A.17})$$

Recalling the facts that an integral of a derivative of a periodic function over the period equals zero and that $\sigma^0(x)$ and $\frac{du^0(x)}{dx}$ are independent of the y scale, one can conclude that

$$\sigma^0(x) = \frac{\frac{du^0(x)}{dx}Y}{\int_Y \frac{1}{E(y)} dy}. \quad (\text{A.18})$$

Now, replacing equation A.18 in equation A.16 one gets

$$E(y) \left[\frac{du^0(x)}{dx} + \frac{\partial u^1(x, y)}{\partial y} \right] = \frac{\frac{du^0(x)}{dx}Y}{\int_Y \frac{1}{E(y)} dy}, \quad (\text{A.19})$$

and rearranging,

$$\frac{\partial u^1(x, y)}{\partial y} = \frac{du^0(x)}{dx} \left(\frac{Y}{E(y) \int_Y \frac{dy}{E(y)}} - 1 \right). \quad (\text{A.20})$$

Integrating equation A.20, one can conclude that $u^1(x, y)$ has the form

$$u^1(x, y) = \chi(y) \frac{du^0(x)}{dx} + \xi(x), \quad (\text{A.21})$$

where $\chi(y)$ depends only on the microscopic variable, y , and ξ is an integration constant, function only on the macroscopic variable, x , due to the integration on the variable y . Hence, from equations A.21 and A.16 one can write the stress as

$$\sigma^0(x) = E(y) \left[\frac{du^0(x)}{dx} + \frac{\partial \chi(y)}{\partial y} \frac{du^0(x)}{dx} \right], \quad (\text{A.22})$$

and its derivatives as

$$\frac{d}{dy} \left[E(y) \left(1 + \frac{\partial \chi(y)}{\partial y} \right) \right] = 0. \quad (\text{A.23})$$

An important consideration is that χ assumes the same values in opposite faces of Y , as a result of the periodicity consideration. Therefore, $\chi(0) = \chi(Y)$. Integrating equation A.23, one gets

$$E(y) \left[1 + \frac{\partial \chi(y)}{\partial y} \right] = a, \quad (\text{A.24})$$

where a is a constant. Rewriting equation A.24, one gets

$$\frac{\partial \chi(y)}{\partial y} = \frac{a}{E(y)} - 1, \quad (\text{A.25})$$

and integrating on the microscopic scale, y ,

$$\chi(y) = \int_0^Y \left(\frac{a}{E(y)} - 1 \right) dy + b, \quad (\text{A.26})$$

where b is an integration constant. Now, using the periodicity condition, $\chi(0) = \chi(Y)$, and isolating the constant a , equation A.26 becomes

$$a = \frac{Y}{\int_0^Y \frac{1}{E(y)} dy}. \quad (\text{A.27})$$

Comparing the equations A.22 and A.24,

$$\sigma^0(x) = a \frac{du^0(x)}{dx}, \quad (\text{A.28})$$

and replacing the value of the constant a , one obtains

$$\sigma^0(x) = \frac{1}{\frac{1}{Y} \int_0^Y \frac{dy}{E(y)}} \frac{du^0(x)}{dx}. \quad (\text{A.29})$$

Equation A.29 has a very similar form of a unidimensional linear elastic problems for a homogeneous material. Also, one notices that $\sigma^0(x)$ and $\frac{du^0(x)}{dx}$ are independent on the microscale. For a linear elastic homogeneous material, the problem can be written as

$$\sigma(x) = E \frac{du(x)}{dx}. \quad (\text{A.30})$$

The only difference between equations A.29 and A.30 is the Young's Modulus. Thus, it is defined the homogenized Young's Modulus as

$$E^H = \frac{1}{\frac{1}{Y} \int_0^Y \frac{dy}{E(y)}}, \quad (\text{A.31})$$

and equation A.29 becomes

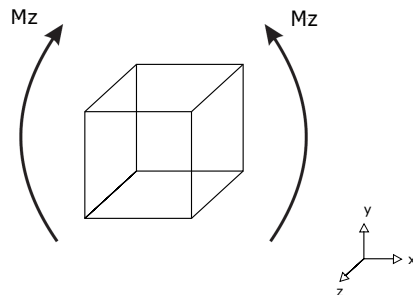
$$\sigma^0(x) = E^H \frac{du^0(x)}{dx}, \quad (\text{A.32})$$

which can be used in the macroscale of the problem, as the method suggests.

APPENDIX B – TRILINEAR ISOPARAMETRIC HEXAHEDRAL ELEMENT WITH INCOMPATIBLE MODES

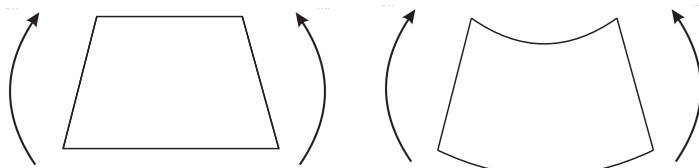
It shall be regarded that when a finite element is submitted to a pure bending load, as shown in figure 94, the accuracy of the results attained with elements with linear interpolation tends to be low. This phenomenon occurs due to the fact that this finite element responds in shear rather than bending, behaviour illustrated in figure 95, in which the exact expected solution and the numerical solution for this kind of element are shown. This spurious shearing is responsible for an artificial overly stiff behaviour. Clearly, a possibility would be use a higher order element, however, the objective is to achieve a good behaviour without introducing additional nodes (HUGHES, 2000). This becomes interesting when is considered that the higher order elements in comparison to the ones with linear interpolation requires a considerably higher computational effort. Several approaches are used to obtain good results without compromising the computational effort, and at this work is used the Incompatible Modes Element.

Figure 94 – Pure bending in a finite element



Source: Author's production, 2016

Figure 95 – Low order approximation and exact solution for a bending case



Source: Author's production, 2016

The development here presented is made as an expansion of the concepts presented by (HUGHES, 2000) and (COOK, 1995) for the four node element, bearing in mind to use this concepts in relation to the eight node element.

From the standard expansion for the approximation of the displacement in terms of trilinear shape functions of a typical element, the quadratic modes are added as

$$\mathbf{u}^h(\xi, \eta, \zeta) = \sum_{a=1}^8 N_a(\xi, \eta, \zeta) \hat{\mathbf{u}}_a^e + \sum_{a=9}^{11} N_a(\xi, \eta, \zeta) \alpha_a^e, \quad (\text{B.1})$$

where $\hat{\mathbf{u}}^e$ are the nodal displacements of the e -th element, α_a^e are the generalized displacements of the e -th, associated to the incompatible modes, ξ , η and ζ are the natural coordinates and N_a are the shape function. This expansion is used in order to obtain the strain-displacement matrix of the element or directly the local stiffness matrix and only, not being used to obtain the body forces of the element.

Following the coordinate system adopted in figure 96, the shape function for the standard eight node trilinear isoparametric element are given by

$$N_1 = \frac{1}{8} (1 - \xi)(1 - \eta)(1 + \zeta), \quad (\text{B.2})$$

$$N_2 = \frac{1}{8} (1 + \xi)(1 - \eta)(1 + \zeta), \quad (\text{B.3})$$

$$N_3 = \frac{1}{8} (1 + \xi)(1 - \eta)(1 - \zeta), \quad (\text{B.4})$$

$$N_4 = \frac{1}{8} (1 - \xi)(1 - \eta)(1 - \zeta), \quad (\text{B.5})$$

$$N_5 = \frac{1}{8} (1 - \xi)(1 + \eta)(1 + \zeta), \quad (\text{B.6})$$

$$N_6 = \frac{1}{8} (1 + \xi)(1 + \eta)(1 + \zeta), \quad (\text{B.7})$$

$$N_7 = \frac{1}{8} (1 + \xi)(1 + \eta)(1 - \zeta), \quad (\text{B.8})$$

$$N_8 = \frac{1}{8} (1 - \xi)(1 + \eta)(1 - \zeta), \quad (\text{B.9})$$

and the incompatible modes add three quadratic shape function in the

form

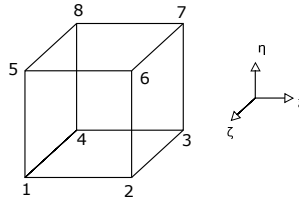
$$N_9 = (1 - \xi^2) \quad (B.10)$$

$$N_{10} = (1 - \eta^2) \quad (B.11)$$

$$N_{11} = (1 - \zeta^2). \quad (B.12)$$

It is worth mentioning that there are no nodes associated to the incompatible modes, and they can be thought as internal element degrees of freedom. Also, the addition of the incompatible modes result in the element displacements being discontinuous between the nodes of the element (HUGHES, 2000).

Figure 96 – Nodes and coordinates system for the eight node element



Source: Author's production, 2016

As the incompatible modes are unique to each element, they can be eliminated on the element level. This leads to a condensed stiffness matrix, with the same dimension of the standard eight node element.

From the standard definition of the stiffness matrix, one has

$$\mathbf{K}^e = \int_{\Omega^e} \mathbf{B}^{eT} \mathbf{C} \mathbf{B}^e d\Omega, \quad (B.13)$$

where \mathbf{C} is the fourth order elasticity tensor, Ω^e is the element domain and \mathbf{B} is the strain-displacement matrix, written as

$$\mathbf{B}^e = [\mathbf{B}_d^e \quad \mathbf{B}_{\alpha}^e], \quad (B.14)$$

where

$$\mathbf{B}_d^e = [\mathbf{B}_1^e \quad \mathbf{B}_2^e \quad \mathbf{B}_3^e \quad \mathbf{B}_4^e \quad \mathbf{B}_5^e \quad \mathbf{B}_6^e \quad \mathbf{B}_7^e \quad \mathbf{B}_8^e] \quad (B.15)$$

refers to the standard nodal displacements and

$$\mathbf{B}_{\alpha}^e = [\mathbf{B}_9^e \quad \mathbf{B}_{10}^e \quad \mathbf{B}_{11}^e] \quad (B.16)$$

refers to the incompatible displacements of the element. Each B_a are defined in the usual way and normal size (6×3). Consequently, matrix \mathbf{B} has 6 rows and 33 columns and the local stiffness matrix, obtained with this expanded strain-displacement matrix, has 33 rows and 33 columns, and can be written in a partitioned form as

$$\mathbf{K}^e = \begin{bmatrix} \mathbf{K}_{dd} & \mathbf{K}_{d\alpha} \\ \mathbf{K}_{\alpha d} & \mathbf{K}_{\alpha\alpha} \end{bmatrix}, \quad (\text{B.17})$$

where \mathbf{K}_{dd} is the usual 24×24 stiffness matrix for the eight node trilinear isoparametric element, $\mathbf{K}_{d\alpha} = \mathbf{K}_{\alpha d}^T$ has dimension 24×9 and $\mathbf{K}_{\alpha\alpha}$ has dimension 9×9 .

Bearing in mind that there are no forces corresponding to the incompatible modes, one can write the equilibrium problem as

$$\begin{bmatrix} \mathbf{K}_{dd} & \mathbf{K}_{d\alpha} \\ \mathbf{K}_{\alpha d} & \mathbf{K}_{\alpha\alpha} \end{bmatrix} \begin{bmatrix} \hat{\mathbf{u}}^e \\ \boldsymbol{\alpha}^e \end{bmatrix} = \begin{bmatrix} \mathbf{f} \\ \mathbf{0} \end{bmatrix}. \quad (\text{B.18})$$

From the above equation, one can write

$$\mathbf{K}_{\alpha d} \hat{\mathbf{u}}^e + \mathbf{K}_{\alpha\alpha} \boldsymbol{\alpha}^e = \mathbf{0}, \quad (\text{B.19})$$

and solving for $\boldsymbol{\alpha}^e$ one obtains

$$\boldsymbol{\alpha}^e = -\mathbf{K}_{\alpha\alpha}^{-1} \mathbf{K}_{\alpha d} \hat{\mathbf{u}}^e. \quad (\text{B.20})$$

The value of $\boldsymbol{\alpha}$ can be eliminated from the equilibrium problem using the above equation, leading to a standard 24×24 stiffness matrix, given by

$$\mathbf{K}_{est}^e = \mathbf{K}_{dd} - \mathbf{K}_{d\alpha} \mathbf{K}_{\alpha\alpha}^{-1} \mathbf{K}_{\alpha d}. \quad (\text{B.21})$$

Equation B.21 is the local stiffness matrix of the incompatible modes of the element, and its acquisition procedure is frequently referred as Static Condensation in the related literature. From this point on, the global stiffness procedure is performed in the usual way and the nodal displacements can be achieved with the usual equilibrium problem.

The stress computation is made in an usual way, including the contribution of the incompatible modes as

$$\begin{aligned} \boldsymbol{\sigma}(\mathbf{x}) &= \mathbf{D}(\mathbf{x}) \boldsymbol{\epsilon}(\mathbf{x}) \\ &= \mathbf{D}(\mathbf{x}) \left[\sum_{a=1}^8 \mathbf{B}_a(\mathbf{x}) \hat{\mathbf{u}}_a^e + \sum_{a=9}^{11} \mathbf{B}_a(\mathbf{x}) \boldsymbol{\alpha}_a^e \right]. \end{aligned} \quad (\text{B.22})$$

According to Lesaint (1976), an element with arbitrary shape presents erratic behaviour and fail the patch test. However, this erratic behaviour does not occur in elements with rectangle or parallelogram forms, which are used at this work.

APPENDIX C – VALIDATION OF THE HOMOGENIZATION

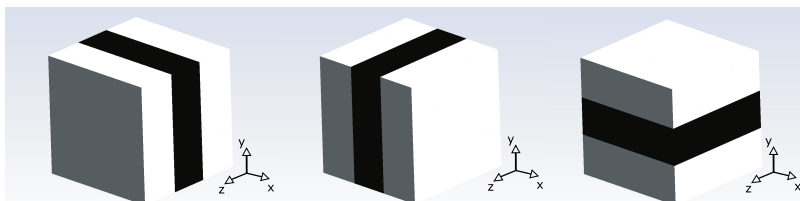
This appendix shows the validation of the mechanical and thermal homogenization procedure implemented in this work. Simple topologies were chosen in order to compare the results obtained with established mathematical theories and with results found into literature.

MECHANICAL VALIDATION

Reinforcement in the Principal Planes

The first model used consists in a reinforcement in a given plane of the base cell. Reinforcement in the three principal planes, xy , yz and xz , are analysed separately and the homogenized tensors are evaluated. The models for the base cell used in the simulations are shown in figure 97, where the voids are represented in white and the reinforcements in black, and the data used in the homogenization program is shown in table 12.

Figure 97 – Reinforcement in the planes xy , yz and xz , respectively



Source: Author's production, 2016.

Table 12 – Data for the plane reinforcement cases

Young's Modulus (E^0) [Pa]	200.0
Poisson's Coefficient (ν)	0.0
Minimum Density (ρ)	10^{-6}
Mesh	50x50x50

The mechanical homogenized tensors, for the cases shown in figure

97, are given in a general form, respectively, by

$$\mathbf{C}^H = \begin{bmatrix} C_{1111}^H & 0 & 0 & 0 & 0 & 0 \\ & C_{2222}^H & 0 & 0 & 0 & 0 \\ & & 0 & 0 & 0 & 0 \\ & & & C_{1212}^H & 0 & 0 \\ & & & & 0 & 0 \\ sym. & & & & & 0 \end{bmatrix},$$

with $C_{1111}^H = C_{2222}^H$,

$$\mathbf{C}^H = \begin{bmatrix} 0 & 0 & 0 & 0 & 0 & 0 \\ & C_{2222}^H & 0 & 0 & 0 & 0 \\ & & C_{3333}^H & 0 & 0 & 0 \\ & & & 0 & 0 & 0 \\ & & & & C_{2323}^H & 0 \\ sym. & & & & & 0 \end{bmatrix},$$

with $C_{2222}^H = C_{3333}^H$ and

$$\mathbf{C}^H = \begin{bmatrix} C_{1111}^H & 0 & 0 & 0 & 0 & 0 \\ & 0 & 0 & 0 & 0 & 0 \\ & & C_{3333}^H & 0 & 0 & 0 \\ & & & 0 & 0 & 0 \\ & & & & 0 & 0 \\ sym. & & & & & C_{1313}^H \end{bmatrix},$$

with $C_{1111}^H = C_{3333}^H$.

As expected, the components that depend on the non reinforced axis have negligible values and so the coupled components, due to the null value of Poisson's Coefficient.

As a comparison, the mixture rule is used, and, as shown by Mendonça (2005) the Young's Modulus of a composite media, in a certain direction, can be found by

$$E^H = V_f E^0 + (1 - V_f) E_v^0, \quad (C.1)$$

where E^0 is the base material's Young's Modulus, E_v^0 is the voids Young modulus, given by

$$E_v^0 = \rho E^0, \quad (C.2)$$

V_f is the volumetric fraction of material, and the shear modulus is given by

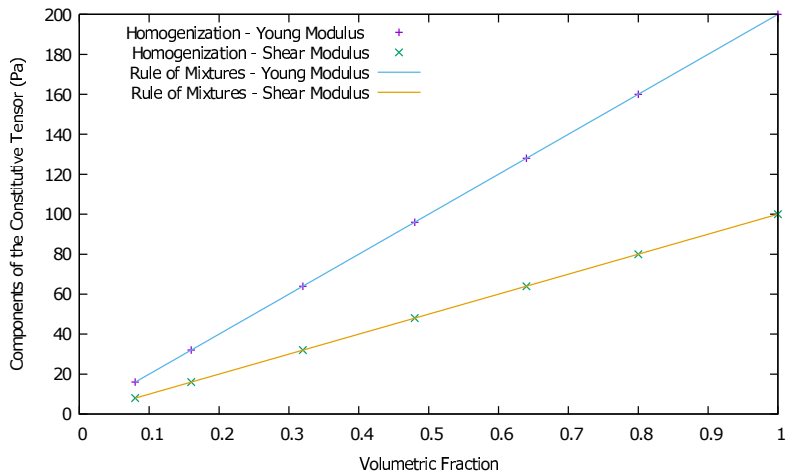
$$G^H = V_f G^0 + (1 - V_f) G_v^0, \quad (C.3)$$

where G^0 is the base material's shear modulus and G_v^0 is the void's shear modulus, given by

$$G_v^0 = \rho G^0. \quad (C.4)$$

For each case, it is used a range of material fraction from zero, where there is no reinforcement at all, to one, where one has a solid media. The results obtained with the homogenization procedure, and with the mixture rule are shown in figure 98.

Figure 98 – Young and shear modulus versus volumetric fraction. In the full lines the mixture rule solution. In the discrete points the homogenization solution



Source: Author's production, 2016.

As the Poisson's coefficient adopted in the simulations is equal to zero, the components C_{1111}^H , C_{2222}^H and C_{3333}^H of the homogenized tensor provide directly the Young's Modulus in its respective directions. Due to the symmetry of the three geometries, the normal components of the tensors are equal among themselves, just changing its directions. Thus, the

components C_{1111}^H and C_{2222}^H for the first case are equal to the components C_{2222}^H and C_{3333}^H for the second case and for the components C_{1111}^H and C_{3333}^H for the third case.

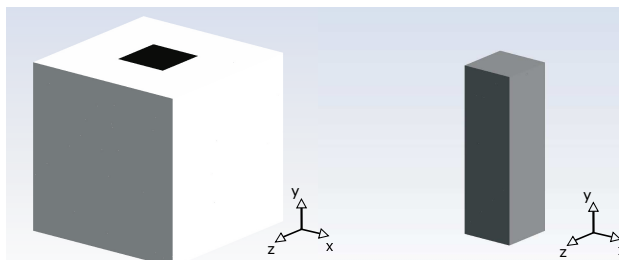
Also, the components C_{1212}^H , C_{2323}^H and C_{1313}^H provides directly the Shear Modulus of the media, and as for the normal components, the values of the shear components are equal among the three studied cases.

Figure 98 shows the comparison of the results obtained with the homogenization procedure and with the mixture rule. As the components for the three cases are numerically the same, this graphic represents the results for all cases. Continuous lines represent the results for the mixture rule, equations C.1 and C.3, and the discrete points represent the solution obtained with the homogenization method. The blue line (or top line), and the associated discrete points represent the Young's Modulus and the green line (bottom) and the associated discrete points represent the Shear Modulus.

Uniaxial Reinforcement

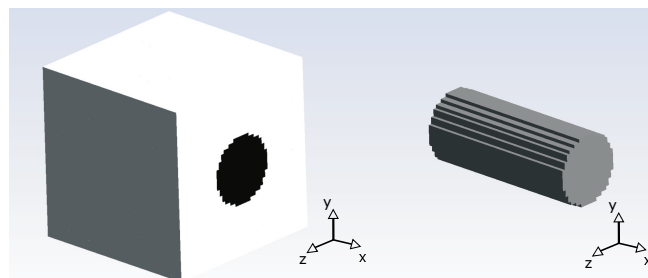
For the second validation, two unidimensional reinforcement were used. The first one consists in a squared reinforcement in y direction, with geometry depicted in figure 99. The second one consists in a circular reinforcement in x direction, as shown in figure 100. In both figures, the white portion represents the voids and the dark portion represents the base material. The data used for both cases is shown in table 13.

Figure 99 – Square reinforcement



Source: Author's production, 2016.

Figure 100 – Circular reinforcement



Source: Author's production, 2016.

Table 13 – Data for uniaxial reinforcement cases

Young's Modulus (E^0) [Pa]	200.0
Poisson's Modulus (ν)	0.0
Minimum Density (ρ)	10^{-6}
Mesh	50x50x50

For the square reinforcement in the y direction, the homogenized mechanical tensor has the form

$$C^H = \begin{bmatrix} 0 & 0 & 0 & 0 & 0 & 0 \\ & C_{2222}^H & 0 & 0 & 0 & 0 \\ & & 0 & 0 & 0 & 0 \\ & & & 0 & 0 & 0 \\ & & & & 0 & 0 \\ & & & & & 0 \end{bmatrix}.$$

sym.

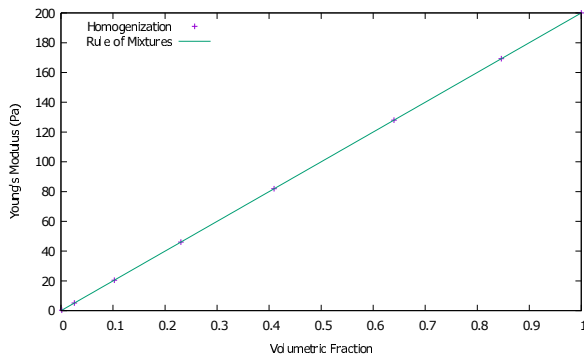
For the circular reinforcement in x direction case the homogenized tensor is given by

$$C^H = \begin{bmatrix} C_{1111}^H & 0 & 0 & 0 & 0 & 0 \\ 0 & 0 & 0 & 0 & 0 & 0 \\ & & 0 & 0 & 0 & 0 \\ & & 0 & 0 & 0 & 0 \\ & & 0 & 0 & 0 & 0 \\ & & 0 & 0 & 0 & 0 \end{bmatrix}.$$

Once again, the comparative is used with regard to the mixture rule, equation C.1, but in this case, only for the longitudinal component of the tensor in which the reinforcement is applied.

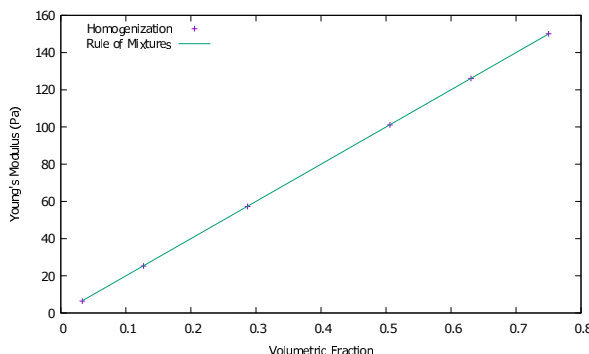
Figures 101 and 102 show the comparison between the Young's Modulus obtained by the rule of mixtures and the homogenized components for the cases with square reinforcement in y and circular reinforcement in x , respectively.

Figure 101 – Young's modulus versus volumetric fraction, square reinforcement in y direction



Source: Author's production, 2016.

Figure 102 – Young's modulus versus volumetric fraction, circular reinforcement in x direction



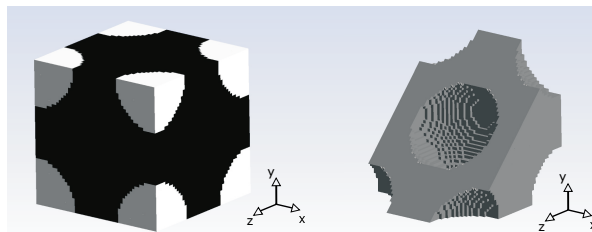
Source: Author's production, 2016.

For these simple geometries, the comparisons show that the homogenization method provides good results.

Spheres

The next validation consists in a base cell in which a sphere is withdraw from the middle and an eight of a sphere is withdraw from each corner of the cell, as shown in the figure 103, where the voids are represented in white and the base material is represented in black. The data used in the simulations is shown in table 14.

Figure 103 – Hollow sphere model



Source: Author's production, 2016.

Table 14 – Simulation data

Young's Modulus (E^0) [Pa]	200.0
Poisson's Modulus (ν)	0.25
Minimum Density (ρ)	10^{-9}
Mesh	50x50x50

The homogenized constitutive elastic tensor for this case has the form

$$C^H = \begin{bmatrix} C_{1111}^H & C_{1122}^H & C_{1133}^H & 0 & 0 & 0 \\ C_{2222}^H & C_{2233}^H & 0 & 0 & 0 & 0 \\ C_{3333}^H & 0 & 0 & 0 & 0 & 0 \\ & & & C_{1212}^H & 0 & 0 \\ & & & & C_{2323}^H & 0 \\ & & & & & C_{1313}^H \end{bmatrix},$$

sym.

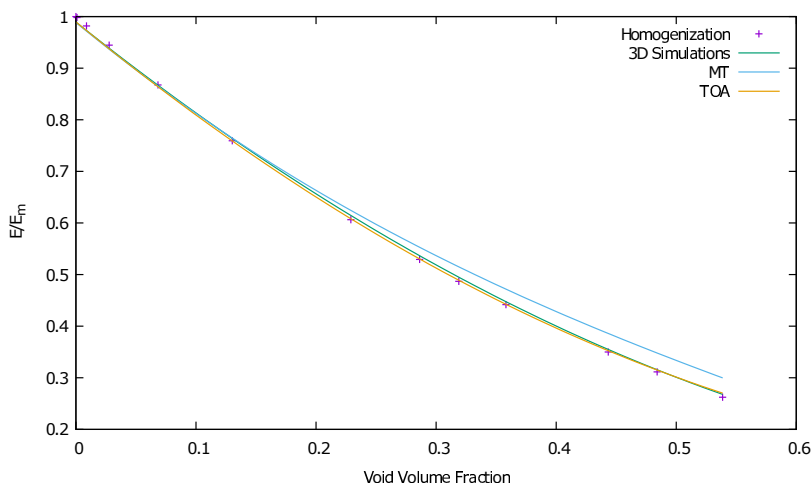
with $C_{1111}^H = C_{2222}^H = C_{3333}^H$, $C_{1122}^H = C_{1133}^H = C_{2233}^H$ and $C_{1212}^H = C_{2323}^H = C_{1313}^H$.

Through the elastic constitutive homogenized tensor is possible to determinate the effective physical properties of the media, such as the Young's Modulus, the Poisson's Modulus, the Bulk Modulus and the Shear Modulus, as a function of the volume of the void spheres. The results presented by Segurado and Llorca (2002) are used as a comparison with the results obtained for the simulations.

The authors use a random distribution of void sphere in an unitary domain and evaluates its effective elastic properties through a three dimensional finite element analysis (3D Simulations). Also, they compare their results with three analytical methods: the Mori-Tanaka mean-field analysis (MT), the generalized self-consistent method (GSC) and Torquato's third-order approximation (TOA).

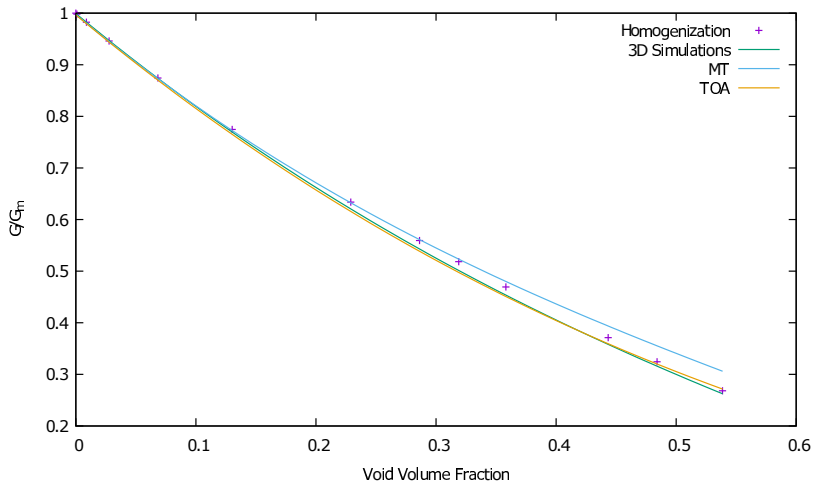
A volume fraction of void sphere between 0.0 and 0.5 is used in regard of the total volume of the domain. Figures 104, 105, 106 and 107 show the results comparison.

Figure 104 – Young's modulus



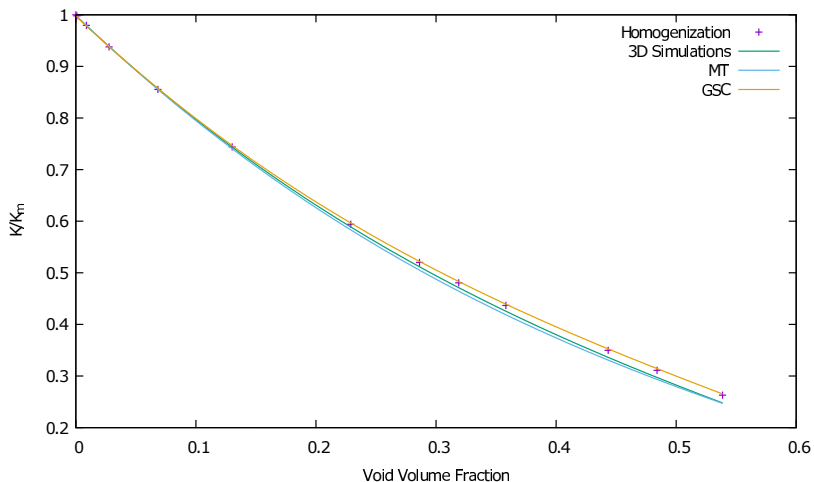
Source: Author's production, 2016

Figure 105 – Shear modulus



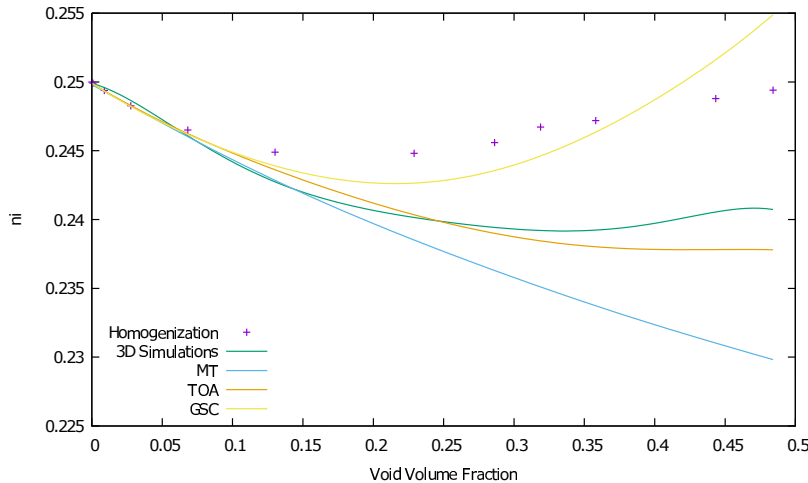
Source: Author's production, 2016

Figure 106 – Bulk modulus



Source: Author's production, 2016

Figure 107 – Poisson's coefficient



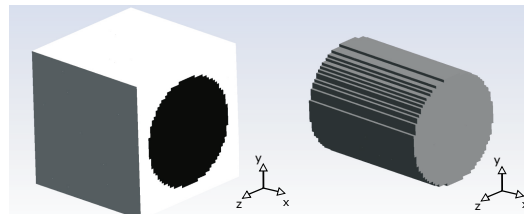
Source: Author's production, 2016

Once again, the comparisons show that the homogenization procedure provides good results. Although the results presented for the Poisson's Coefficient, figure 107, seems to deviate from the results used as comparison, the scale of this figures shows that the numerical results are very close to each other and that the Poisson's coefficient do not vary significantly in this range of volume fraction.

Composites

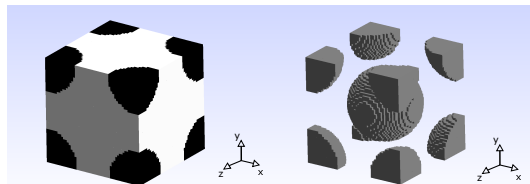
Another possibility of the use of the homogenization method, is to evaluate the properties of a media composed of two or more materials. The last mechanical validation presented use two different kind of materials on the geometry of the base cell, forming a composite. Two cases were chosen, the first one, shown in figure 108, is a glass fibre in an epoxy matrix, and the second one, shown in figure 109, is a glass sphere in an epoxy matrix. For both figures, the white portion represents the epoxy matrix and the black portion represents the glass reinforcement. The data used in the simulations is shown in table 15.

Figure 108 – Glass fibre with volumetric fraction of 0.51 in an epoxy matrix



Source: Author's production, 2016.

Figure 109 – Glass spheres volumetric fraction of 0.54 in an epoxy matrix



Source: Author's production, 2016.

Table 15 – Simulation data

Glass Young Modulus (E_f) [GPa]	70.0
Glass Poisson Modulus (ν_f)	0.20
Matrix Young Modulus (E_m) [GPa]	3.0
Matriz Poisson Modulus (ν_m)	0.38
Mesh	50x50x50

For the case shown in figure 108, the Young's Modulus in the longitudinal direction of the fibre it is calculated by the mixture rule, equation C.1, and the Young's Modulus in the transversal direction of the fibre, and the Shear Modulus are calculated by the equations proposed by Halpin (1969), given by

$$\frac{P}{P_m} = \frac{1 + \zeta \eta V_f}{1 - \eta V_f}, \quad (C.5)$$

where

$$\eta = \frac{\frac{P_f}{P_m} - 1}{\frac{P_f}{P_m} + \zeta}, \quad (C.6)$$

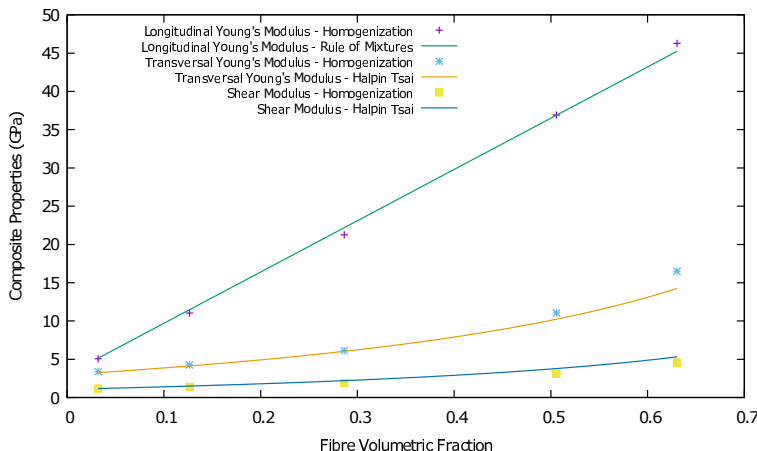
where P is the required property and ζ represents a measure of the reinforcement, which depends on the form of the cross section of the fibre. Mendonça (2005) suggests for circular fibres, a value of $\zeta = 2$. The constitutive elastic tensor, obtained with the homogenization procedure, for this case, is given by

$$C^H = \begin{bmatrix} C_{1111}^H & C_{1122}^H & C_{1133}^H & 0 & 0 & 0 \\ C_{2222}^H & C_{2233}^H & C_{3333}^H & 0 & 0 & 0 \\ C_{1212}^H & C_{2323}^H & C_{1313}^H & 0 & 0 & 0 \\ sym. & & & & & \end{bmatrix},$$

with $C_{2222}^H = C_{3333}^H$, $C_{1122}^H = C_{1133}^H$ and $C_{1212}^H = C_{1313}^H$.

The comparison between the results obtained with the homogenization method and with the equations mentioned are shown in figure 110

Figure 110 – Properties of the epoxy matrix reinforced by glass fibres



Source: Author's production, 2016.

The constitutive tensor for the case shown in figure 109 has the form

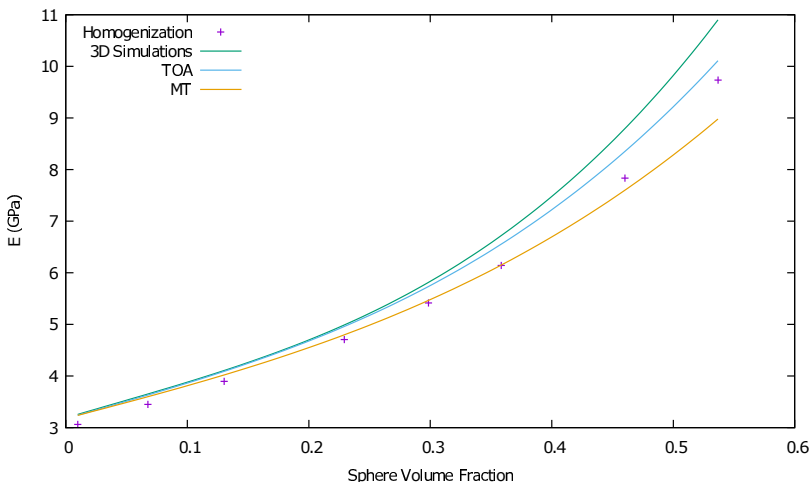
$$C^H = \begin{bmatrix} C_{1111}^H & C_{1122}^H & C_{1133}^H & 0 & 0 & 0 \\ C_{2222}^H & C_{2233}^H & 0 & 0 & 0 & 0 \\ C_{3333}^H & 0 & 0 & 0 & 0 & 0 \\ & C_{1212}^H & 0 & 0 & 0 & 0 \\ & & C_{2323}^H & 0 & 0 & 0 \\ & & & C_{1313}^H & 0 & 0 \end{bmatrix},$$

sym.

with $C_{1111}^H = C_{2222}^H = C_{3333}^H$, $C_{1122}^H = C_{1133}^H = C_{2233}^H$ and $C_{1212}^H = C_{2323}^H = C_{1313}^H$.

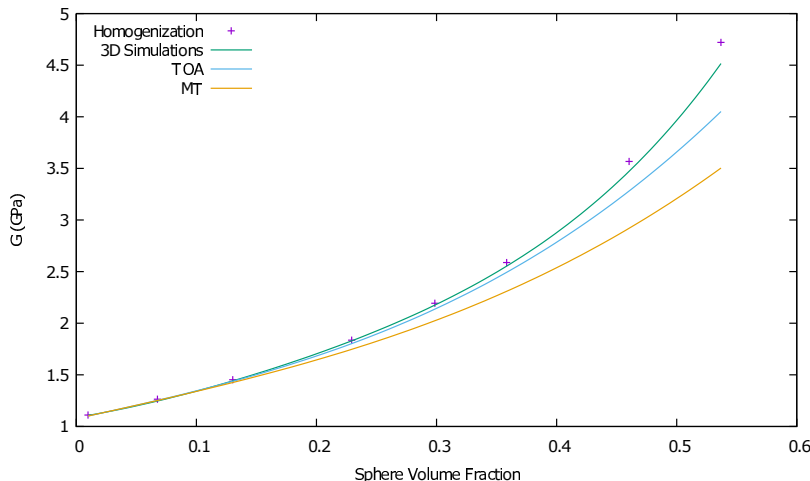
For this case is used the work of Segurado and Llorca (2002) as comparison. The authors use a unitary domain in which 30 glass fibres spheres are allocated randomly into an epoxy matrix. A three dimensional finite element analysis (3D Simulations) is made by the authors and compared with TOA and MT methods. The comparison of the results for the Young's Modulus and for the Shear Modulus are shown in figures 111 and 112.

Figure 111 – Properties of the epoxy matrix reinforced by glass spheres - Young's modulus



Source: Author's production, 2016.

Figure 112 – Properties of the epoxy matrix reinforced by glass spheres - Shear modulus



Source: Author's production, 2016.

THERMAL VALIDATION

This section aims to validate the thermal homogenization code written. Two models were chosen to do the validation. The first one consists in the reinforcement in the principal planes of the base cell, and the second ones is the a model of open cell hollow spheres. Mathematical models and results found into the literature are used for the comparison.

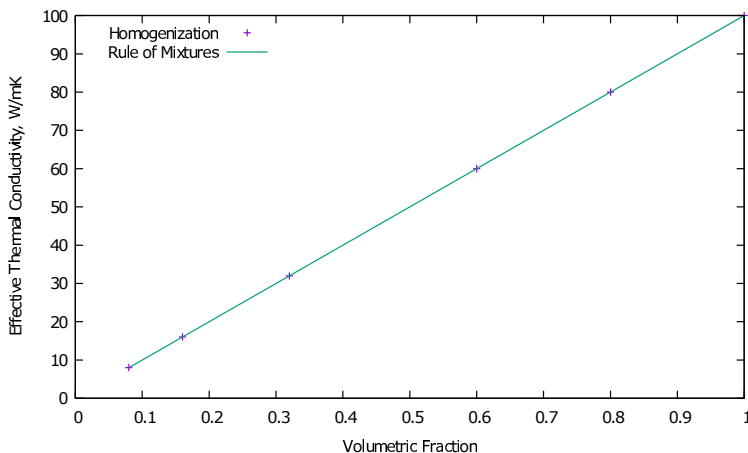
Reinforcement in the Principal Planes

The first model chosen is equal to the first model used in the mechanical validation, and can be seen in figure 97. The data used in the simulations is shown in table 16. As comparison, the rule of mixtures is used.

Table 16 – Data for the plane reinforcement cases

Thermal Conductivity (Kt^0) [$\text{Wm}^{-1}\text{K}^{-1}$]	100.0
Minimum Density (ρ)	10^{-6}
Mesh	50x50x50

Figure 113 – Effective thermal conductivity versus volumetric fraction. In the full line is the mixture rule solution. In the discrete points is the homogenization solution



Source: Author's production, 2016.

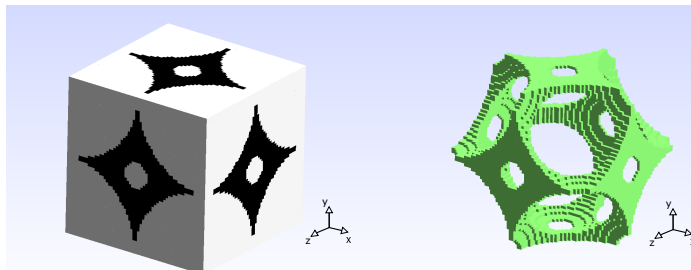
Open Cell Hollow Spheres

The second validation consist in a open cell hollow sphere structure, as shown in figure 114. The data used in the simulations is shown in table 17. The effective thermal conductivity is calculated through the homogenization method and the results given by Krishnan, Garimella and Murthy (2008) are used as a comparison. The authors use a direct simulation to evaluate the thermal conductivity properties of an open cell foam formed by a body centred cell (BCC). Figure 115 shows the result comparison.

Table 17 – Data for the plane reinforcement cases

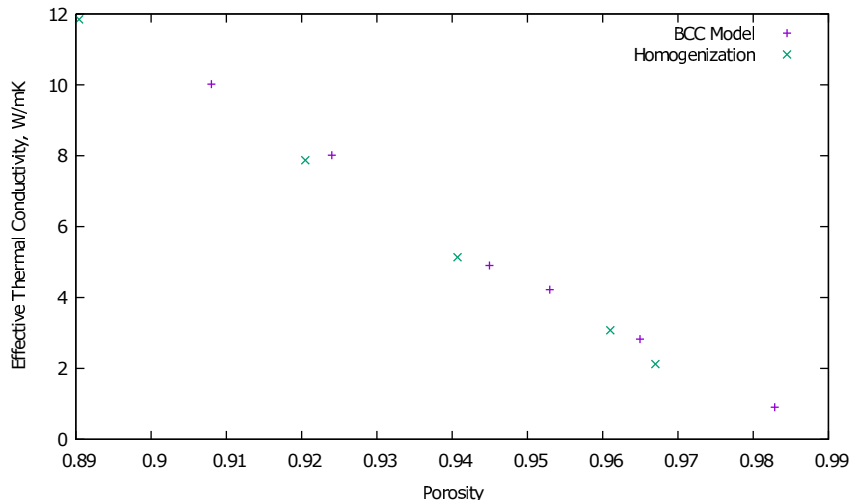
Thermal Conductivity (Kt^0) [$Wm^{-1}K^{-1}$]	218.0
Minimum Density (ρ)	10^{-6}
Mesh	50x50x50

Figure 114 – Open cell hollow sphere structure



Source: Author's production, 2016.

Figure 115 – Thermal properties validation



Author's production, 2016.

APPENDIX D – SENSITIVITY VALIDATION

This chapter aims to validate the derivatives of the components of the fourth order elasticity tensor. The central finite difference is used. Let the function $f(x)$, written in Taylor's series, truncated on the first order term. For a forward perturbation, h , one can write

$$f(x+h) = f(x) + f'(x)h, \quad (\text{D.1})$$

and for a backward perturbation,

$$f(x-h) = f(x) - f'(x)h. \quad (\text{D.2})$$

Using the expression D.1, one can obtain an expression for the derivatives of the function in regard to the forward finite difference, given by

$$f'(x) = \frac{f(x+h) - f(x)}{h}. \quad (\text{D.3})$$

All the same, the expression D.2 can be used to determinate the derivatives in regard to the backward finite difference, so

$$f'(x) = \frac{f(x-h) + f(x)}{h}. \quad (\text{D.4})$$

Besides, using the difference of the expressions D.1 and D.2,

$$f(x+h) - f(x-h) = 2f'(x)h, \quad (\text{D.5})$$

the derivatives of the function in regard to the central difference can be obtained as

$$f'(x) = \frac{f(x+h) - f(x-h)}{2h}. \quad (\text{D.6})$$

For the validation of the analytical derivatives of the homogenized constitutive tensor in regard to the pseudo-densities, the central finite difference is used in order to compare the results.

A range of five different perturbations were used in the central difference method, equation D.6, in order to compare with the analytical derivatives, equation 5.27.

Tables 18, 19 and 20 show the comparison for all components of the homogenized constitutive tensor for the five perturbations. A mesh of

$20 \times 20 \times 20$ elements was used and the derivatives were calculated based on an element chosen randomly. It expected a value that approaches 1.0, indicating that the derivatives calculated for both methods have the same value.

Table 18 – Validation of the analytical derivatives through the central finite difference method

C/h	1×10^{-1}	1×10^{-2}	1×10^{-3}	1×10^{-4}	1×10^{-5}
C_{111}^H	0.99655	0.99996	0.99999	0.99999	0.99999
C_{112}^H	0.99522	0.99995	0.99999	0.99999	0.99999
C_{113}^H	0.99506	0.99995	0.99999	1.00000	1.00000
C_{112}^H	0.99838	0.99998	0.99999	0.99999	0.99999
C_{1123}^H	1.00267	1.00002	1.00000	1.00000	1.00000
C_{1113}^H	1.00071	1.00001	1.00001	1.00001	0.99999
C_{222}^H	0.99681	0.99996	0.99999	1.00000	1.00000

Table 19 – Validation of the analytical derivatives through the central finite difference method

C/h	1×10^{-1}	1×10^{-2}	1×10^{-3}	1×10^{-4}	1×10^{-5}
C_{223}^H	0.99538	0.99995	0.99999	1.00001	0.99999
C_{2212}^H	1.00366	1.00004	1.00000	1.00000	1.00000
C_{222}^H	1.00249	1.00003	1.00000	1.00000	1.00000
C_{2213}^H	1.00007	1.00000	1.00000	1.00000	1.00000
C_{333}^H	0.99708	0.99997	1.00000	1.00000	1.00000
C_{3312}^H	0.98826	0.99988	1.00000	1.00000	1.00000
C_{332}^H	0.99232	0.99992	1.00000	1.00000	1.00000

Table 20 – Validation of the analytical derivatives through the central finite difference method

C/h	1×10^{-1}	1×10^{-2}	1×10^{-3}	1×10^{-4}	1×10^{-5}
C_{3313}^H	0.99945	0.99999	1.00000	1.00000	1.00000
C_{212}^H	0.99853	0.99999	1.00000	1.00000	1.00000
C_{1223}^H	0.99972	0.99998	0.99999	0.99999	1.00000
C_{1213}^H	0.99829	0.99998	0.99999	1.00000	1.00000
C_{2323}^H	0.99818	0.99998	1.00000	1.00000	1.00000
C_{2313}^H	0.98669	0.99987	1.00000	1.00000	1.00000
C_{1313}^H	0.99801	0.99998	0.99999	0.99999	1.00000